Analysis of Mutants of Tyrosyl-tRNA Synthetase by X-ray Crystallography

by

Michael David Fothergill

A dissertation submitted to the Imperial College of Science and Technology in candidature for the Diploma of the Imperial College, and to the University of London in candidature for the degree of Doctor of Philosophy.

Department of Chemistry
Imperial College of Science and Technology
London SW7 2AY.

October 1988

"O SON OF BOUNTY!"

"Out of the wastes of nothingness, with the clay of My command I made thee to appear, and have ordained for thy training every atom in existence and the essence of all created things."

Baha'u'llah

Acknowledgements

I would like to thank the following people for their friendship and support over the last three years;

from my supervisor's group -

Miss Tamara Gray, for teaching me how to do enzyme preps; Mr. Jack Waring Knill-Jones, for general advice and encouragement; Drs. Eric First and Robin Leatherbarrow for help with various chapters; Dr. Frankie Lau for sharing my more than academic interest in Sainsbury's tandoori chicken; Dr. Mark Bycroft for making me finish this thesis; Dr. Colin Longstaff for his sporting camaraderie and political acumen; Drs. Danuta Mossakowska and Alison Campbell for helpful advice; Dr. Tim Wells and Mr. Sanjoy Ray for proofreading and constructive criticism; Miss Sophie Jackson for help with the Guardian Crossword puzzle;

and from the Biophysics group -

Drs. Peter Brick, Andrew Leslie, Katy Brown, Kim Henrick, Charles Collyer and Alan Wonnacott. K. H. and A. J. W. deserve particular mention for their unselfish efforts on my behalf.

Finally, I would like to thank my supervisor, Professor Alan Fersht, F.R.S., for his creative suggestions and support and Professor David Blow, F.R.S., for allowing me to work in his laboratory.

Abstract

This thesis is an account of the analysis of four mutants of the tyrosyl-tRNA synthetase from *Bacillus stearothermophilus* by X-ray crystallography.

Analysis of the mutant Cys→Gly-35 shows that the removal of a residue thought to form a hydrogen bond with the enzyme-bound intermediate, tyrosyl adenylate causes a structural change at a neighbouring residue also involved in catalysis. This can be related to kinetic data from the double-mutants made at these residues which show that they are not independent of one another.

The crystal structure of the mutant Tyr→Phe-34 shows that the deleted hydroxyl group is not replaced by a water molecule in the mutant enzyme-substrate complex. This implies that the free energy of an unpaired hydrogen bond has been determined.

The X-ray analysis of the mutant Thr→Cys-51 complexed with tyrosyl adenylate revealed that a disulphide bridge is formed between residues Cys-35 and Cys-51, in the crystal, in the absence of reducing agents. The analysis of the same mutant complexed with tyramine shows no disulphide bridge. Kinetic studies in the presence of reducing agents showed the enzyme to have improved catalytic activity (Ho & Fersht, 1986). The crystal structure of the reduced form suggests that this may result from the formation of new hydrogen bond between the sulphydryl group of Cys-51 and the 3'OH oxygen of the substrate.

Analysis of the mutant Asp→Asn-194, shows no structural change. Data from kinetics, linear free energy relationships and the crystal structure suggests that the carboxyl side chain of this residue may interact with the magnesium in the transition state of the formation of tyrosyl adenylate.

In addition to the crystallographic work, the model of the penta-coordinate transition-state (Leatherbarrow *et al.*, 1985) has been augmented in response to recent work (Fersht *et al.*, 1988) where residues in a region of the enzyme several Angstroms away from the active site of the enzyme have been shown to bind the transition-state of the formation of tyrosyl adenylate. An induced fit mechanism has been proposed, where this loop region folds over the active site as the reaction proceeds. A polypeptide segment, comprising residues 220-240 in this crystallographically disordered region, has been modelled in such a conformation. A magnesium binding site has been built into the model using data from the mutants at position 194.

CONTENTS

Acknowledgements
Abstract
Contents
List of Figures
List of Appendices

Page

CHAPTER 1: INTRODUCTION

1.1.1	Introduction	14
1.1.2	Protein Engineering of Tyrosyl-tRNA Synthetase.	17
1.1.3	Crystal Structures	19
1.1.4	Model of Tyrosyl Adenylate	22
1.1.5	Model of Transition-State	22
1.1.6	The Use of Binding Energy in Catalysis	26
1.1.7	Linear Free Energy Relationships	30
1.1.8	The Double Mutant Test	33
1.1.9	Hydrogen Bonding	39

CHAPTER 2: METHODS

2.1.1	Purification of Mutant Enzymes	41
2.1.2	Purification Procedure	42
2.1.3	Preparation of 2 Litre Culture	43
2.1.4	Cell Harvesting and Lysis	43
2.1.5	Ammonium Sulphate Precipitation	44
2.1.6	FPLC Purification	44
2.1.7	Enzyme Assays	45
2.1.8	SDS-Polyacrylamide Gel Electrophoresis	45
2.1.9	Optimization of YTS Expression	46
2.2.1	Crystallisation	51
2.2.2	Crystallisation of Mutant Enzymes	51
2.2.3	Crystal Mounting and Data Collection	52
2.2.4	Truncated Monoclinic Form	53
2.3.1	Synchrotron Radiation	54
2.3.2	Film Measurement	54

2.3.3	Densitometry	55
2.3.4	Orientation	55
2.3.5	Oscillation	56
2.3.6	Measurement of Oscillation Data	56
2.3.7	Postrefinement	57
2.3.8	Reduction of Data	58
2.4.1	Electron Density Maps	59
2.4.2	Refinement of Structures	59

CHAPTER 3: Analysis of Cys→Gly-35 Mutant

3.1.1	Introduction	62
3.1.2	Purification and Crystallisation	63
3.1.3	Data Collection and Structure Refinement	63
3.1.5	Difference Maps of Complex With Tyrosine	64
3.1.6	Difference Maps of Complex With Tyrosyl Adenylate	68
3.2.1	Interpretation of Structural Changes in Tyrosine Complex	72
3.2.2	Interpretation of Structural Changes in Tyrosyl Adenylate Complex	72
3.2.3	Relationship Between Changes in Structure and Activity	72

CHAPTER 4: Analysis of Tyr→Phe-34 Mutant

4.1.1	Introduction	76
4.2.1	Purification and Crystallisation	77
4.2.2	Data Collection and Structure Refinement	77
4.2.3	Difference Map of the Complex With Tyrosine	77
4.2.4	Interpretation of Complex With Tyrosine	78
4.3.1	Relationship Between ΔG_{app} and ΔG_{bind} in Tyr→Phe-34	81

CHAPTER 5: Analysis of Thr→Cys-51 Mutant

5.1.1	Introduction	84
5.1.2	Purification and Crystallisation	85
5.1.3	Data Collection and Structure Refinement	85
5.1.4	Difference Maps of Complex With Tyrosyl Adenylate	86
5.1.5	Difference Maps of Complex With Tyramine	89
5.2.1	Discussion	93

CHAPTER 6: Analysis of Asp→Asn-194 Mutant

6.1.1	Introduction	98
6.1.2	Purification and Crystallisation	98
6.1.3	Data Collection and Structure Refinement	99
6.2.1	Difference Map of the Complex With Tyrosine	99
6.3.1	Results of Crystallographic Analysis	99
6.4.1	Discussion	100

CHAPTER 7: Transition State Model

7.1.1	Introduction	108
7.1.2	Model Building	108
7.2.1	Results of Model Building	109
7.3.1	Discussion	112

CHAPTER 8: Conclusions 120

References 124

List of Figures

Fig 1.1	Crystal structure of tyrosyl-tRNA synthetase.	18
Fig 1.2	A kinetic scheme for the formation of tyrosyl adenylate.	20
Fig 1.3	Residues believed to interact with tyrosyl adenylate in the active site of tyrosyl-tRNA synthetase.	23
Fig 1.4	Representation of the mechanism of formation of tyrosyl adenylate.	24
Fig 1.5	Drawing of the reaction transition state as modelled from the crystal structure of tyrosyl adenylate.	25
Fig 1.6	Comparison of free energy profiles for four mutant tyrosyl-tRNA synthetases with that of the wild type enzyme.	28
Fig 1.7	Difference free energy diagrams for several active site mutants of tyrosyl-tRNA synthetase.	29
Fig 1.8	A linear free energy relationship between the binding energy utilised in the transition-state for the reaction and that of the E.Tyr-AMP.PPi complex.	32
Fig 1.9	The double mutant test.	34
Fig 1.10	An example of a pair of additive double mutants which are relatively far apart in sequence and space.	35
Fig 1.11	An example of non-additive double mutants which are far apart in sequence, but close together in space.	37
Fig 1.12	An example of non-additive double mutants which are close together in sequence and space.	38
Fig 2.1	Typical SDS-polyacrylamide gel of a preparation of tyrosyl-tRNA synthetase.	47

Fig 3.1	Difference map showing loss of side chain in the mutant Cys→Gly-35 complexed with tyrosine.	65
Fig 3.2	Difference maps of above structure after 5 cycles of refinement, showing small structural changes.	66
Fig 3.3	Difference map after refitting the model, showing that Ile-52 has more than one conformation.	67
Fig 3.4	An electron density map of the mutant Cys→Gly-35 complexed with tyrosyl adenylate, showing density for the substrate.	67
Fig 3.5	Difference map of the mutant Cys→Gly-35 complexed with tyrosine, where the side chains of Thr-51 and Ile-52 have been removed from the model. Shows unbiased electron density for these side chains.	70
Fig 3.6	Same as Fig 3.5 but for the mutant Cys→Gly-35 complexed with tyrosyl adenylate. In comparison with Fig 3.5, this figure shows a change in the preferred conformation of the side chain of Ile-52, and increased disorder of Thr-51.	70
Fig 3.7	Double mutant data for Cys→Gly-35 paired with Thr→Pro-51 and Thr→Cys-51 respectively.	73
Fig 4.1	Difference electron density map showing the loss of the hydroxyl group in the mutant Tyr→Phe-34.	79
Fig 4.2	Electron density map of the mutant Tyr→Phe-34 after several cycles of refinement, showing density for the substrate, tyrosine.	80
Fig 4.3	Diagram showing that a water molecule will not fit between the substrate hydroxyl and the mutant residue, phenylalanine 34.	82

Fig 5.1	Difference electron density map of the mutant Thr→Cys-51 showing density for tyrosyl adenylate and a disulphide bridge formed between Cys-35 and Cys-51.	87
Fig 5.2	Electron density map after 30 cycles of refinement. Density for the disulphide bridge and the substrate is shown.	88
Fig 5.3	Difference electron density map showing the mutant Thr→Cys-51 complexed with tyramine. The cysteines are reduced in this structure.	90
Fig 5.4	An electron density map showing the substrate analogue tyramine and cysteines 35 and 51 after several cycles of refinement.	91
Fig 5.5	The active site region of the refined structure of the native enzyme complexed with the inhibitor tyrosinyl adenylate.Shows the side chain of Thr-51 and the ribose ring of the substrate analogue.	95
Fig 5.6	Same as Fig 5.5 but the coordinates of the mutant Thr→Cys-51 have been superimposed in place of those of the native enzyme. Shows a hydrogen bond could form between the γ-sulphur of Cys-51 and the 3'OH group of the inhibitor.	96
Fig 6.1	A plot of the difference between the crystallographic temperature factors for the main (above) and side chain atoms of the mutant Asp→Asn-194 and that of the native structure. This shows that the mutation has little effect on the distribution of disorder.	101

Fig 6.2	The active site region of the refined structure of tyrosyl-tRNA synthetase complexed with the inhibitor, tyrosinyl adenylate. Residue Asp-194 is shown.	102
Fig 6.3	The refined structure of the mutant Asp→Asn-194.	103
Fig 6.4	Difference free energy diagram of mutants Asp→Asn-194 and Asp→Ala-194.	104
Fig 6.5	A linear free energy relationship between the E.Tyr-ATP$^{\neq}$ complex and the equilibrium constant for the formation of the E.Tyr-AMP complex.	106
Fig 7.1	The active site region of the refined structure of tyrosyl-tRNA synthetase complexed with the inhibitor, tyrosinyl adenylate.	110
Fig 7.2	The penta-coordinate transition-state as described in Leatherbarrow *et al.*, (1985).	111
Fig 7.3	Difference free energy diagrams for the active site mutants Lys→Ala or Asn-82; Arg→Ala or Gln-86; also Lys→Ala or Asn-230 and Lys→Ala or Asn-233 which are in the mobile loop region of the enzyme.	113
Fig 7.4	Crystallographic temperature factors for main chain. B values averaged for backbone C, N and C_α taken from Brick & Blow (1987) and unpublished data.	114
Fig 7.5	Representation of the active site region of tyrosyl-tRNA synthetase showing lysines 82, 230, 233 and arginine 82.	115

Fig 7.6 Representation of a model of the folded loop conformation of tyrosyl-tRNA synthetase, showing the interactions made between residues 82, 86, 230, 233 and the β and γ phosphates of the penta-coordinate transition-state. 116

Fig 7.7 A close up view of Fig 7.6, concentrating on the active site region around the α, β and γ phosphates of the penta-coordinate transition-state. The magnesium has been modelled coordinated to four water molecules and the oxygens of the β and γ phosphates. 117

List of Appendices

Appendix A:	Details of Data Collected on Mutant Enzymes	128
Appendix B:	Refinement Statistics for Mutant Enzymes	130
Appendix C:	Definitions of ΔG_{app} and ΔG_{bind}	136
Appendix D:	Bacterial Strains and Media	137
Appendix E:	Comparison of B Values for Mutant and Native Structures	139

CHAPTER 1

1.1.1 Introduction

Site-directed mutagenesis (Zoller & Smith, 1983), is a technique which allows a piece of DNA to be mutated at a specific region, as little as a single base pair, to any other sequence of nucleotides. When applied to the gene coding for a protein or enzyme, mutations can be made which will change the codons for any amino acid residue in the polypeptide chain. When the nucleotide sequence of the gene has been determined, this technique can be used to mutate any residue in the protein to one of the naturally occuring set of 20 amino acids. This particular application of the technique is termed protein engineering. Since its introduction in 1982 (Winter *et al.*, 1982), protein engineering has been used to investigate the properties of several proteins, especially the catalytic behaviour of enzymes. This has been widely reviewed (Leatherbarrow & Fersht, 1986; Gerlt, 1987; Knowles, 1987).

Enzymology has mainly drawn upon two fields; kinetics and protein crystallography. Before the development of protein engineering, apart from a few notable exceptions, it was often very difficult to relate structural and kinetic data for many enzymes. In 1982, the catalytic mechanism of tyrosyl-tRNA synthetase was completely unknown, yet the structures of enzyme bound species were known from X-ray crystallography and accurate kinetic data were available. It was only after the extensive application of site-directed mutagenesis to the enzyme that the catalytic mechanism was elucidated (Fersht, 1987). This work has set a precedent for a renaissance in enzymology. It is now the accepted standard for a serious investigation of an enzyme. Protein engineering has emphasised the importance of protein crystallography and has revitalised enzyme kinetics.

This thesis describes the analysis of four mutants of the tyrosyl-tRNA synthetase from *Bacillus stearothermophilus* by X-ray crystallography. At the outset of the work described in this thesis, one of the major concerns in protein engineering was whether the interpretation of the results of a site-directed mutagenesis experiment were complicated by structural changes occuring in mutant proteins beyond the replacement of an amino acid. At that time (1985), very few mutant enzymes had been analysed by X-ray crystallography. Since then, however, several crystal structures of mutants have been published. A few examples are discussed below.

A crystal structure of a thermostable mutant of subtilisin (Asn→Ser-218) has been reported (Bryan et al., 1986). This enzyme was isolated by screening random mutants at a temperature (70° C) which would inactivate wild-type subtilisin BPN'. X-ray analysis showed little change in structure apart from improved H-bond geometry between the main chain N-H of Ser-204 to the hydroxyl oxygen of Ser-218 as opposed to the native Asn carbonyl oxygen atom. In the mutant structure, the hydroxyl of Ser-218 fits in the plane of the main chain N-H of Ser-204. The fact that the side chain is shorter also allows better packing of two antiparallel β-strands which define the conformation around the mutation, shortening two intersheet hydrogen bonds by 0.16 Å and 0.1 Å respectively.

A number of crystal structures of mutant T4 lysozymes have been determined (Alber et al., 1987; Grutter et al., 1987). Mutations have been made in order to discover the contribution of particular residues to the stability of the folded state of the protein. For T4 lysozyme, the difference in free energy of folding between wild type and mutant proteins was determined by reversible thermal denaturation (Alber et al., 1987). Comparison of the wild-type and mutant crystal structures allows some interpretation of the effect of the mutation on protein

stability. A detailed study (Alber et al., 1987) of the effects of 13 different amino acid substitutions at position 157 of T4 lysozyme (Thr in wild-type enzyme) has been reported. Crystal structures and thermal denaturation/renaturation data were described in detail. Residue 157 was chosen for mutation since a temperature sensitive mutant (Thr→Ile-157) was previously isolated (Grutter et al., 1987).

As might be expected, it was found that the most stable lysozyme variants contained hydrogen bonds analogous to those in the native enzyme. Other mutants caused local changes in solvation e.g., a new water molecule occupied the cavity created by the Thr→Gly mutation, and the His, Asp and Asn mutants adopt different conformations even though they might be expected to be the most conservative of the set of 13 replacements. The temperature sensitive mutation, Thr→Ile-157, caused a reduction in stability of the protein of 2.9 kcal/mol (42° C, pH 2.0), the least stable of the set of 13 mutant enzymes. Analysis of the crystal structure shows localised changes, though the main reason for the reduction of stability is the deletion of an H-bond to the main chain N-H of Asp-159. The protein was quite tolerant to the Thr→Phe substitution; only 2.4 kcal/mol energy of stabilization was lost to the enzyme.

Further work (Matsumura et al., 1988) was directed at the determination of the hydrophobic stabilization by making a similar series of 13 substitutions at position 3. (Ile in native structure). This residue located in the interior of the protein, surrounded by the side chains of Met 6, Leu 7 and Ile 100 and the main chain of Cys 97. The residue is about 80% inaccessible to solvent (Matsumura et al., 1988). The overall conclusion of the work was that it was the degree of stabilization is proportional to the hydrophobicity of the substituted residues and that this is a function of the surface area accessible to

solvent in the folded state. Only two mutants could be crystallised; Ile→Val and Ile→Tyr. The former is almost identical to the native structure but the latter undergoes a structural rearrangement where the tyrosine rotates 120° so that it is largely exposed to solvent.

At the start of this study, the only evidence for a lack of gross structural change resulting from the mutation of the enzyme was that most of the mutants retained some catalytic activity. The original purpose of the work in this thesis was to find out to what extent, if any, structural changes had occured on the creation of a mutant enzyme. Previous work on tyrosyl-tRNA synthetase which is relevant to the mutants analysed in this thesis will be discussed.

1.1.2 Protein Engineering of Tyrosyl-tRNA Synthetase.

Tyrosyl-tRNA synthetase from *Bacillus stearothermophilus* has been cloned, sequenced and expressed in *E. coli* (Winter *et al.*, 1982 & 1983). The enzyme (Fig 1.1) is a dimer of 2 x 47316 Da, and catalyses the following reactions;

$$E + Tyr + ATP \rightleftarrows E.Tyr\text{-}AMP + PP_i \qquad (1)$$

$$E.Tyr\text{-}AMP + tRNA^{tyr} \rightarrow E + Tyr\text{-}tRNA^{tyr} + AMP \qquad (2).$$

The first reaction has been studied in detail. A stable intermediate, tyrosyl adenylate is formed on the enzyme with a stoichiometry of one mol/dimer (Fersht, 1975). Its formation and destruction on the enzyme can be monitored by stopped-flow fluorescence (Fersht *et al.*, 1975) and isotope exchange kinetics (Calendar & Berg, 1966). The tight binding of the intermediate permits accurate determination of the concentration of active enzyme by active-site

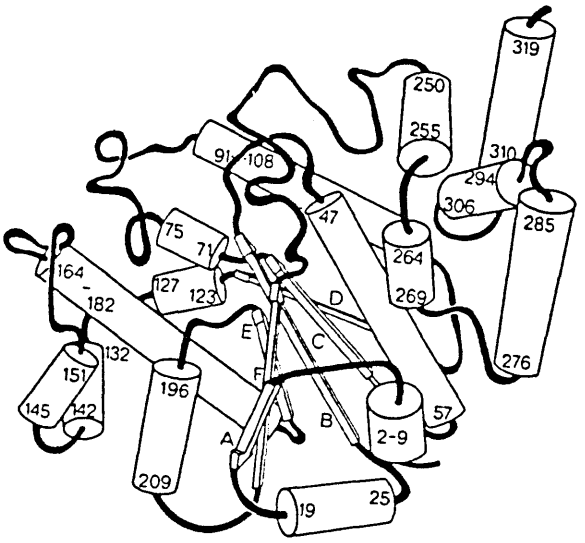


Fig 1.1 Schematic representation of the crystal structure of a monomer of tyrosyl-tRNA synthetase from *Bacillus stearothermophilus*. The ordered region, residues 1-319, is shown (from Bhat *et al.*, 1982).

titration (Fersht *et al.*, 1975). The enzyme is incubated with excess tyrosine and Mg.ATP in the presence of inorganic pyrophosphatase. The hydrolysis of PP_i promotes product formation in the equilibrium shown in eq. 1 and thus complete saturation of active sites is achieved. In the presence of radiolabelled tyrosine, collection of the complex on nitrocellulose filters allows the concentration of active sites to be assayed by liquid scintillation counting. The combination of isotope exchange and pre-steady state kinetics provides a complete determination of the rate and binding processes in eq.1. This equation can be expanded as shown (Fig 1.2).

The dissociation constants K_t, K'_a and K_{pp} and the forward and backward rate constants (k_3 and k_{-3}) through the transition state for the reaction can be measured. K_t is determined from equilibrium dialysis or isotope exchange kinetics. K'_a, K_{pp} and the rates for the formation and destruction of tyrosyl adenylate (k_3 and k_{-3}) are measured in the pre-steady state. It can be shown (Wells, 1987 chap 6) that $k_3/K'_a = k_{cat}/K_{M(ATP)}$ for the forward reaction given the kinetic scheme in Fig 1.2. The rate constant for the forward reaction, k_3 and K'_a can be determined by stopped flow fluorescence. The $k_{cat}/K_{M(ATP)}$ term can be determined by isotope exchange kinetics.

1.1.3 Crystal Structures

Crystallographic studies of tRNA synthetases which have yielded a high resolution structure will be briefly reviewed before describing those concerning the tyrosyl enzyme.

With the exception of tyrosyl-tRNA synthetase, the only other high resolution structure is that of methionyl-tRNA synthetase from *Escherichia coli* (Zelwer et al., 1982). Crystals of the glutaminyl enzyme

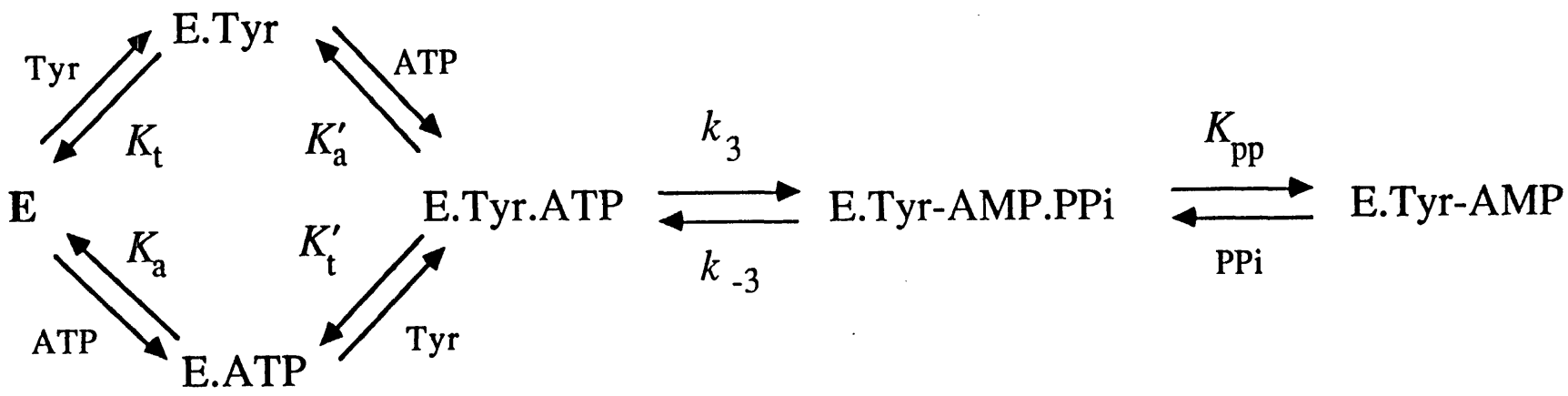


Fig 1.2 A kinetic scheme for the formation of tyrosyl adenylate (after Fersht, 1987).

complexed with its cognate tRNA (also from *E.coli*) which diffract to at least 2.8 Å resolution have been reported (Perona et al., 1988). The seryl enzyme from *E.coli* (Leberman et al., 1987) and the phenylalanyl enzyme from *Thermus thermophilus* have also been crystallised and shown to diffract to 2.8 and 2.9 Å respectively. Further work, especially the probing of the tRNA complex will have to await the determination of these structures.

Two crystal structures of tyrosyl-tRNA synthetase have been determined. The first, of the full length molecule (Bhat *et al.*, 1982) lacks the C-terminal 99 amino acids since they are disordered in the crystalline state. The space group is $P3_121$ and the crystallographic 2-fold axis is coincident with the dimer axis and the asymmetric unit is the monomer. The overall structure (Fig 1.1) is α/β. The structure has been solved at 2.1 Å resolution with R=21%. The reliability index, or R-factor is defined as the following;

$$R=\Sigma||F_o|-|F_c||/\Sigma F_o, \qquad (3)$$

where F_o is the observed structure factor amplitude for a given reflection and F_c is the value for that reflection as calculated from the model, and the summation is over all reflections.

A second crystal structure of a deletion mutant of the enzyme lacking the disordered region of the molecule has also been determined. The crystals are monoclinic space group $P2_1$, and the asymmetric unit is a dimer. This structure (Brick & Blow, 1987) has been solved at 2.5 Å with R=18.1%. The structure is very similar but not identical to that of the full length molecule. In particular, the molecular 2-fold axis is not perfect and the two subunits although very similar are not identical. The tyrosine binding site is better occupied in the truncated molecule.

1.1.4 Model of Tyrosyl Adenylate

The structure of enzyme bound tyrosyl adenylate has been revealed from crystallographic work (Rubin *et al.*, 1981). Residues thought to interact with it (Fig 1.3) have since had their role confirmed by site-directed mutagenesis and their contribution to the enhancement of rate and binding processes has been quantified (Fersht, 1987 and references therein).

1.1.5 Model of Transition-State

The catalytic mechanism of the formation of tyrosyl adenylate was postulated to involve an in-line nucleophilic substitution where the negatively charged carboxyl oxygen of the tyrosine attacks the α-phosphorus of the ATP, displacing the β-phosphorus to form pyrophosphate (Lowe & Tansley, 1984; Leatherbarrow *et al.*, 1985), (Fig 1.4). The transition state would therefore be pentacoordinate and would necessarily involve the movement of the β and γ phosphates of the bound ATP. Since it was known from kinetic data that most of the binding energy used to form tyrosyl adenylate was realised in the transition state, it was presumed that the structure of the transition state might resemble that of tyrosyl adenylate. It was, therefore, reasonable to build a model of the putative pentacoordinate transition state around the crystallographically determined structure of tyrosyl adenylate. The β and γ phosphates were attached to the α-phosphorus of the tyrosyl adenylate and a pentacoordinate species was created.

Exploration of the conformational space available to the phosphate groups suggested that the side chains of Thr-40 and His-45 hydrogen bonded to them (Fig 1.5). The kinetic analysis of the double mutant

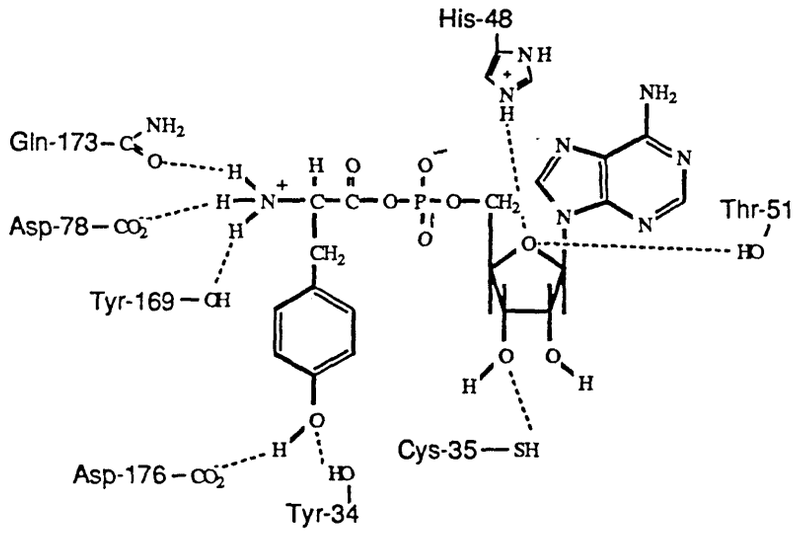


Fig 1.3 Residues believed to interact with tyrosyl adenylate in the active site of tyrosyl-tRNA synthetase (from Fersht, 1987).

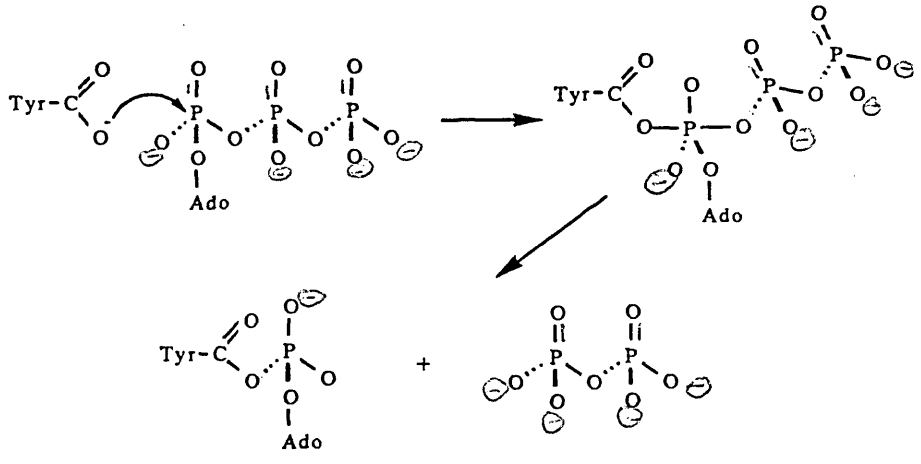


Fig 1.4 Representation of the mechanism of formation of tyrosyl adenylate as proposed (Leatherbarrow et al., 1985). Note the change in geometry around the beta and gamma phosphates.

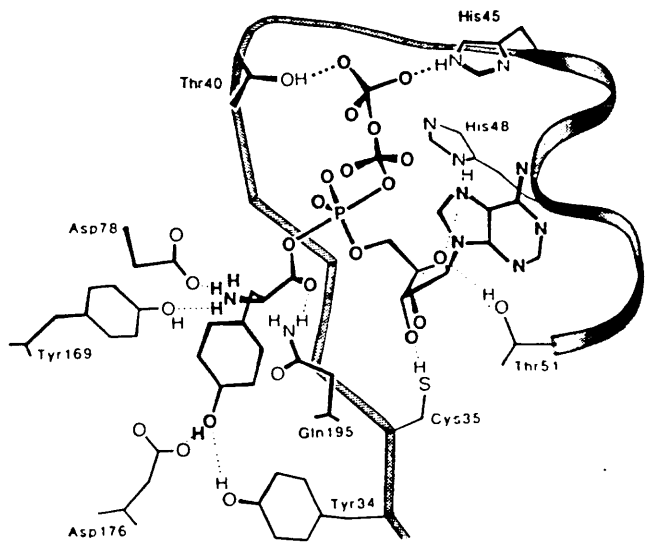


Fig 1.5 Drawing of the reaction transition state as modelled from the crystal structure of tyrosyl adenylate (reproduced from Leatherbarrow *et al.*, 1985).

Thr→Ala-40;His→Gly-45 groups gave precisely the expected results for a model based on transition-state stabilization; k_3 is lowered by 3.2 x 10^5 but K_S for ATP is raised by only a factor of 5 (Leatherbarrow *et al.*, 1985).

Recent work (Fersht *et al.*, 1988) has shown other residues to make interactions in the transition-state of the formation of tyrosyl adenylate. Protein engineering studies of residues Lys-82, Arg-86, Lys-230 and Lys-233 have shown these residues contribute several kcal/mol binding energy in the transition-state of the reaction. The ϵ-NH_3 groups of Lys-230 and Lys-233 however, are at least 8 Å away from the pyrophosphate region of the transition-state model as it was built (Leatherbarrow *et al.*, 1985) into the crystal structure of the unligated form of tyrosyl-tRNA synthetase. Binding of substrates must induce a conformational change on the enzyme which brings these residues into contact with the phosphate moiety of the reaction transition-state. The four residues lie in crystallographically disordered regions of the molecule. In particular, Lysines 230 and 233 are located in a loop comprising residues 220-240, some of which have high crystallographic temperature factors. It has been suggested (Fersht *et al.*, 1988), therefore, that this mobile loop region folds over the active-site of the enzyme during the reaction. A model of such a folded conformation is described in chapter 7.

1.1.6 The Use of Binding Energy In Catalysis.

The initial characterization of active site mutants and the implication of a penta-coordinate transition-state in the reaction were achieved using isotope exchange kinetics only, apart from the transition-state mutants described above where in some cases the rates of tyrosyl adenylate formation were so slow that the time course of an

active site titration could be followed by manual sampling of radiolabelled enzyme on to nitrocellulose filters. With this exception, no pre-steady state analysis had been performed on the mutant enzymes, yet the catalytic mechanism had been elucidated. This shows the power of steady-state analysis when pre-steady state work has proven the existence and accumulation of intermediates on the reaction pathway.

The pre-steady state experiments allow the true rate constants for individual steps in (Fig 1.2) to be measured. This permits a thermodynamic analysis of the reaction. Two equations are used to calculate the standard free energy change for each stage of the reaction;

$$\Delta G = RT\ln K_S \qquad \text{(for binding processes)} \qquad (4)$$

$$\Delta G = -RT\ln k + RT\ln(k_B.T/h) \qquad \text{(for rate processes)} \qquad (5).$$

The results of the thermodynamic analysis can be plotted as a free energy profile of the reaction (Fig 1.6). By subtracting two profiles e.g., mutant from wild type, one can produce a difference free energy diagram (Fig 1.7) which shows the apparent contribution to binding of a residue to a state in the reaction pathway (Wells *et al.*, 1986). This enzyme uses most of its binding energy to sequester tyrosyl adenylate which would otherwise diffuse out of the active site and covalently modify any other nucleophile in the cell (Wells, 1987, chap 6). The rest of the binding energy is used to bind the transition-state for the reaction and the amino acid tyrosine. Binding energy for rate enhancement must be sacrificed for the sake of substrate specificity, since the enzyme must bind the correct amino acid. Less binding energy is put into the Mg^{++}.ATP complex, since specificity is less

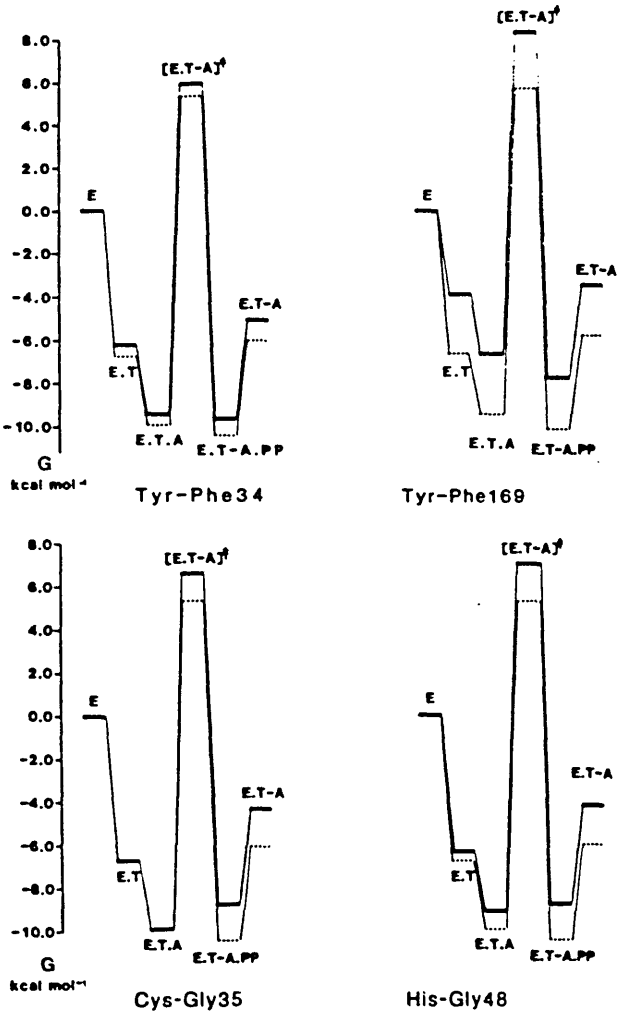


Fig 1.6 Comparison of free energy profiles for four mutant tyrosyl-tRNA synthetases with that of the wild type enzyme (from Wells & Fersht, 1986).

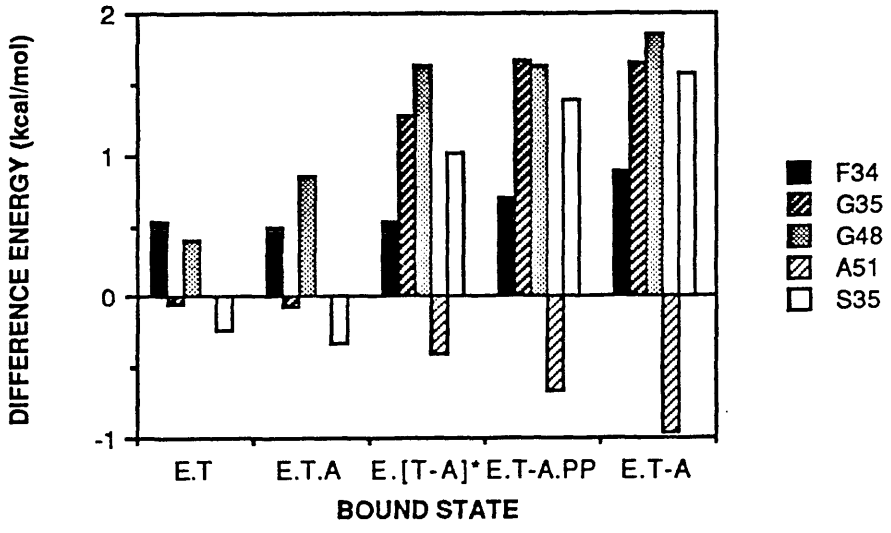


Fig 1.7 Difference free energy diagrams for several active site mutants of tyrosyl-tRNA synthetase.

important and the parameter k_{cat}/K_M can be maximised for this enzyme (since it is a two substrate reaction, $k_{cat}/K_t.K'_a$ must be optimised).

A general feature borne out by these experiments is that hydrogen bonds which have been deleted by mutagenesis are not directly involved in the chemical processes but are at some distance from the seat of the reaction; the α-phosphate. Thus catalysis or the distribution of binding energy and rate enhancement, is delocalised around the active site of the enzyme. This is probably true for all enzymes, but some residues not only contribute binding energy but are covalently modified as part of the catalytic process. Removal of these residues by site-directed mutagenesis causes a severe reduction in activity e.g., the active site serine 221 of subtilisin, which when mutated to alanine causes a drop in k_{cat} of 2×10^6 (Carter & Wells, 1987 & 1988).

1.1.7 Linear Free Energy Relationships

It is known that the modification of the nucleophilicity of a functional group e.g., the hydrolysis of various benzoic acid esters will alter its reactivity (Fersht 1985, chap 2). If the physical processes being modelled are the same in each experiment, then a plot of the natural log of the rate constant for the reaction versus the log of the equilibrium constant should be linear. This is called the Brønsted or Hammett relationship. The delocalised nature of catalysis in tyrosyl-tRNA synthetase (Fersht, 1987) has allowed a series of such systematic variations in the reactivity of mutant enzymes to be created by protein engineering. The Brønsted theory predicts that a series of mutants should fit to a single linear free-energy relationship (LFER) when comparing rate and equilibrium constants for any given step on the reaction pathway. The theory is presented below. For a given

reaction (Fersht *et al.*, 1986),

$$X \rightleftarrows Y \qquad (6)$$

the following relationship is assumed;

$$k = AK^{\beta} \qquad (7)$$

where k is the rate constant and K the equilibrium constant. Taking the natural logarithm gives

$$\log k = \text{constant} + \beta \log K. \qquad (8).$$

Transition state theory predicts that $\log k \propto \Delta G^{\neq}$ therefore

$$\Delta G^{\neq} = \text{constant} + \beta \Delta G_e. \qquad (9).$$

The physical meaning of β is given as follows; if β is close to zero then the structure of the transition-state must resemble that of the reactants; conversely, if β is close to a value of one then the transition-state must resemble the products. An example (Fersht *et al.*, 1986; Fig 1.8) for tyrosyl-tRNA synthetase is presented. A plot of log k_3 versus log k_3/k_{-3} (forward and backward rates through the transition state respectively) gives a straight line of slope β = 0.83. The reaction is the step from the Michaelis complex E.T.A to the product complex E.Tyr.AMP.PP_i. This suggests that 83% of the binding energy used to form the product complex is realised in the transition state for this reaction. It also serves to add support to the kinetic arguments made earlier that the transition-state for the formation of tyrosyl adenylate and tyrosyl adenylate itself are similar in structure.

Linear free energy relationships can be produced for any of the steps in the reaction which encompass a rate and equilibrium process

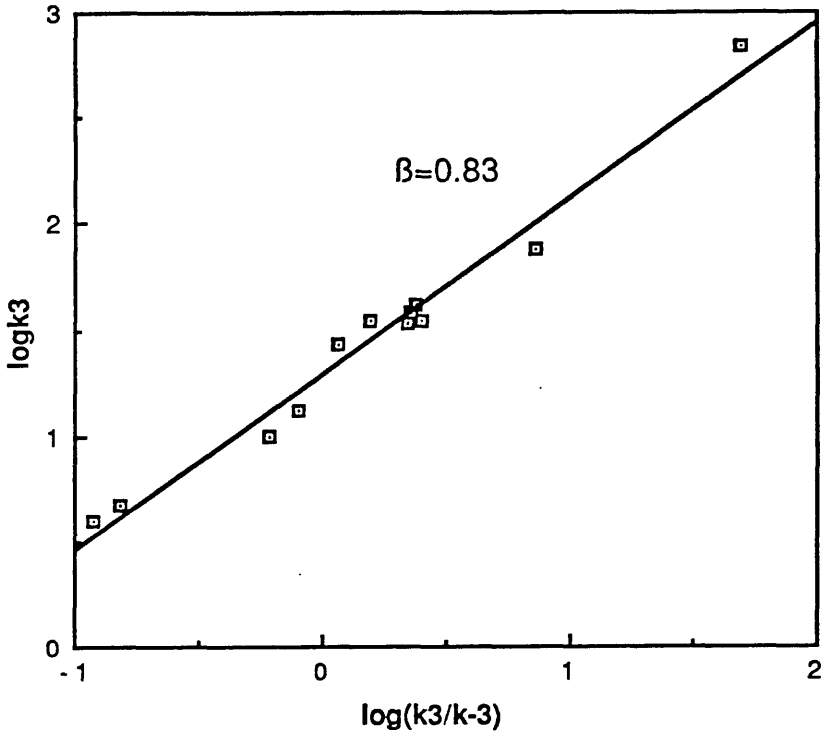


Fig 1.8 A linear free energy relationship between the binding energy utilised in the transition-state for the reaction and that of the E.Tyr-AMP.PPi complex is shown (after Fersht, 1986).

(which has been measured experimentally). The great significance for the mechanistic enzymologist is that they imply that the structure of reactants, transition-states and products are similar in structure in all mutants analysed, otherwise no such linearity would be observed. One of the major concerns of the investigators is that the structure and catalytic mechanism of mutant enzymes are not fundamentally altered by point mutations in the active site. The existence of LFERs show that structural artefacts can be ruled out unless they are of a benign nature.

1.1.8 The Double Mutant Test

A second method using protein engineering which permits the detection of discrepancies or artefacts in a mutagenesis experiment is the "double mutant" test (Carter *et al.*, 1984; Fig 1.9). Many mutants fit reasonably well on the LFER plots and produce plausible difference energy diagrams, but there is no way to check for small artefacts caused by the mutation itself. The idea is to make two (or more) mutations at residues involved in catalysis separately and together as a double mutant enzyme. If the residues are far away in space and sequence, they are likely to be independent of one another. Assuming that the mutants do not cause structural perturbations, then the kinetics of the double mutant should be equal to the sum of the single mutant data. An example where they are is with the Cys-35; His-48 pair (Fig 1.10), where the corresponding single and double point mutations to Gly produce additive kinetic data. The problem here is that structural perturbations could occur in both single and double mutations to a similar extent and both be mutually independent of one another; this may be the case in this pair of residues since crystallographic studies of the single mutants show structural changes. An example where the

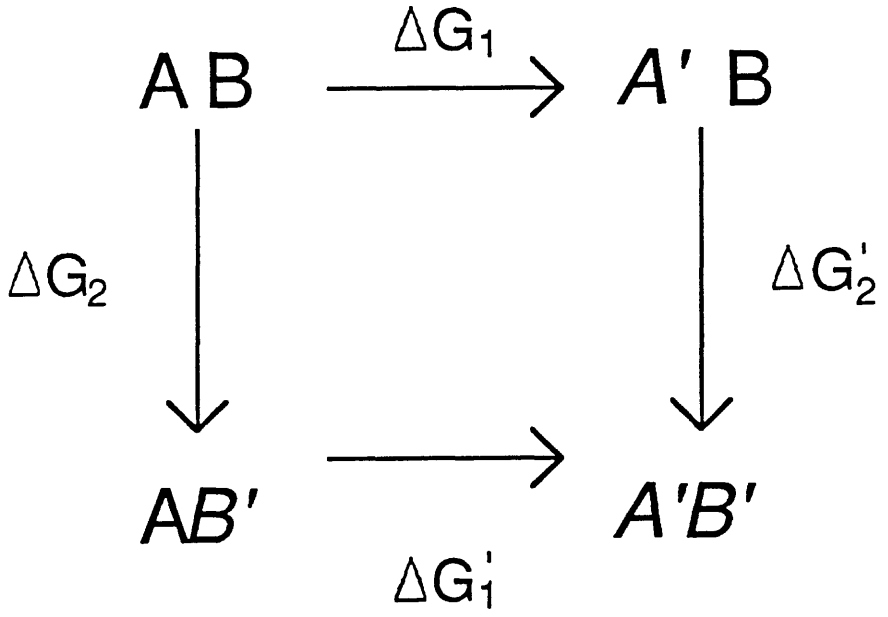


Fig 1.9 The double mutant test is designed to show whether two residues are independent of one another. If so, then $\Delta G_1 = \Delta G_1'$ and $\Delta G_2 = \Delta G_2'$ (after Carter *et al.*, 1984).

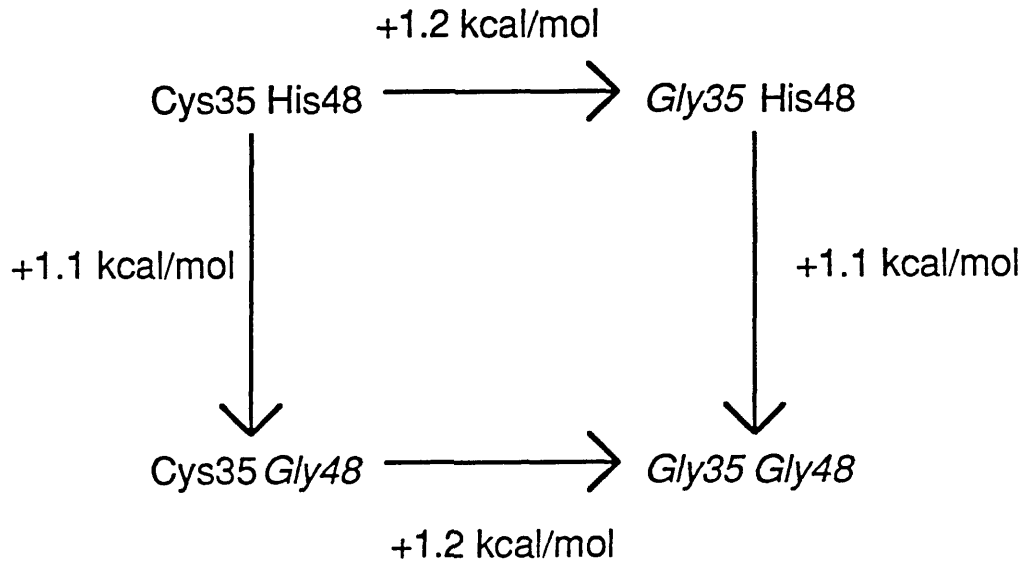


Fig 1.10 An example of a pair of additive double mutants. These are relatively far apart in sequence and space (after Carter *et al.*, 1984).

mutations are close in space (but far away in sequence) is the pair Cys-35 and Thr-51. The double mutant cycles (Fig 1.11) to Gly and Pro/Cys at positions 35 and 51 respectively show a consistent non additivity of 0.4 kcal/mol. Although the residues are close together in space and therefore might not be expected to be independent of each other, it is difficult to know whether the non-additivity is a measurement of a structural perturbation which only occurs in one set of single point mutations (e.g., Cys→Gly-35) and not in the double mutant enzymes. A further degree of complexity is possible; the His-48 Thr-51 pair. These residues are reasonably close in space and sequence. The double mutant data (Fig 1.12) are non-additive in all possible permutations of the data and to differing degrees with different mutant residues. It is clear that structural changes could occur which might be transmitted through the helical region between residues 48 and 51. Precise quantification of these effects requires X-ray crystallography. Work on His→Gly-48 (Brown, 1988) shows structural perturbations that affect residue 51. This concurs with the above data from the double mutant test which suggest the residues are not independent. Crystallographic work on Cys→Gly-35 shows an alteration in structure affecting position 51 which is an artefact of the amino acid replacement. This discussed is in chapter 4.

In summary, although the double mutant test is more sensitive than an LFER it becomes most powerful when combined with crystallography.

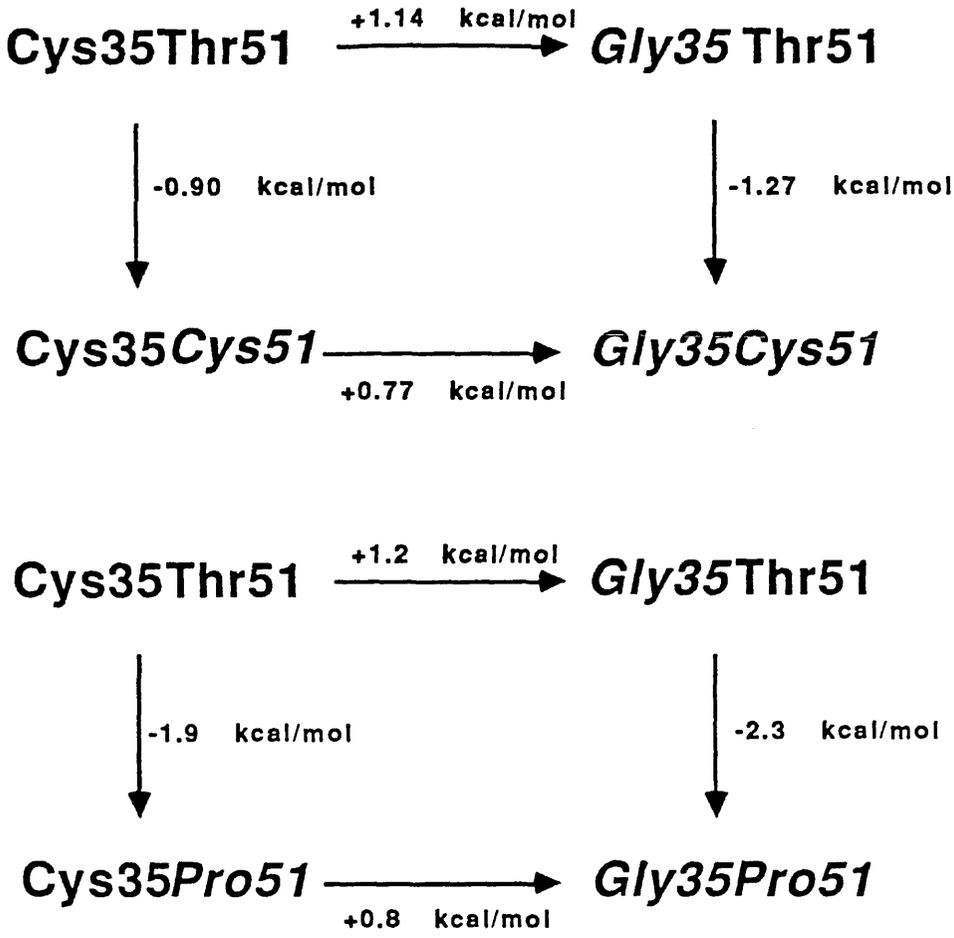


Fig 1.11 An example of non-additive double mutants which are far apart in sequence, but close together in space (after Carter *et al.*, 1984 and Fersht *et al.*, 1985).

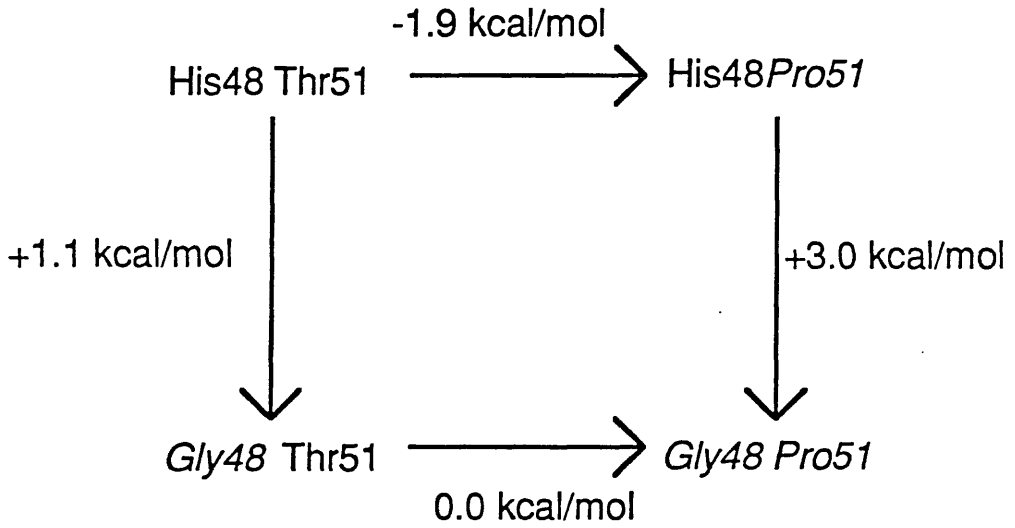


Fig 1.12 An example of non-additive double mutants which are close together in sequence and space (after Carter *et al.*, 1984).

1.1.9 Hydrogen Bonding

One must consider the relationship between the true or theoretical hydrogen bond energies and the apparent values obtained from the mutagenesis experiment. Otherwise interpretation of the experimental data will be difficult. The simplest case, the deletion of an uncharged donor or acceptor will be analysed. The formulation of Jencks and Hine (Fersht, *et al.*, 1985) can be applied to the system as follows;

$$E\text{-}H\cdot\cdot OH_2 + HOH\cdot\cdot B\text{-}S = E\text{-}H\cdot\cdot B\text{-}S + HOH\cdot\cdot OH_2 \quad (10)$$

$$E\ HOH\cdot\cdot OH_2 + HOH\cdot\cdot B\text{-}S = E\ HOH\cdot\cdot B\text{-}S + HOH\cdot\cdot OH_2 \quad (11)$$

where equation (11) represents the mutant and (10) the native enzyme. The donor and acceptor species are uncharged in these equilibria, and they make similar types of hydrogen bond pairs on either side of the equations in both cases. The energies of these interactions are also of similar magnitude and will tend to cancel out. Subtraction of equation (11) from (10) will leave (10) unchanged as the acceptor species remains solvated in (11). It is assumed water associated with the enzyme does not make any unfavourable interactions with the enzyme in this case. ΔG_{app}, the apparent binding energy measured in a mutagenesis experiment of this specific type will correspond to the free energy change occuring in equation (10). Equation (10) represents the free energy of transfer of the donor on the enzyme and the acceptor on the substrate from water to their binding environment, or ΔG_{bind} (Fersht, 1988). A central aim of the protein engineering experiments carried out in this laboratory was to measure this quantity. The experimentally determined strengths of hydrogen bonds between uncharged donor and acceptor groups are in the range 0.5-1.8 kcal/mol (Fersht, 1988). (The kinetic properties of the enzyme permit interaction

energies quoted can be measured to within +/- 0.1 kcal/mol.)

In the mutant enzyme, it is also possible that no water binds in the region of the protein vacated by the side chain deletion. Here, one would be measuring the energy of creation of an unpaired donor or acceptor on the substrate rather than the above formal definition of the hydrogen bonding group binding energy, ΔG_{bind}. The only way to distinguish between these two cases is by crystallographic analysis of the mutant enzyme substrate complex. An example, the mutant Tyr→Phe-34, is described in chapter 4.

Purification of Mutant Enzymes

2.1.1 Choice of *E. coli* Strain for Enzyme Expression.

The gene coding for the tyrosyl-tRNA synthetase from *Bacillus stearothermophilus* has been cloned, expressed (Winter *et al.*, 1982) and sequenced (Winter *et al.*, 1983). The vector, M13 (Messing, 1983) is a filamentous phage which requires the F-pilus to be present in the host *E. coli* strain for transfection. The purification of tyrosyl-tRNA synthetase as described in Lowe *et al.*, 1985 has been altered by the introduction of kanamycin selection for the maintenance of F-pilus infection in cultures of *E. coli.* In order to improve yields for crystallization the *E. coli* strain HB101F (Russel *et al.*, 1986) was employed. This strain carries an F-pilus which confers kanamycin resistance on the cells. By adding kanamycin (described below in detail) to the cultures of HB101F at all stages in the preparation procedure, the constant presence of the F-pilus was ensured. This resulted in improved yields (e.g., 100 mg/L c.f. 5-10 mg/L using *E.coli* JM101 for the expression of truncated Tyr→Phe-34). The JM101 strain (Messing, 1983) will only retain the F-pilus when grown on minimal media. This is because this particular strain of *E. coli* lacks the ability to synthesise proline from simple precursors, and this facility is conferred upon it by the F-pilus which carries the Pro^+ marker. The media used for enzyme preparations, TY broth, contains excess amino acids, including proline. Thus there was no longer any selection for the retention of the F-pilus.

2.1.2 Purification Procedure

Plaque Purification.

An overnight culture of HB101F was grown by inoculation of 5ml of sterile 2xTY broth containing 50 μg/ml kanamycin with a single colony taken from a kanamycin H-plate (also 50 μg/ml) and agitating the medium for 12 hours at 37°C. Stocks of M13 encoding the mutant tyrosyl-tRNA synthetase proteins were diluted serially in sterile water to encompass a range of 10^2-10^4 pfu/ml. 100μL of each dilution was mixed with 200μL of an overnight culture of HB101F. The resulting material was mixed with 3 ml of molten H-top agar (42°C) and plated out on kanamycin H-plates and incubated overnight at 37°C. Plates containing 50-200 plaques were used when picking plaques for over-expression. About 20-30 plaques were picked with sterile toothpicks and used to inoculate 5ml of a 1:100 dilution of overnight HB101F containing 50 μg/ml kanamycin. The resulting cultures were grown for 5 hours in an orbital shaker (New Brunswick Scientific) at 37°C, with vigorous aeration (300 rpm). Each cloned culture was spun down for 10 minutes in a bench top centrifuge at about 3000 rpm. The supernatant phage were decanted into sterile 25 ml universals (Sterilin) and stored at 4°C. The cell pellets were vortexed in 300 μL of 10 mM Tris-HCl pH 7.78, 1 mM EDTA, 5 mM β-mercaptoethanol and 0.1 mM PMSF. The suspended pellets were sonicated for 30 seconds using a small (2 mm tip) probe using a Heat Systems Ultrasonics sonicator, and heated to 56°C for 30 mins to denature the majority of host proteins, including proteases. Strains and media used in this thesis are detailed in Appendix D.

In order to check the degree of expression of tyrosyl-tRNA synthetase, the sonicated material for each clone was analysed by SDS-polyacrylamide gel electrophoresis, against a purified standard.

Clones which gave good expression were selected for large scale culture.

2.1.3 Preparation of 2L Culture

A hundred fold dilution of an overnight culture of HB101F was prepared as follows; 1 ml of bacteria was added to 100 ml sterile 2xTY broth containing 50 μg/ml kanamycin. After about an hour of agitation in an orbital shaker (300 rpm) at 37°C, 5 ml of phage was added to the culture. Next morning, the cells were spun down, checked for continuing over-expression of tyrosyl-tRNA synthetase as previously described and the resulting phage supernatant was used for inoculation of the large scale culture. A second overnight culture of HB101F was diluted 500 fold as follows; 1 ml of cells was added in turn to four 2 L flasks each containing 500 ml of sterile 2xTY broth and 50 μg/ml kanamycin. The resulting culture was grown for 2-3 hours at 37°C in an orbital shaker and then each flask was inoculated with 10ml of phage from the previous 100 ml culture. The culture was incubated overnight in an orbital shaker (300 rpm) at 37°C.

2.1.4 Cell Harvesting and Lysis

After overnight incubation, the culture was spun down in 6x500ml bottles (Sorvall GS-3 rotor) at 8000 r.p.m. for 20 min at 4°C. The pellets were resuspended in 50 ml of 10 mM Tris-HCl pH 7.78, 1 mM EDTA.Na_2, 0.1 mM PMSF, 10 mM 2-mercaptoethanol and sonicated for 2 mins using a 10 mm probe. The resulting lysate was heated to 56°C in a water bath for 30 mins and then spun down at 18000 r.p.m. (Sorvall SS-34 rotor) for 30 mins at 4°C to pellet cell debris.

2.1.5 Ammonium Sulphate Precipitation

Solid ammonium sulphate (enzyme grade, Sigma) was slowly added to the lysate while stirring it at 4° C to create a 70% saturated solution (0.434 g/ml). After 30 minutes the salt had dissolved and the precipitate was pelleted by centrifugation at 20000 rpm for 30 mins at 4° C in the Sorvall SS-34 rotor. The supernatant was decanted and discarded, and the resulting material resuspended in the FPLC start buffer (20 mM Bis-Tris-HCl pH 6.0, 5 mM 2-mercaptoethanol, 0.1 mM PMSF) and dialysed overnight against 2 L of the same buffer.

2.1.6 Ion-exchange Chromatography

The mono-Q 10/10 Fast Protein Liquid Chromatography column (Pharmacia, Uppsala) column was pre-equilibrated in 20 mM Bis-Tris-HCl pH 6.0, 5 mM 2-mercaptoethanol, 0.1 mM PMSF. The ammonium sulphate dialysate was loaded into a 10 ml superloop through a 2.5 cm 0.22 micron Durapore filter in a Swinnex filtration unit. The protein was then pumped on to the column and washed at 2 ml/min with the above buffer until all unbound material had been eluted. A gradient of 50-400 mM NaCl, 20 mM Bistris buffer was then applied to the column at 1 ml/min over a 40 min period. The protein eluted at a concentration of 250 mM NaCl. After washing several column volumes of 1 M NaCl through the column it was re-equilibrated in 20 mM Tris-HCl pH 7.78, 5 mM 2-ME, 0.1 mM PMSF. The sample was diluted 1:3 with the new buffer and the whole process was repeated at pH 7.78. The protein eluted at a concentration of abou 330 mM NaCl. It was found that two cycles of FPLC purification resulted in protein pure enough for crystallisation. Yields varied between different

mutants from about 10 mg/L (Thr→Cys-51) to 100 mg/L (truncated Tyr→Phe-34) of cell culture.

2.1.7 Enzyme Assays

Column fractions and samples for crystallization were all assayed by active-site titration. For the chromatography, accuracy was not important and a typical enzyme assay was performed as follows; 5 μl of a fraction was mixed with 20 μl of active-site cocktail (2 mM Mg.ATP/10 μM [^{14}C] tyrosine (500 mCi/mmol)/unit/ml inorganic pyrophosphatase (Sigma) in 144 mM Tris-HCl buffer, pH 7.78, 10 mM $MgCl_2$ and 0.1 mM PMSF). The sample was left at room temperature for about 1 min in order to allow the enzyme bound tyrosyl adenylate to form. In solution, the enzyme forms 1 mol of bound tyrosyl adenylate per dimer under these conditions. The radioactively-labelled enzyme-bound intermediate was trapped by vacuum filtration through a nitrocellulose filter (0.22 μm pore 2.5 cm diameter, Sartorius). Filters were washed with dilute Tris-HCl pH 7.78 before use. After drying, the filters were scintillation counted using PPO/POPOP as the scintillant. The specific activity of ^{14}C tyrosine in the assay was obtained from a standard sample applied directly to the nitrocellulose. From this the active site titre of the enzyme could be obtained.

2.1.8 SDS-Polyacrylamide Gel Electrophoresis.

Protein samples (ca. 10 μg) from each stage of the preparation were prepared for SDS-gel electrophoresis (Laemmli, 1970) by adding an equal proportion of buffer contain 10 mM Tris-Bicine pH 8.5, 25% glycerol, 0.02% bromophenol blue, 2% SDS and 10% 2-mercaptoethanol. Typically, 10 μL of sample and 10 μL of sample buffer were mixed

and heated in a hot block at 100°C for 2 mins. The samples and standards were then loaded on to a 10% polyacrylamide gel (83 x 65 x 2 mm). The gel mix contained 10% acrylamide, 0.3% bis-acrylamide and 0.1% sodium dodecyl sulphate (SDS) in 0.1 M glycine buffer pH 9.0. The polymerisation reaction was started by adding a few granules of solid ammonium persulphate and tetramethyl-ethylenediamine (TEMED) to 0.25%. The running buffer consisted of 0.1 M glycine buffer, pH 9.0, and 0.1% SDS. The samples were loaded into the gel (typically 5 μL) and a constant 40 V potential difference was applied until the bromophenol blue marker entered the gel. Then the voltage was increased to 75 V until the marker reached the bottom of the gel.

Gels were stained using 0.3% Coomassie blue (R) stain dissolved in 50:40:10 methanol:water:acetic acid for 30 minutes. Destaining consisted of two 30 minute washes in 50:40:10 methanol:water:acetic acid and then overnight in 10% aq. acetic acid. A representative gel of an enzyme purification is shown (Fig 2.1). It shows the enzyme has been purified to over 95% of total protein.

2.1.9 Optimization of Enzyme Expression

A 2 litre preparation of tyrosyl-tRNA synthetase typically produces 20 mg of purified protein. While this degree of expression is adequate for crystallization experiments, often, however, clones were obtained which gave low to negligible yields. There were two reasons for this. The first was the problem of selection against the F', which was solved by the introduction of HB101F described above. The second is the problem of achieving a suitably high multiplicity of infection.

In order to achieve complete infection of a culture by M13, it must not only be 100% F^+, but there must be an excess of phage over bacteria of about 100:1 (multiplicity of infection). In a plaque

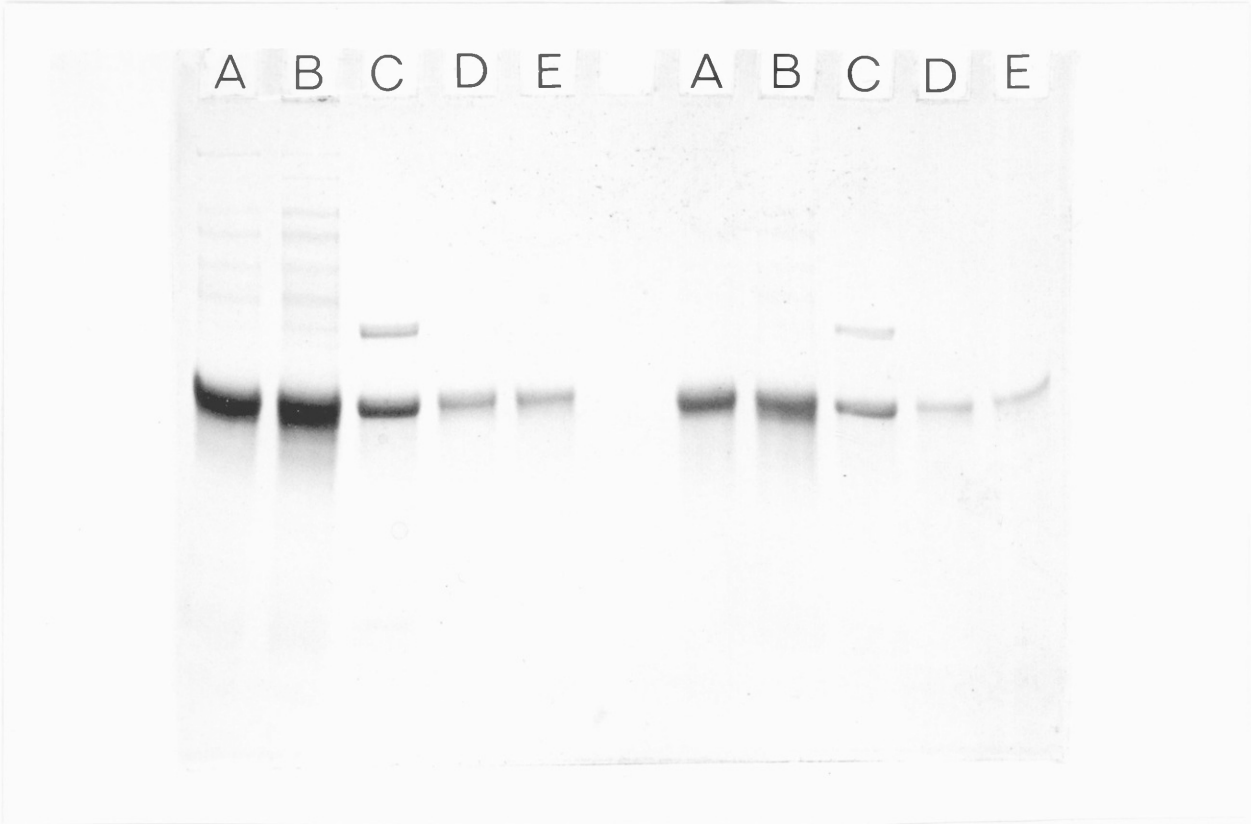


Fig 2.1 Typical SDS-polyacrylamide gel of a preparation of tyrosyl-tRNA synthetase. Lanes A to E are as follows; A; cell lysate after heat treatment (56° C, 30 mins); B; same material after 70% ammonium sulphate cut; C; FPLC purification, pH 6.0; D; FPLC purification, pH 7.78; E; standard. The mutant is Tyr→Phe-34.

purification procedure, the expected titre of phage (plaque forming units) is about 10^{14}/ml. In a typical preparation, an overnight culture of HB101F is diluted 1:100 in sterile 2xTY broth and grown for 3-4 hours in an orbital shaker (300 rpm), at 37°C. At this point the cells will be in log phase and are most readily transfected by M13. Phage are usually added to the culture at a dilution of 1:100. If the phage titre is about 10^{14} pfu/ml this will result in a final concentration of approximately 10^{12}/ml. The titre of an overnight HB101F culture varies depending on the aeration of the flask. In a 20 ml universal, an A_{660nm} of about 8 is reached overnight. This corresponds to about 10^8 cells/ml. Therefore the excess of phage over bacteria will be greater than 10^4 for a log phase culture.

In practice, when JM101 was still being used, a small sub-culture of cells were grown to log phase in a universal and then inoculated with a 1:100 dilution of phage and incubated for 30 mins. The resulting material (5ml) was distributed between four 2 litre flasks each containing 500ml of 2xTY broth. The flasks were then agitated overnight in an orbital shaker (300 rpm) at 37°C. Cells were then harvested, lysed and run out on a gel. Even when the total yields of protein were reasonable (5mg/L) the gels of culture lysates showed worse over expression than the original plaque purification gels. An example was the truncated mutant Tyr→Phe-34. Plaque purification in either TG2 or JM101 resulted in poor over-expression on protein gels. Even after screening 60 different clones, none showed very good over-expression, and when 2 litre preparations were carried out the yields of protein were often poor. The introduction of HB101F at the plaque purification stage, however, enhanced both the apparent over-expression on gels and the yield of mutant protein (yields increased from about 5 mg/L to 10 mg/L).

The largest increase in over-expression occured, however, when the

preparation was fortuitously carried out with a minor short cut. In this experiment, 5 ml of phage supernatant from an over-expressing clone was added to 500 ml 2xTY broth containing 50 μg/ml kanamycin and a 5 ml overnight culture of HB101F. No sub-culture was used, and the cells were not grown to log phase before inoculation with phage. The result of this was that the excess of phage over cells was at least 10^3 fold higher than usual. Assuming a phage titre of 10^{14}, one would expect no difference in M13 infection and degree of over-expression. The fact that the 500 ml culture was not grown to log phase before infection with M13 meant that one would expect the cell pellets to be smaller after an overnight culture, as the infection with M13 slows down cell growth. This was indeed the case with the Tyr→Phe-34 preparation, but not markedly. When the cells were lysed and run on a gel, however, it was immediately apparent that the levels of expression obtained were identical to that observed in the plaque purification. The resulting yield was about 100 mg of protein. For this mutant, the improvement was at least 10 fold, from about 10 mg/L to 100-200 mg/L in subsequent preparations repeated in this way.

The only logical explanation for this is that the phage titres must have been abnormally low. This was verified by serial dilution and plaque assay of the phage supernatant inoculum. The titre was found to be about 10^{11}, about 10^3 fold lower than the literature estimates for M13 yields. The reason for this is not clear. One possibility is that the better over-expression of tyrosyl-tRNA synthetase significantly competes with expression of phage proteins and nucleic acid metabolism. Scaling up the preparation in a fermenter requires large amounts of phage (50 ml), but gives identical results.

The mutant Thr→Cys-51 was prepared using this method, however the overall increase in expression was only twofold; from about 5 mg/L to 10 mg/L, but the prep became very reliable. This lower expression

was probably due to the fact that this mutant was made using a version of M13 where upstream control sequences had been deleted from the genetic construct (G. Winter, unpublished; J. W. Knill-Jones, personal communication). Further work to improve yields would require investigation of the time course of tyrosyl-tRNA synthetase expression and the optimum cell density at which to inoculate a culture with phage. The preparation is always grown overnight - this may infact be unnecessary or even deleterious because of cell death. In a typical preparation, the A_{660nm} of the culture barely doubles overnight. Cell growth is retarded by phage infection. This suggests that the best yields will result from a complete infection of the highest possible log phase cell density. The degree of aeration of a culture determines the maximum cell density at which growth remains exponential. Therefore, since a fermenter is designed to achieve good aeration, a series of inoculations of cultures should be carried out at varying cell densities (as measured by the A_{660nm}), and the resulting final cell densities and yields of tyrosyl-tRNA synthetase should be quantitated. Optimization of these two parameters should give the most convenient conditions for a preparation to produce a good yield of mutant protein.

2.2.1 Crystallization

Crystals of tyrosyl-tRNA synthetase from *Bacillus stearothermophilus* were first grown (Irwin *et al.*, 1976) by vapour diffusion from 50% ammonium sulphate in the presence of Tris acetate pH 7.3 and 10 mM $MgCl_2$, using the hanging drop method (McPherson *et al.*, 1982). They are trigonal with cell dimensions a=b=64.5 Å, c=238 Å, $\alpha=\beta=90^\circ$ and $\gamma=120^\circ$. The space group is $P3_121$ and they diffract to about 2 Å resolution. The external morphology is a hexagonal prism and will be termed the hexagonal plate form. Tetragonal bipyramids can also be grown under these conditions but they have never been shown to diffract X-rays. Crystals of the truncated enzyme (Winter *et al.*, 1983) have been grown (Brick *et al.*, 1987) from polyethylene glycol (PEG). They are monoclinic with space group $P2_1$ and cell dimensions a=95.5 Å, b=67.1 Å, c=61.4 Å, $\alpha=90.0^\circ$, $\beta=90.78^\circ$ and $\gamma=90.0^\circ$. The conditions for crystallization are 12% PEG (4K), 100 mM Tris-acetate pH 7.3, 10 mM $MgCl_2$ mixed 1:1 with protein (usually 10 mg/ml in 100 mM Tris-Ac pH 7.3) in the drop and 12% PEG in the well.

2.2.2 Crystallization of Mutant Enzymes

The three full length mutants of tyrosyl-tRNA synthetase and the single truncated mutant were all crystallised under the same conditions as the native enzymes. Tyrosine (1 mM) was added to all trials with full length enzymes, since it has been found that crystal growth of the hexagonal plate form is enhanced in the presence of substrate. Saturating tyrosine was also added to the truncated enzyme. Protein was purified as described above and concentrated using Centricon 30 disposable membranes which have a 30,000 Mwt. threshold. This also allowed buffer exchange from the preparative Tris-HCl pH 7.78 buffer

to crystallisation buffer (100 mM Tris-acetate pH 7.3). The relationship between A_{280nm} and concentration of active sites for pure enzyme has been calculated (Fersht *et al.*, 1975) to be 1 mg/ml=1.39 OD units. Prior to crystallisation, the enzyme was concentrated to at least 10 mg/ml as determined by both active-site titration and A_{280}, using a Centricon 30 centrifugal concentrator (Amicon). Crystals produced were always isomorphous with respect to the native form with one exception, described below.

Attempts to diffuse tyrosyl adenylate into crystals by soaking hexagonal plates in the presence of tyrosine and ATP result in cracked crystals. It was reported (Rubin *et al.*, 1981) that crystals soaked in the presence of saturating tyrosine and 12 mM ATP cracked and then reannealed over a 14 day soak. No such reannealing was ever observed with mutants. Mutant enzymes described in this thesis were co-crystallised with ATP and tyrosine in order to circumvent the cracking phenomenon. Typical conditions for crystallisation were; 50% ammonium sulphate, 100 mM Tris-acetate pH 7.3, 10 mM $MgCl_2$, 1 mM tyrosine and 10 mM Mg.ATP. This experiment had never been tried before and the result was a hexagonal bipyramid form, with both mutant and eventually wild-type enzymes. Unlike the small crystals produced previously large (200 μm edges) flattened ellipsoids were produced with ill-defined edges. Attempts to collect a full data set on these crystals has been hampered by the fact that they are unstable in the X-ray beam.

Co-crystallisation experiments performed with mutants at 4°C occasionally resulted in the previously reported hexagonal plate form. A complete set of reflection data was collected for a co-crystal of the mutant Cys→Gly-35 and its analysis is described in chapter 3. The crystallisation conditions of the mutants described in this thesis are tabulated in Appendix A.

2.2.3 Crystal Mounting and Data Collection

Hexagonal Plates

The hexagonal plate form was harvested into 55% ammonium sulphate, Tris-acetate pH 7.3, 10 mM $MgCl_2$, tyrosine (1 mM) and/or ATP (10 mM). Crystals were mounted in 1mm glass capillary tubes upright on a plate face normal to the hexagonal face. The crystallographic c-axis is parallel to the six-fold axis apparent in the external morphology. The Laue symmetry ($P3_121$) is such that a 30° rotation around the c-axis will constitute a unique data set. Because the c-axis is long (238 Å), its associated reciprocal lattice spacings will be small. Hence oscillation about this axis will allow a greater number of reflections to be measured on a single film without significant overlap. This, in combination with the symmetry, means that a unique set of reflection data can be collected economically for this unit cell, using only 14 consecutive film packs at 2.5 Å resolution. The oscillation range used was 2.5° and this includes two extra film packs which ensure that the unique region is completely encompassed given that orientation of the crystal is not accurately determined until after the experiment.

2.2.4 Truncated Monoclinic Form

Crystals were harvested into 14% PEG (4K), 100 mM Tris-acetate pH 7.3, 2 mM tyrosine, 10 mM $MgCl_2$. They were mounted so that at phi=0°, the X-rays were parallel to the crystallographic 2-fold. Since they are monoclinic, at least 90° of unique data must be collected. This was achieved by rotating about the normal to the crystallographic 2-fold.

2.3.1 Synchrotron Radiation

All oscillation data were collected on flat films at the SRS facility at Daresbury. Each cassette contained 3 films, allowing the full dynamic range of diffracted intensities to be recorded. A pair of aluminium foils were used to attenuate the 0.88 Å data sets, abutting the A and B / B and C films respectively in each pack. Wavelengths of 0.88 Å and 1.488 Å were used for different sets of data (see Appendix A). The data were recorded with an Arndt-Wonnacott oscillation camera (Enraf Nonius, Delft) using CEA Reflex 25 film on flat cassettes. Crystals were cooled to about -5°C with the exception of the truncated form (4°C). The synchrotron source consists of a linear accelerator coupled to powerful electromagnets arranged in a ring. When electrons are injected into the ring and accelerated to 2 GeV they give off a broad spectrum of X-rays. The correct positioning of the ports in combination with the use of monochromators allows a particular wavelength suitable for protein crystallography to be sampled. Furthermore, a localised powerful magnetic field can be used to distort the flow of electrons and alter the wavelength of the X-rays. The 0.88 Å source is produced by this method.

2.3.2 Film Measurement

The CCP4 suite of programs was used. Many of the programs originated in the MRC Laboratory of Molecular Biology at Cambridge. A brief description of the strategy of film processing and software is given below.

2.3.3 Densitometry

All films were scanned and digitised using a Scandig microdensitometer (Joyce Loebl). The raster step size was 50 μm and the optical density range 0.0 to 2.0 units.

2.3.4 Orientation

In order to correctly index and accurately measure a series of contiguous films, one must know the orientation of the of the crystal (degrees) and the unit cell dimensions (Å) to better than one part in a hundred. Otherwise the classification and summation of partial reflections will not be possible. Even if misindexing does not occur, many reflections will simply not be predicted. To determine the cell parameters and orientation, still photographs were taken at 0 and 90° from the start of the oscillation experiment. The film image files were searched for fiducial spots and the direct beam which act as reference markers. Spots suitable for the refinement procedure were selected. An initial estimate of the misorientation angles (measured manually from the stills), cell parameters and wavelength was used to predict and index strong spots in the central region of the film. The deviations between observed and calculated spot positions were minimised and the cell parameters and orientation were refined using a least squares procedure (Nyborg & Wonnacott, 1977 Chap 8). The process was repeated until greater than 90% of the spots on both films were indexed and the refinement converged. The precision varied considerably between data collected from different crystals and is tabulated in Appendix A. With good crystals it is possible to achieve an error in orientation and cell dimensions of less than one part in a

hundred. The cell dimensions for different mutants are almost identical to that of the wild type (a=b=64.5 Å, c=238.0 Å, $\alpha=\beta=90^\circ$ and $\gamma=120^\circ$). They deviate by about one part in two hundred. Accurate determination of the orientation parameters is therefore paramount at the outset of the film measurement procedure. The post-refinement process (described further on) ensures that the cell parameters and orientation are continuously monitored during the oscillation experiment, and with good crystals it will refine them to an error of a few parts in a thousand.

2.3.5 Oscillation

The positions and indices of reflections appearing on oscillation films was predicted using the cell parameters and orientation data. A suitable oscillation range was chosen to minimise the number of overlapping reflections. Mosaic spread was modelled either isotropically or with separate vertical and horizontal components as directed by the post-refinement process described later.

2.3.6 Measurement Of Oscillation Data

The data were measured using the program MOSFLM (first described by Nyborg & Wonnacott, 1977 and subsequently; Leslie, 1987), after several changes such as the introduction of profile fitting for the measurement of reflection intensities. Each film image contained the A, B and C films for one cassette. The refined cell parameters and crystal orientation determined by the analysis of the still photographs were used to predict the spot positions and indices of reflections appearing on oscillation films. Fiducial marks and optionally the direct beam itself were used to refine the film/drum coordinate

transformation. In the ideal case, the cassette would be perpendicular to and centred on the X-ray. In practice, however, the cassettes are slightly misaligned. Parameters defining the deviation from perpendicularity and are refined in successive cycles of a least-squares algorithm starting from the central area of the film and proceeding outward radially to the edges of the film. These parameters are stored and used as input for the measurement of the B and C films. Strong spots are searched out and used for the final refinement of the transformation. The program always measures the A films first (closest to the X-ray beam). Typically four consecutive film packs were scanned and their respective A films were manually fitted and then four film packs were processed in batch mode on a VAX 750. Profile fitting was used for all data sets.

2.3.7 Postrefinement

After processing the first two A films, common partial reflections were used to refine the cell parameters and orientation matrix of the crystal during the rotation experiment. If these parameters differed significantly from the estimates taken from still photographs then the spot positions and indices were predicted again and the film measurement process repeated. This was repeated until postrefinement showed no change in cell parameters and orientation. Then four consecutive packs were processed using these cell and orientation parameters. Postrefinement analysis was carried out between packs 1 and 2, 2 and 3 and 3 and 4 in order to check for crystal slippage. If no significant slippage was found, then the next four film packs were analysed using the cell and orientation parameters from the postrefinement analysis of packs 3 and 4. Postrefinement analysis was carried out between each set of four e.g., 4 and 5, 8 and 9, 12 and 13

as well as within each batch in order to check that the pattern was not predicted over too great an oscillation range given the experimentally determined degree of crystal slippage. In the truncated data analysis, slippage was such a problem that prediction was only accurate over two packs.

2.3.8 Reduction of Data

Intra-pack scaling (between the A, B and C films of a pack) and averaging of scaled measurements was performed after correcting for obliquity and film absorption. The scaled reflection data were averaged and their standard deviations calculated. Corrections for Lorentz, polarization and transmission effects were applied. The agreement between symmetry related reflections (if present on a film pack) was monitored. This proved to be very useful for reflection data collected on the full length enzyme since the symmetry related reflections are only found when the films are indexed correctly. The separation of reflections on these films, with a rotation axis dimension of 238 Å (c-axis) was of the order of 50 μm along the c*-axis at 2.5 Å resolution. The effect of this was that it was difficult to align the 'l' indices. Occasionally, misindexing occured and was detected by analysis of the symmetry related reflections. The 'l' indices of reflections were permuted accordingly and satisfactory agreement between symmetry related reflections was obtained. Scaling between packs and over the complete data set was achieved using the algorithm of Fox & Holmes (1966). The results of film measurement and data reduction of the mutants described in this thesis is tabulated in Appendix A.

2.4.1 Electron Density Maps

Initial electron density maps were computed using structure factor amplitudes from the mutant and native datasets and phases calculated from the current model available in this laborarory of tyrosyl-tRNA synthetase (R-factor 21%, 2.1 Å resolution, truncated enzyme R-factor 18%, 2.5 Å resolution (Brick & Blow, 1987)). Typically, two electron density maps, (F_{mut}-F_{wt} , α_{wt}) and ($3F_{mut}$-$2F_{wt}$) α_{wt}) were calculated for each mutant and displayed using the program FRODO (Jones, 1985) with the wild type model. After modelling the mutation and subsequent refinement with PROLSQ (Hendrickson, 1985), further maps (F_o-F_c, α_{calc}) and ($3F_o$-$2F_c$, α_{calc}) were calculated. Electron density maps were computed using the CCP4 protein crystallography package.

2.4.2 Refinement of Structures

The mutant structures were refined using the least-squares algorithm PROLSQ (Hendrickson, 1985). The use of linear regression requires that the number of observational equations exceeds the number of parameters which have to be refined, and further conditions must be found under which the equations describing the function to be minimised behave in a linear fashion. The structure factor equation;

$$F_{(hkl)} = \Sigma\, f_n.\exp 2\pi i(hx_n+ky_n+lz_n)$$

is not linear. A linear approximation however, can be derived using a Taylor expansion. This approximation is only accurate for small shifts in parameter values. For the purposes of crystallographic refinement by the method of least-squares, it is therefore necessary to compute partial derivatives and hence shifts for the parameters in the structure factor equations in a cyclical process. Large shifts would

result in convergence to a false minimum. The overall aim is to minimise the sum of the squares of the differences between the observed and calculated structure factor amplitudes. Crystal structures which have a low R-factor ($\Sigma||F_o|-|F_c||/\Sigma F_o$) are not necessarily correct. Successful refinement requires that a structure of geometric rigour and intuitive chemical sense can be arrived at which converges to a low R-factor. For small molecule diffraction studies, the R-factor is often less than 5%. The reason for this is that the number of observed diffraction data exceeds the number of parameters (atomic coordinates, temperature factors) to be refined by a factor of about 7 to 1. An approximately correct trial structure should converge to a very low R-factor with little intervention by the crystallographer. In protein crystallography, however, there is a great paucity of data compared with that of a small molecule structure determination; e.g., a typical small molecule structure consisting of perhaps 20-30 atoms will result in about 100 parameters to be refined (x,y,z and anisotropic U for each atom). A typical data set could contain 2000-3000 observations. This represents an excess of observed data over parameters to be refined of at least 10 fold. A typical set of reflection data after for a mutant of tyrosyl-tRNA synthetase contains approx 20000 observations at 2.5 Å resolution and 2500 atoms (excluding hydrogen); this results in 10000 parameters to be refined and an overdeterminacy of 2:1, which is much less desirable. Geometrical constraints are applied during the refinement process in an effort to compensate for the lack of data. Small molecule diffraction studies have already provided a great deal of accurate information about bond lengths, angles and peptide geometry. Existing knowledge of preferred side chain conformations in proteins (Ponders & Richards, 1987) and main chain Φ and Ψ angles (Ramakrishnan & Ramachandran, 1965), assumption of peptide bond planarity and the topological arrangement

of α-helices and β-sheet structures can all be used to constrain the refinement process.

Intervention by the crystallographer is necessary; hence the computation of the (F_o-F_c, α_{calc}) and ($3F_o$-$2F_c$, α_{calc}) electron density maps. The refinement package restricts the shifts of any one atom during a refinement cycle to a small value (<0.3 Å). Therefore moving a side chain which is completely out of density into density cannot be carried out. In addition until the model is refined to a sufficiently low R-factor, choosing the correct conformation of a side chain within density is difficult. The situation may be improved by the introduction of restrained molecular dynamics refinement, which in theory at least should allow the sampling and preferential selection of all conformational space as part of the refinement process, and reduce the amount of model building required. This will not affect the rate at which highly refined structures are produced. This is dependent on the search for isomorphous derivatives. Details of the refinement statistics for the mutants described in this thesis are tabulated in Appendix B.

CHAPTER3 Analysis of Cys→Gly-35 Mutant.

3.1.1 Introduction

Residue Cys-35 of the tyrosyl-tRNA synthetase has the distinction of being the first residue in an enzyme of known three-dimensional structure to be modified by site-directed mutagenesis (Winter et al., 1982). Crystallographic studies suggest that its side chain sulphydryl group hydrogen bonds to the 3'-OH of the ribose ring of tyrosyl adenylate. As this residue is conserved in another aminoacyl-tRNA synthetase (Barker & Winter, 1982), mutations of the cysteine residue were originally made to search for a contribution of the thiol group to catalysis (Winter et al., 1982). Construction of the free energy profile for the formation of tyrosyl adenylate shows that Cys-35 contributes no binding energy to ATP in the E.Tyr.ATP complex but stabilises the transition state for the formation of E.Tyr-AMP by 1.3 and Tyr-AMP by 1.6 kcal/mol, relative to a glycine at position 35 (Wells & Fersht, 1986). These values fall within the range of 0.8-1.5 kcal/mol which is found experimentally for a large number of apparent H-bond energies determined in this laboratory and elsewhere (Fersht, 1988a). The double-mutant test however, indicated an interaction between positions 35 and 51 (Carter et al., 1984). The sum of the individual changes in binding energy on mutating Cys→Gly-35 and Thr→Pro-51 differ by 0.4 kcal/mol from the total change in the double mutant Cys→Gly35;Thr→Pro-51. The significance of the small non-additivity was unknown. In order to try to interpret this at the molecular level crystal structures of TyrTS(Cys→Gly-35) complexed with tyrosine and tyrosyl adenylate respectively were determined.

3.1.2 Purification and Crystallisation.

TyrTS(Cys→Gly-35) was purified and crystallised as described in chapter 3. A single large crystal (0.4 mm in smallest dimension) was chosen for data collection. Crystals of the tyrosyl adenylate complex were grown by co-crystallization in the presence of saturating tyrosine, 10 mM ATP, 10 mM $MgCl_2$ and 100 mM Tris/acetate pH 7.3, at 4° C.

3.1.3 Data Collection and Structure Refinement.

A complete set of data for the complex with tyrosine was collected to 2.5 Å resolution as described in chapter 2. Altogether, 20549 independent reflections were measured out of a total of 43782 giving an R-merge of ~ 5.3% . A data set of poorer quality was collected for the co-crystal with tyrosyl adenylate. In this experiment, 19912 independent reflections were measured out of a total of 42188 reflections with an overall R-merge of 10.6%. These data were good to 2.7 Å resolution. A more detailed description of the results of data collection and processing is given in Appendix A.

3.1.5 Difference Maps of Complex With Tyrosine.

A more detailed discussion of the types of electron density maps calculated and the use of computer graphics to display and interpret them is given in chapter 2. The initial map ($(F_{mut}-F_{wt})$, native phases) at 2.5 Å resolution contained a large negative peak (Fig 3.1) corresponding to the wild-type sulphur atom (and β-carbon) of Cys-35. The F_o-F_c map shows two peaks adjacent to Thr-51 and Ile-52 (Fig 3.2). Inspection of the $3F_o-2F_c$ map showed the density of the side chain at Ile-52 to be contiguous with the new density, and this was interpreted as an alternate side chain conformation (Figs 3.2 and 3.3). The conventional interpretation of this is that the side chain exists in two conformational states, each of which is significantly occupied and ordered. In this case, one state adopts the wild-type conformation and the other differs.

The peak adjacent to the side chain of Thr-51 was the β-carbon of this residue in a new conformation and the side chain had to be modelled into the $3F_o-2F_c$ map (Figs 3.2 and 3.3). Thr-51 exists in one conformation only. Both the mutant and native torsion angles (Fig 3.3 legend) are found with similar incidence in existing tertiary structures (Ponder & Richards, 1987).

It was not possible to refine both alternate conformations together using the refinement program implemented at Imperial College. The quality of the data and model are not high enough to make it worthwhile. In practice, the alternate conformations of Ile-52 were refined separately. Refining alternate conformations gave almost identical models. The current residual after several cycles of

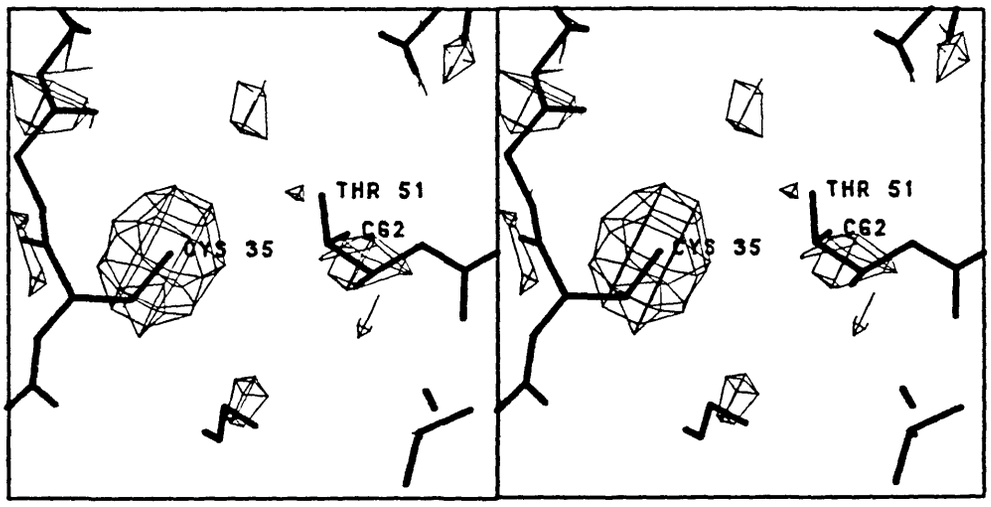


Fig 3.1 Difference map (F_{mut}-F_{wt}, α_{wt}) at 2.5 Å resolution, contouring at 3σ. Negative density shown only. Loss of sulphur atom is clear.

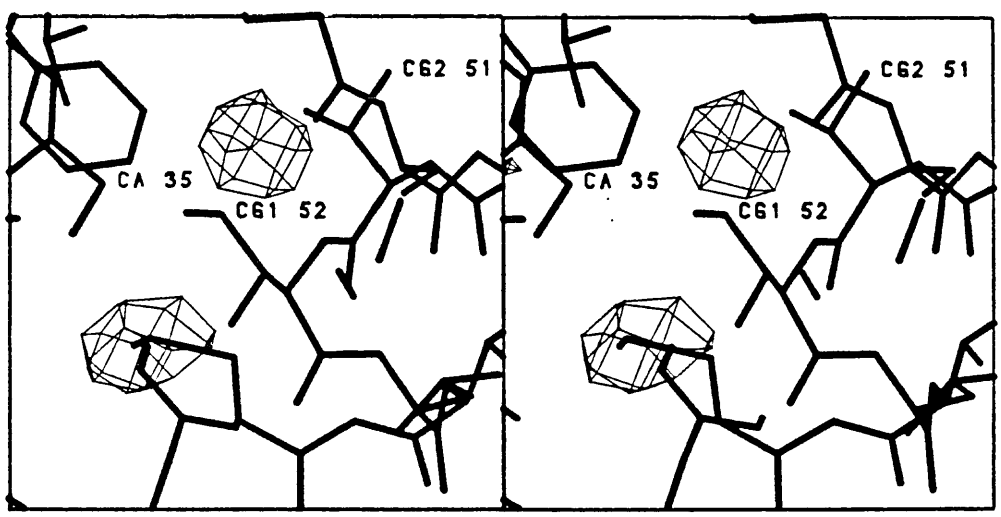


Fig 3.2 Difference map (F_o-F_c, α_{calc}) after 5 cycles of refinement. Contouring is at 3σ, positive density only.

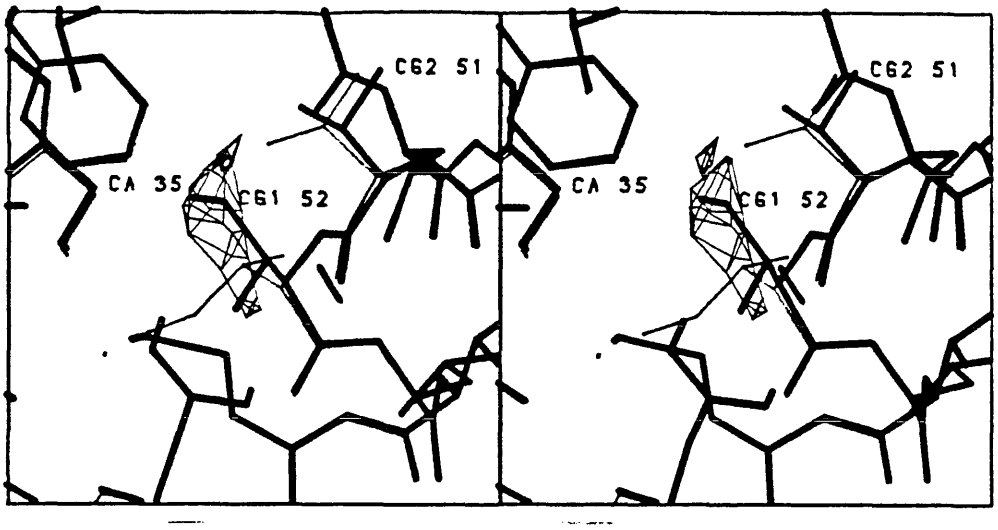


Fig 3.3 Difference map (F_o-F_c, α_{calc}) after refitting the model. After 10 of cycles refinement, the model differed as follows; Thr-51 Chi 1 native 62°, mutant -65°; Ile-52 Chi 1 native -64°, mutant -166°; Chi 2 native -161°, mutant 56°. Contouring is at 3σ, positive density for alternate conformation (native in this case) of Ile-52. Mutant conformation is shown in thin line.

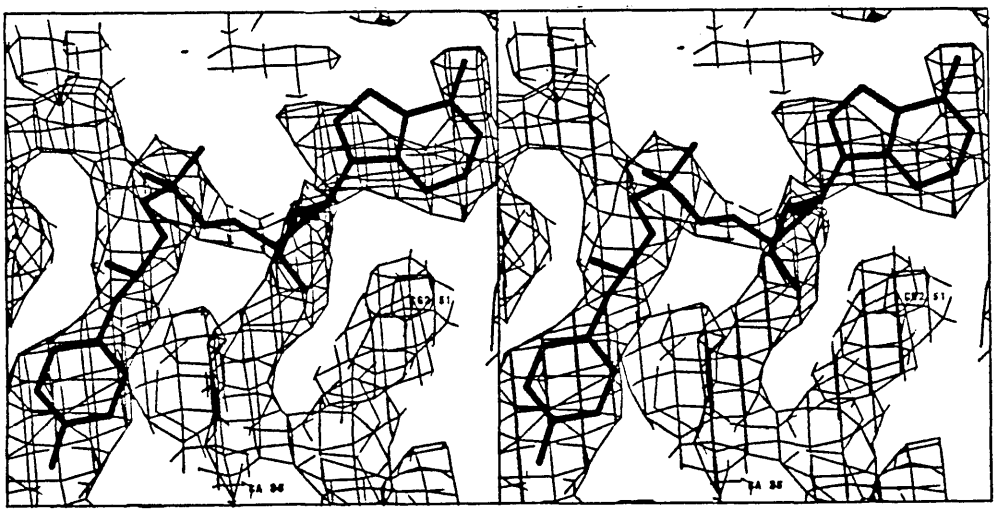


Fig 3.4 A 2.7 Å ($3F_o$-$2F_c$, α_{calc}) map calculated with tyrosyl adenylate omitted from the model. Contouring is at 1σ.

restrained least squares refinement using PROLSQ (Hendrickson, 1985) is 23.6% at 2.5 Å resolution compared with 21% (2.1 Å resolution) for the native structure (Blow & Brick, 1985). A more detailed description of the refinement statistics is tabulated in Appendix B. The main chain conformation was almost unchanged (rms deviation from native 0.10 Å) and the structure is effectively isomorphous (overall rms dev. 0.22 Å). The mean B value (temperature factor) for the structure was 17.06 $Å^2$ compared with 15.66 $Å^2$ for the native structure (Blow & Brick, 1985), and the overall difference between the two was 1.39 $Å^2$. The mean temperature factors for the residues 35 and 51 did not change significantly, after allowing for the increase for the whole structure, but the value for Ile-52 increased from 12.78 $Å^2$ to 18.53 $Å^2$ (difference 5.75 $Å^2$) as would be expected if it adopts more than one conformation. The difference in main chain temperature factors is plotted in Appendix E.

3.1.6 Difference Maps of Complex With Tyrosyl Adenylate.

This structure was treated in exactly the same way, using the models from the tyrosine structure. The electron density for the adenylate is shown in Fig 3.4. In order to compare the electron density for the Thr-51 and Ile-52 side chains in the tyrosine and tyrosyl adenylate structures, F_o-F_c and $3F_o$-$2F_c$ maps were computed with models without these side chains. As in the tyrosine complex, both data sets were refined separately in each alternate side chain conformation. The models resulting from this process were almost identical (main chain rms dev. 0.11 Å, overall 0.19 Å) and were used to compute the omit maps. The R-factor values did not differ

significantly from the tyrosine structure; details are tabulated in Appendix B. The mean temperature factor for the structure was 16.58 $Å^2$, compared with 15.66 $Å^2$ for the native structure, a difference of 0.92 $Å^2$. The mean temperature factor of residue 35 did not change significantly, after allowing for the overall increase in the structure, but the values for residues 51 and 52 rose significantly, especially the side chain of Thr-51 which increased from 12.33 $Å^2$ to 21.55 $Å^2$, a difference of 9.22 $Å^2$. The difference in main chain temperature factors is plotted in Appendix E.

Inspection of the difference density (Figs 3.5 and 3.6) clearly shows that when tyrosyl adenylate is present, the alternate conformation at Ile-52 appears to have almost reverted to that of the wild type, and the density for Thr-51 shows increased disorder, as reflected in the higher B value for the side chain. In an effort to model these changes, the coordinates of both conformations of the Thr-51 and Ile-52 (wild type and mutant in each case) have been used to calculate and hence model density for these side chains. By varying the occupancies of the different conformations, it is possible to produce reasonably convincing representations of the observed density. It is appreciated that refining the alternate conformations seperately is unsatisfactory, since the occupancy, temperature factor and coordinates of each conformation cannot be determined accurately. Attempts to model density for alternate conformations of residues 51 and 52 to try to provide crystallographic support for what appears to be a perturbation effect were hampered by the fact that the coordinates of the alternate conformations could not be refined properly. Modelling electron density for side chains requires an accurate set of coordinates, if it is to be meaningful. Fortunately, however, the spatial separation between the

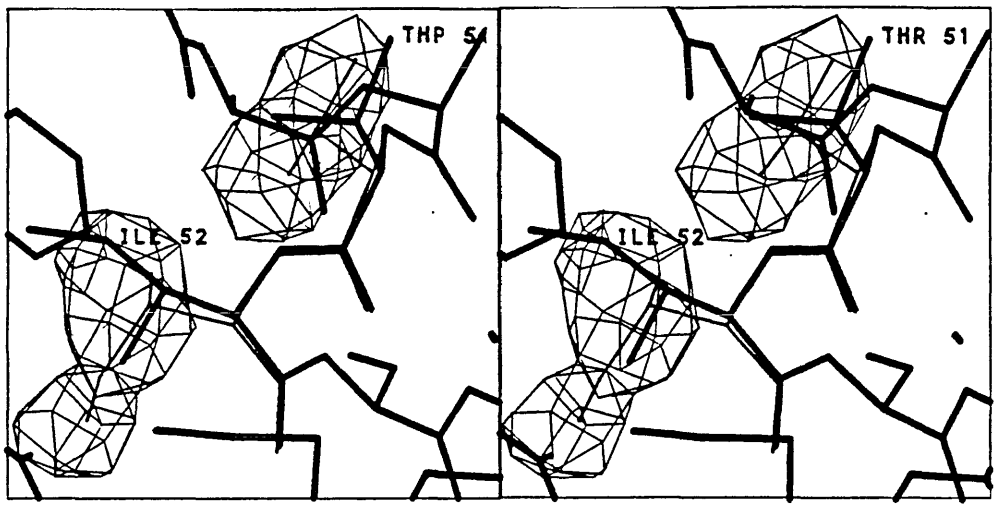


Fig 3.5 Difference map (F_o-F_c, α_{calc}) at 2.5 Å resolution of the tyrosine structure, where Thr-51 and Ile-52 side chains have been removed from the model. Contouring at 3σ, positive density only.

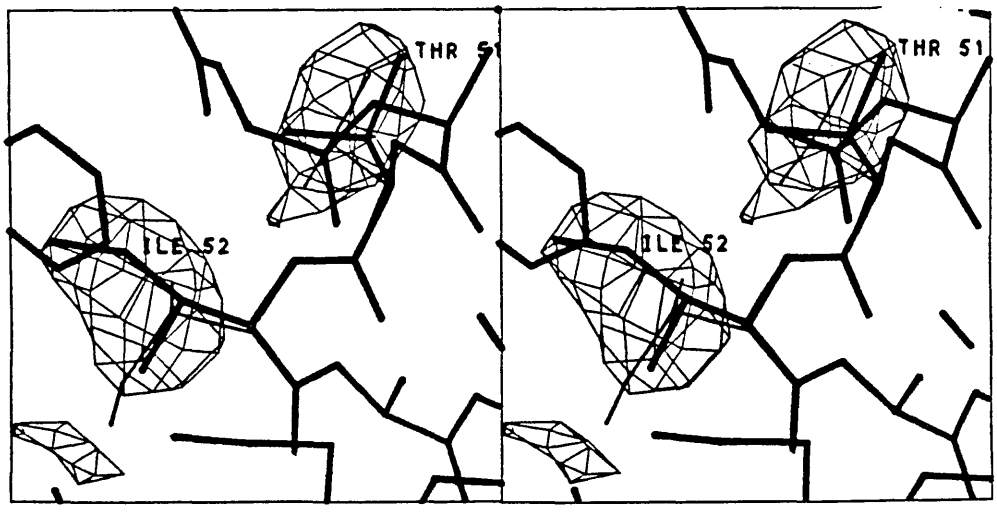


Fig 3.6 Same as Fig 3.5 but for the tyrosyl adenylate structure (2.7 Å resolution).

two conformations of Ile-52 is such that it seems reasonable to say that a change in occupancy has occured on the formation of tyrosyl adenylate regardless of its magnitude. The same is true for Thr-51, but it is not possible to show whether the side chain adopts two conformations which are close in space or generalised disorder results on binding of tyrosyl adenylate. As far as the mechanistic interpretation (3.2.3) is concerned, crystallography need only show that a perturbation exists. Other methods (the double mutant test, 1.1.8) can quantitate its effects more accurately, but as will be discussed, they can only be interpreted in this way in the light of such structural data.

3.2.1 Interpretation of Structural Changes In Tyrosine Complex.

Two changes in structure were observed on mutation of Cys→Gly-35. The side chain of Thr-51 rotates about the C_α-C_β bond so that the γ-methyl group partly occupies the space vacated by the $-CH_2SH$ of Cys-35. The side chain of Ile-52 becomes disordered. Although glycine residues are the most flexible links in the protein main chain, mutation of Cys→Gly-35, leaves the α-carbon backbone unchanged. The observed changes in structure are thus a consequence of the creation of a cavity in the protein on deletion of the side chain and the movement of side chains of other amino acids to occupy the cavity.

3.2.2 Interpretation of Complex With Tyrosyl Adenylate.

This structure is very similar to the complex with tyrosine except that Ile-52 tends to revert to the wild type conformation and Thr-51 becomes disordered. The significance of this is discussed below.

3.2.3 Relationship Between Changes in Structure and Activity.

Mutation of Cys→Gly-35 in wild-type enzyme weakens the binding of the transition state for the formation of Tyr-AMP by 1.2 kcal/mol (Carter et al., 1984). The same mutation in the mutant TyrTS(Thr→Pro-51) gives a double mutantthat shows binding that is weaker by only 0.8 kcal/mol. Mutating Cys→Gly-35 in TyrTS(Thr→Cys-51) also weakens binding by 0.8 kcal/mol (Fersht et al,

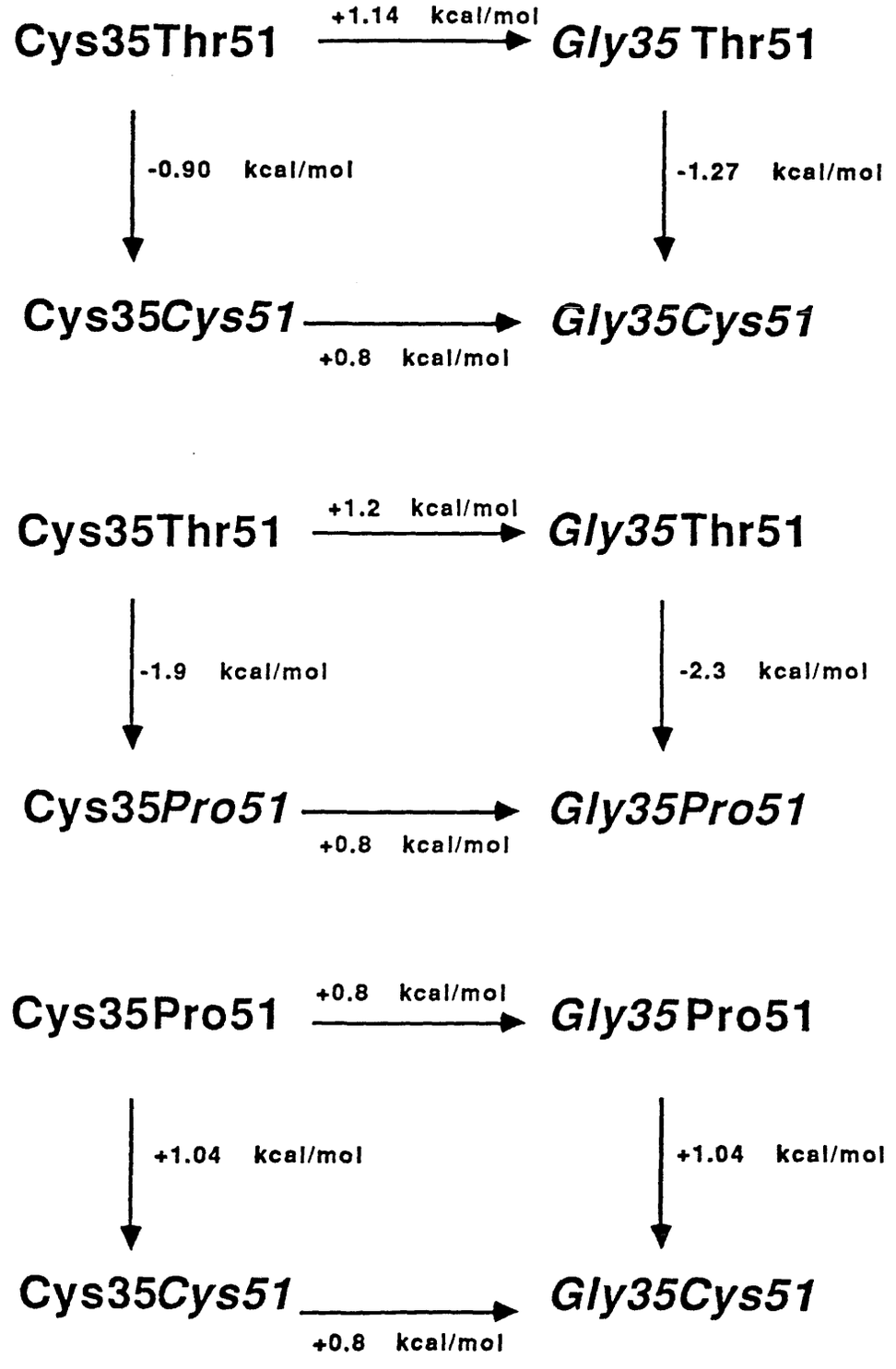


Fig 3.7 Double mutant data for Cys→Gly-35 paired with Thr→Pro-51 and Thr→Cys-51 respectively (Carter *et al.*, 1983 and Fersht *et al.*, 1985).

1985). Expressed as the double mutant test (Fig 3.7), the mutations of Cys-35 and Thr-51 are seen to be non-additive, indicating that the mutations are not independent. The energy changes are calculated for the process E.Tyr + ATP → enzyme-bound transition state ([E.Tyr-ATP]$^{\neq}$). The two structures required for quantitative calculation of the energetics are, therefore, those two complexes. Although the structure of the transition state is not known, data from linear free energy relationships indicate that the interactions between the ribose ring and the enzyme are very close in energy to those in the E.Tyr-AMP complex (Fersht et al, 1987).

One could explain the double mutant data as follows; in both cases mutation of Thr-51 to either Pro or Cys removes the β-carbon of Thr-51. Therefore there is no side-chain group which can fill the void created in the Cys→Gly-35 mutation. Hence such mutations would tend to be structurally independent of the glycine at position 35, and so the mutant enzyme should be functionally unaffected by any second site mutations at position 51 that cannot fill this cavity. This implies that the double-mutant pair Cys→Gly-35;Thr→Pro-51 and Cys→Gly-35;Thr→Cys-51 should be additive; this is shown in Fig 3.7.

The X-ray data clearly show that the binding of substrate perturbs the equilibrium between the two conformations of Ile-52. The preferred state for catalysis is that which most resembles the wild-type structure.

Consider the following system;

$$E \rightleftarrows E'$$

where E' is an alternate conformation of the enzyme which is not favoured for catalysis. The 0.4 kcal/mol discrepancy corresponds to a change in K_{eq} by a factor of 2 between free and substrated states

($\Delta G = -RT\ln K$). The apparent change in density is roughly consistent with this. These data suggest that the H-bond strength at position 35 is 0.8 kcal/mol in the transition-state, and the Cys→Gly-35;Thr-51 value of 1.2 kcal/mol contains an extra 0.4 kcal/mol caused by structural change at Thr-51. The H-bond to the E.Tyr-AMP complex will likewise be revised down from 1.6 to 1.2 kcal/mol. Non-additivities are not likely to yield to such a simple analysis as outlined above. In many cases both residues will move with respect to one another, and probably to different extents in each pair of mutations at a given pair of loci. This will be borne out in the kinetics, which will be non-additive in all possible permutations of the data. In a few cases it may be possible to predict structural changes from double mutant data and simple modelling of the mutant amino acids, providing a crystal structure is available.

This crystal structure has shown that a mutation at a given position involved in hydrogen bonding to the active site of an enzyme can cause a structural change at a neighbouring residue involved in catalysis. This observation serves to re-affirm the sensitivity of the double mutant test as a probe of this phenomenon and gives rise to a revised estimate of the true strength of hydrogen bonding in catalysis. The apparent hydrogen bond strengths measured at position 35 have been revised by 25 and 33% in the transition-state and tyrosyl adenylate complexes respectively as a result of the X-ray analysis. In protein engineering experiments where the observed free energy changes are of the order of 1-2 kcal/mol structural changes need not be beyond the resolution of protein crystallography. This is because the protein engineering experiment measures free energy changes based directly on catalytic properties and only indirectly on structure itself.

CHAPTER 4 Analysis of Tyr→Phe-34 Mutant

4.1.1 Introduction

Crystallographic studies suggest that Tyr-34 hydrogen bonds to the hydroxyl oxygen of the tyrosine substrate (Brick & Blow, 1987). Kinetic experiments showed that Tyr-34 contributes 0.5 kcal/mol binding energy to the E.Tyr complex (Wells & Fersht, 1986). The mutation Tyr→Phe-34 was originally constructed to measure the contribution of this group to specificity (tyrosine vs phenylalanine) and catalysis (Fersht *et al*, 1985). The mutation is conservative; K_S for tyrosine is raised from 12μM to 29 μM and only an OH is removed from a planar ring. Unlike other mutants in the tyrosine pocket which drastically weaken substrate binding (Lowe *et al.*, 1987), the substrate should bind tightly in the crystal. Furthermore, the model of tyrosine in the truncated enzyme crystal structure is significantly better than that of the full length molecule (Brick & Blow, 1987). The crystal structure of this mutant complexed with tyrosine was determined to discover whether or not a water molecule was bound in place of the phenolic hydroxyl group in the active-site of the enzyme, or if further changes in structure had occured as result of the mutation.

4.2.1 Purification and Crystallisation.

ΔTyrTS(Tyr→Phe-34) was purified and crystallised as described in chapter 3. Crystals obtained were typically 0.1 x 0.1 x 0.4 mm and grew in the same form as the wild-type truncated enzyme (Brick & Blow, 1987). Two crystals were chosen for data collection.

4.2.2 Data Collection and Structure Refinement.

A complete set of data for the complex with tyrosine was collected to 2.7 Å resolution at the SRS facility in Daresbury (U.K.) by the oscillation method (Nyborg & Wonnacott, 1977) on flat films, in 120 min (2.0 GeV, ~ 250mA, 0.88 Å). A total of 52718 reflections were reduced to 19113 independent reflections with an R-merge of 8.4%. Experimental details are given in Appendix A.

4.2.3 Difference Map of the Complex With Tyrosine.

Electron density maps were computed and displayed as described in chapter 2. The current residual after several cycles of restrained least squares refinement using PROLSQ (Hendrickson, 1985) was 17.9% at 2.7 Å resolution (rms deviation in bond lengths is 0.018 Å compared with 18.7% (2.5 Å resolution, rms dev. 0.017 Å) for the native structure (Brick & Blow, 1985). Full details of the refinement are given in Appendix B. Comparison of the native and mutant structures shows an overall rms difference of 0.16 Å, comprising 0.12 Å in main chain and 0.19 Å in side chain atoms for subunit A, and for subunit B they are

0.15, 0.11 and 0.18 Å respectively. The mean B value for the A subunit was 25.66 $Å^2$ compared with 26.04 $Å^2$ for the native enzyme; that of the B subunit was 22.18 $Å^2$ compared with the native value of 23.05 $Å^2$.

4.2.4 Interpretation of Complex With Tyrosine.

The initial map ($(F_{mut}-F_{wt})$, wild-type phases) at 2.7 Å resolution showed a negative peak (Fig 4.1) corresponding to the hydroxyl oxygen of Tyr-34. Inspection of the $3F_o-2F_c$ map calculated after refining the mutant model shows convincing density for the substrate and Phe-34 (Fig 4.2). The occupancy of the substrate must be close to full, since the temperature factors after refinement are low; the mean B value for the tyrosine bound in the A subunit was 7.12 $Å^2$ compared with 10.5 $Å^2$ in the native structure; that of the B subunit was 5.9 $Å^2$ relative to the native 7.51 $Å^2$. In addition, the temperature factor for the side chains of residue 34 fell from 7.00 and 11.45 $Å^2$ in the native structure to 4.63 and 6.78 $Å^2$ in the mutant A and B subunits respectively. No other features are present and there is no room for a water to bind in the pocket created in this mutation.

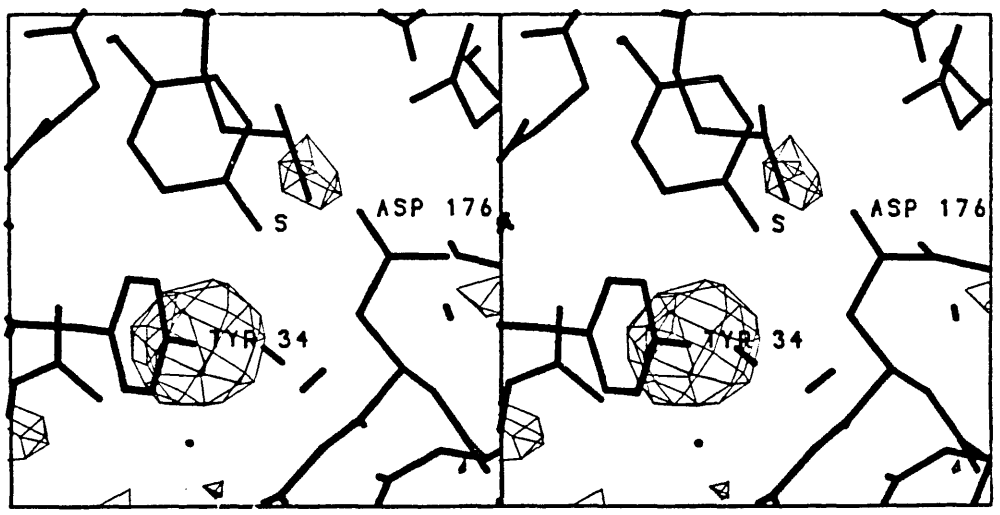


Fig 4.1 Difference map (F_{mut}-F_{wt}, α_{wt}) at 2.7 Å resolution, contouring at 3σ. Negative density shown only. Loss of hydroxyl group is clear. The model is that of the native enzyme complexed with tyrosine. The substrate is labelled "S".

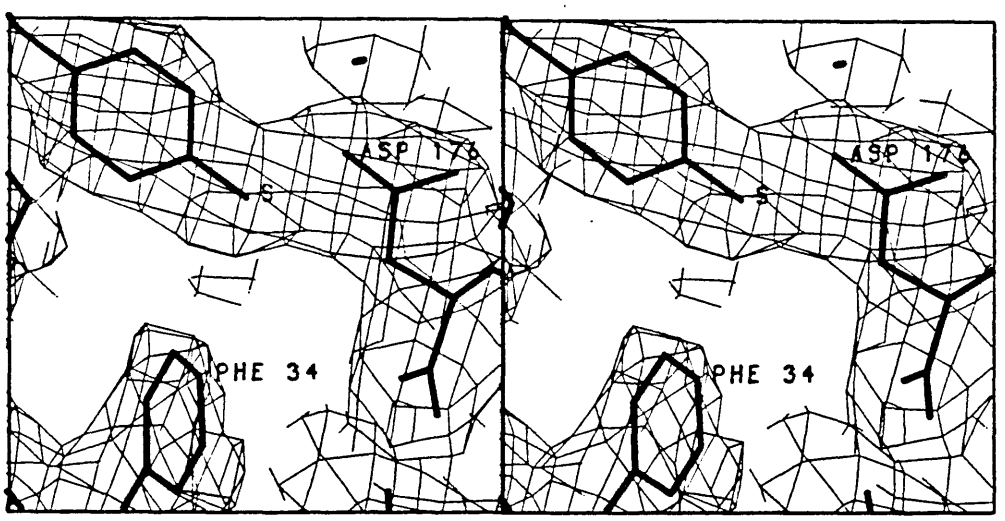


Fig 4.2 Electron density map ($3F_o$-$2F_c$, α_{calc}) after several cycles of refinement. Contouring is at 1σ, resolution 2.7 Å. The refined native (Fig 4.2) and mutant models are almost identical. Note the clear density for the substrate, "S".

4.3.1 Relationship Between ΔG_{app} and ΔG_{bind} in Tyr→Phe-34

After the characterization of several mutant enzymes (Fersht, 1987), a more rigorous and formal analysis of a protein engineering experiment was put forward. Fersht (1988) has suggested that ΔG_{app}, the experimentally determined apparent binding energy will equal ΔG_{bind}, the incremental binding energy of the hydrogen bond, if there are no net hydrogen bonds broken in either mutant or wild type enzyme, there are no structural changes in the E.S complex and one is dealing with an uncharged hydrogen bond. If this is true for a given mutant then a water molecule should hydrogen bond to the substrate in the mutant E.S complex which forms similar interactions to bulk solvent in the free mutant enzyme. If not, then ΔG_{app} is not equal to ΔG_{bind}, but is the energy of an unpaired hydrogen bond. A full derivation of ΔG_{app} and ΔG_{bind} is given in Appendix C. In Tyr→Phe-34, no density for a bound water is apparent, and the groups around the substrate OH group are too close to allow one to bind (Fig 4.3). Therefore the free energy of the creation of an unpaired phenolic hydroxyl oxygen has been experimentally determined.

Protein engineering experiments that are designed to measure the strengths of hydrogen bonds in proteins and their role in biological specificity should not be confined to kinetic methods. A thorough analysis would require two criteria to be satisfied which could only be determined by X-ray crystallography. One is that there is no change in structure on the removal of a hydrogen bonding group on the enzyme. The other is that the solvation state of the enzyme bound substrates, intermediates and products (in theory the transition-state also)

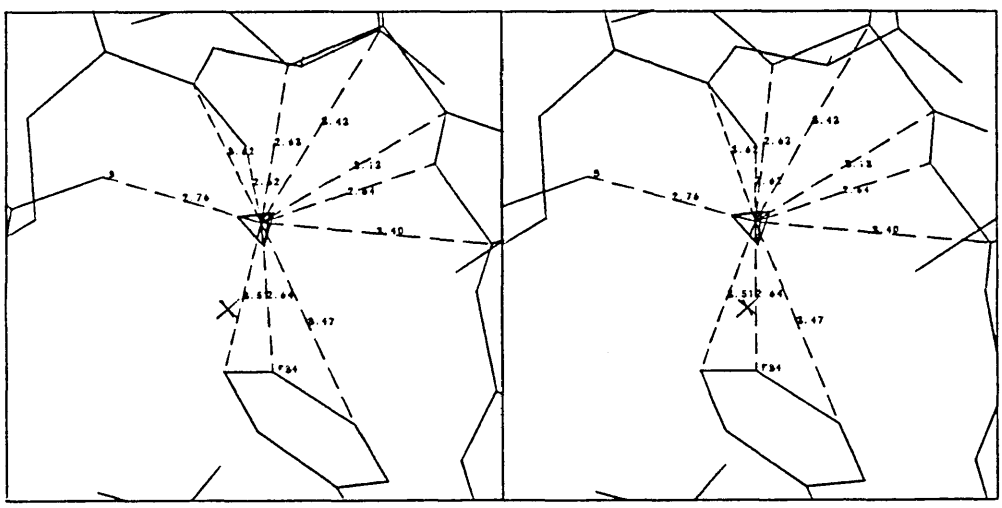


Fig 4.3 An attempt to model a water molecule between the substrate hydroxyl and the mutant residue, phenylalanine 34. Neighbouring residues are too close packed for this to occur in reality.

must be known for the mutant enzyme. If the first criterion is not satisfied, then ΔG_{app} will contain an extra component reflecting the reorganisation of enzyme structure and solvation. If the second cannot be determined, then it will not be possible to know whether the free energy of a paired or unpaired hydrogen bond has been measured by kinetic methods.

CHAPTER 5 Analysis of Thr→Cys-51 Mutant

5.1.1 Introduction

The formation of artificial disulphide bridges as result of site directed mutagenesis experiments has been widely reported and reviewed (Wetzel, 1987). As early as 1982 it had been suggested (D. M. Blow personal communication) that a disulphide bridge might form between residues Cys-35 and Thr-51 of the tyrosyl-tRNA synthetase on mutation of residue 51 to cysteine. These residues are located in the active site of the enzyme. Residue Cys-35 hydrogen bonds to the 3'-OH group of the ribose moiety of tyrosyl adenylate. Residue Thr-51 is also close (3.7 Å) to the ribose but not sufficiently for the γ-OH to make a hydrogen bond with its 4' ring oxygen. Kinetic studies of the Thr→Cys-51 mutant show that it has enhanced affinity for the Michaelis complex, E.Tyr.Mg.ATP. Construction of the free energy profile for the mutant Thr→Cys-51 showed that it contributes an *extra* 1.19 kcal/mol binding energy to ATP in the E.Tyr.Mg.ATP complex and stabilises the transition state for the formation of E.Tyr-AMP by 1.24 and Tyr-AMP by 1.44 kcal/mol (Ho & Fersht, 1986) relative to the wild type enzyme. The aims of this study were to discover whether a disulphide bridge formed in this mutant, and to investigate its enhanced binding of substrates, transition-state and tyrosyl adenylate. Attempts were made to use its improved binding of the Michaelis complex to allow a crystal structure of Mg.ATP bound to the enzyme to be determined.

5.1.2 Purification and Crystallisation.

TyrTS(Thr→Cys-51) was purified and crystallised as described in chapter 2, except 17mM tyramine and 50mM ATP were present, and the temperature was 4° C. Tyramine is similar to tyrosine except that it lacks the carboxylate acid group of the amino acid. This molecule was used to mimic the natural substrate but prevent the formation of tyrosyl adenylate, in an effort to create a dead end complex E.Tyramine.Mg.ATP which would resemble the Michaelis complex, E.Tyr.Mg.ATP, as closely as possible. Crystals obtained were typically 0.1 x 0.4 x 0.4 mm and grew in the same form as the wild-type enzyme (described in chapter 2). A single large crystal (0.4 mm in smallest dimension) was chosen for data collection. Crystals of the tyrosyl adenylate complex were grown by adding 10 mM ATP to crystals grown first in the presence of saturating tyrosine, 10 mM $MgCl_2$ and 100 mM Tris/acetate pH 7.3, at 18° C and subsequently washed with mother liquor containing 17 mM tyramine in an attempt to remove the bound tyrosine. Efforts to remove the tyrosine and replace it with tyramine apparently failed due to formation of tyrosyl adenylate on addition of 10mM ATP.

5.1.3 Data Collection and Structure Refinement.

A complete set of data for the complex with tyramine was collected to 2.5 Å resolution as described in chapter 2. A total of 42874 reflections were reduced to 19980 independents giving an R-merge of 6.3%. A data set was collected for the enzyme bound tyrosyl adenylate complex. In this experiment, 20047 independents were

produced from a total of 43029 reflections with an overall R-merge of 10.6%. These data were good to 2.7 Å resolution. Details of the results of data collection and processing are given in Appendix A.

5.1.4 Difference Maps of the Complex With Tyrosyl Adenylate.

Electron density maps were computed and displayed as described in chapter 2. The current residual after several cycles of restrained least squares refinement using PROLSQ (Hendrickson, 1985) is 22.4% (rms deviation of bond lengths 0.024 Å) at 2.7 Å resolution compared with 21% (2.1 Å resolution) for the native structure (Blow et al., 1985). Comparison of the native and mutant structures shows an overall rms difference of 0.42 Å, comprising 0.32 Å in main and 0.51 Å in side chain atoms respectively. The representation (Fig 5.1) of the $(F_{mut}-F_{wt})$, α_{wt} map of density for the side chain of residue 51 is consistent with the substitution of the relatively electron dense sulphur atom and the formation of a disulphide bond between Cys-35 and Cys-51. There is also clear density for tyrosyl adenylate. A disulphide linkage was built between these residues, and after refinement (Fig 5.2) the $3F_o-2F_c$ map shows convincing density for the substrate and the S-S bridge. The torsion angles for the disulphide bridge are X1 = 175°, X2 = 148°, X3 = 104°, X2' = -144°, X1' = -142°, starting from the C_α of Cys-35 and ending at the C_α of Cys-51. The mean B value for the structure was 19.57 $Å^2$ compared with 15.66 $Å^2$ for the native enzyme. The temperature factors for residues 35 and 51 did not change significantly with respect to the rest of the structure. The average B value for the substrate, tyrosyl adenylate, was 24.44 $Å^2$ compared with 22.00 $Å^2$ for the native molecule complexed with the

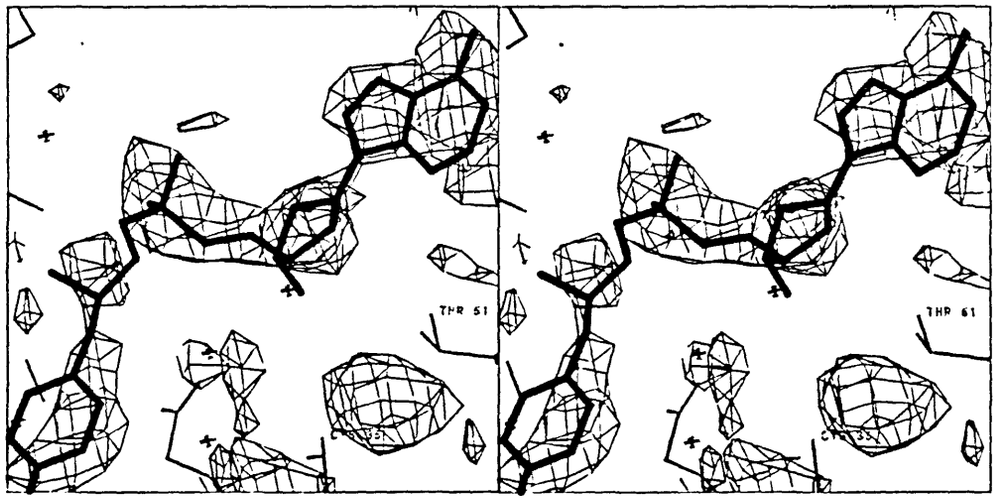


Fig 5.1 Difference map (F_{mut}-F_{wt}, α_{wt}) at 2.7 Å resolution, contouring at 3σ. Positive density shown only. Note electron density between residues 35 and 51, and that for the substrate.

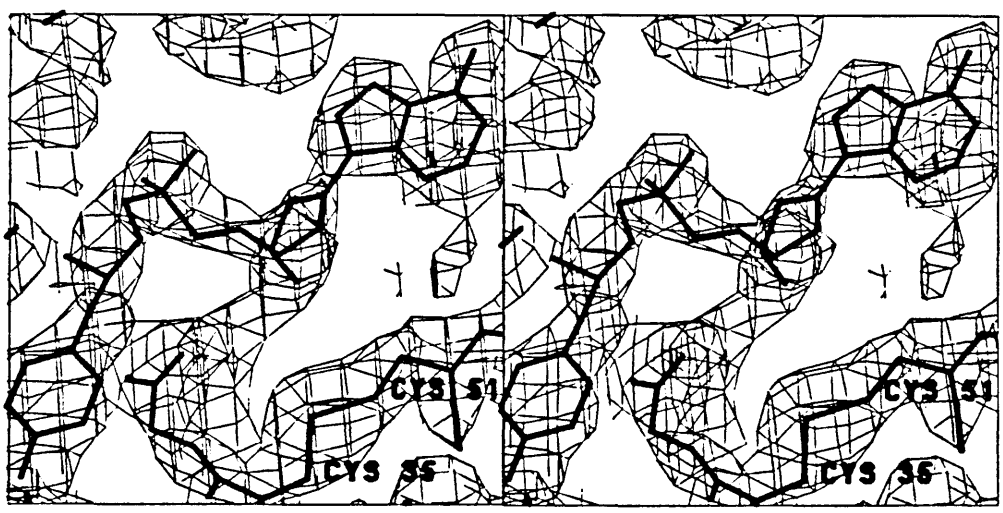


Fig 5.2 Electron density map ($3F_o$-$2F_c$, α_{calc}) after 30 cycles of refinement. Contouring is at 1σ, resolution 2.7 Å. Density for the disulphide bridge and the substrate is clear.

inhibitor, tyrosinyl adenylate. The difference in temperature factors for mutant and native main chain atoms is plotted in Appendix E.

5.1.5 Difference Maps of the Complex With Tyramine.

Electron density maps were computed and displayed as described in chapter 2. The initial maps computed for the complex with tyramine confirmed the mutation but did not clearly show whether there was a disulphide bridge present in this structure. Hence a second set of maps (F_{red}-F_{ox} and $3F_{red}$-$2F_{ox}$), α_{calc}) were calculated. These maps are essentially the same as those described in chapter 2, except that the structure factor amplitudes and phases from the refined structure of the complex with tyrosyl adenylate containing the oxidised disulphide bridge were used to compute a difference electron density map for the complex with tyramine. Further maps (F_o-F_c), α_{calc} and ($3F_o$-$2F_c$), α_{calc} were computed after refinement. The R-factor was 23.3%, rms deviation of bond lengths 0.026 Å and the resolution was 2.5 Å. Comparison of the native and mutant structures shows an overall rms difference of 0.38 Å, comprising 0.25 Å in main and 0.48 Å in side chain atoms respectively. Details of the refinement statistics are given in Appendix B. Inspection of the F_{red}-F_{ox} map (Fig 5.3) shows significant density for the sulphur atom of Cys-51 which is clearly not covalently bonded to that of Cys-35. After refinement, the $3F_o$-$2F_c$ map (Fig 5.4) shows convincing density for tyramine and the reduced sulphydryls at residues 35 and 51. Cys-51 may hydrogen bond to Cys-35. There is some connected density between the two sulphur atoms, but this is not much greater than the rms density (noise level). Oxidation of the sulphydryls may have occured to a limited extent.

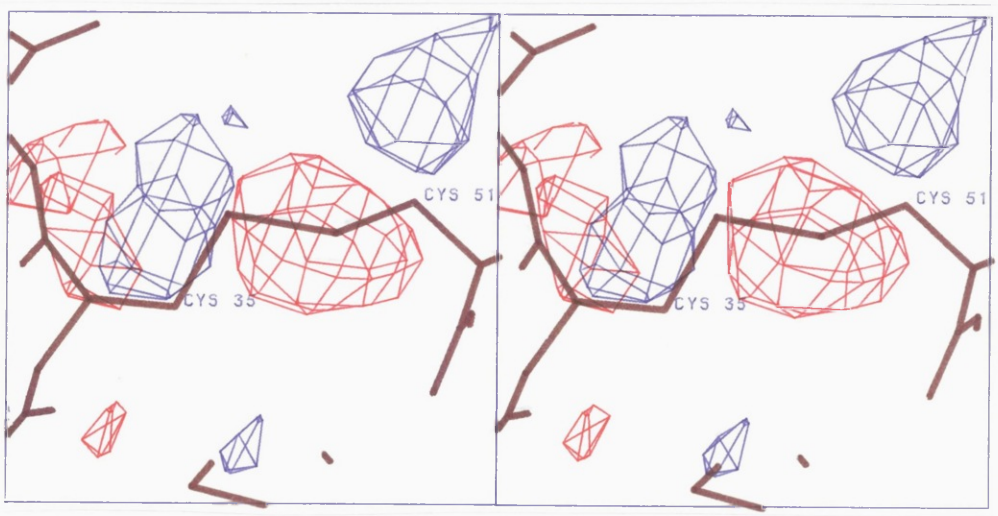


Fig 5.3 Difference map (F_{red}-F_{ox}, α_{ox}) at 2.5 Å resolution. Contouring is at 3σ. Positive density, in blue, adjacent to Cys-51 and negative density, in red, over the disulphide bridge suggests that the sulphur atom is not covalently bonded to Cys-35 in this structure, but protrudes into the active site.

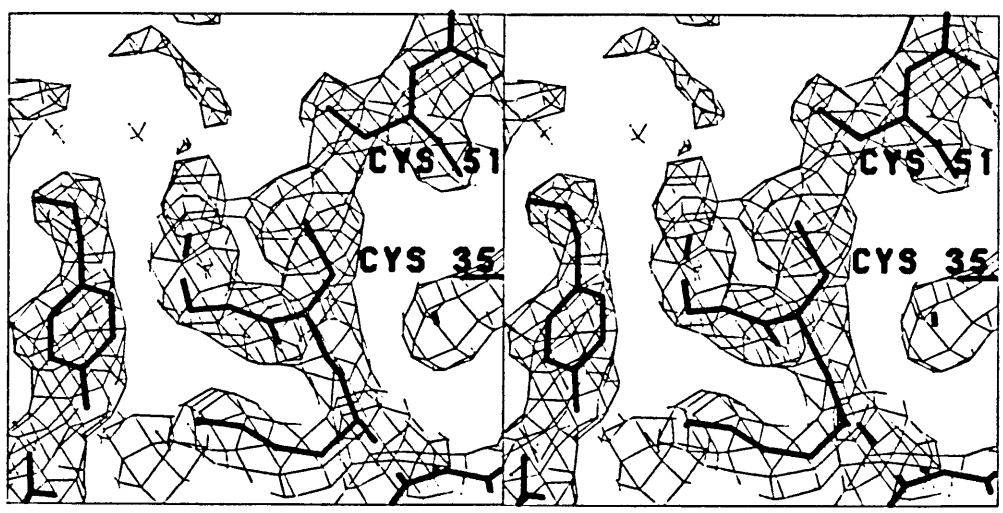


Fig 5.4 An electron density map ($3F_o$-$2F_c$, α_{calc}) showing the substrate analogue tyramine and cysteines 35 and 51 after several cycles of refinement. Contouring is at 1σ, resolution is 2.5 Å.

The torsion angles for the reduced structure are X1 = -168° for Cys-35 and X1 = -57° for Cys-51. The native values are X1 = -175° for Cys-35 and X1 = -58° for Thr-51. The mean temperature factor value for the structure was 27.96 $Å^2$ compared with 15.66 $Å^2$ for the native enzyme. The B values for residues 35 and 51 rose in line with the overall increase in crystallographic disorder observed in this structure. A difference plot of temperature factors is given in Appendix E.

5.2.1 Discussion.

In contrast to the kinetic experiments (Ho & Fersht, 1986) which were performed in the presence of 0.1 mM dithiothreitol, no reducing agents were added to the mother liquor of these crystals. The fact that in the tyrosyl adenylate structure there is a disulphide bond yet in the tyramine structure the sulphydryls are reduced may result from the difference in temperature at which the crystals were grown. The tyramine co-crystals were grown at 4°C, whereas those of the tyrosyl adenylate complex were incubated at 18°C. The reduced temperature may have slowed the oxidation reaction. Wetzel (1987) has reviewed other artificial disulphide bonds created by protein engineering. He cites the unusual example of the disulphide bridge made between positions 39 and 85 of dihydrofolate reductase (Villafranca et al., 1987), where it also proved possible to obtain crystal structures of both the reduced and oxidised forms of the enzyme. It is suggested that since the reduced form was stable in the presence of air and not easily oxidised by standard redox reagents that a thermodynamic barrier must exist for the oxidation of this sulphydryl pair.

Crystallographic studies of tyrosyl-tRNA synthetase have not revealed the structure of the Michaelis complex with Mg^{++}.ATP, possibly reflecting the poor binding of this species to the enzyme. No other mutations have been produced which significantly enhance the binding of the Michaelis complex, E.Tyr.ATP. The wild type K_S for Mg^{++}.ATP is 5 mM, and that of Thr→Cys-51 is 340 μM, a better than 10 fold improvement. In spite of this, no electron density for Mg.ATP was observed in the tyramine structure. There could be a number of reasons for this; one is that the ATP could bind loosely as a

disordered complex; another is that the enzyme could possess ATP-ase activity, although the experiments of Monteilhet & Blow, (1978) suggested that this was not the case if one was dealing with crystals of the pure enzyme, rather than a dilute solution of it.

An explanation of the enhanced binding of the transition-state and tyrosyl adenylate observed in this mutant has been put forward in Fersht *et al.*, 1985 and Ho & Fersht, 1986. The γ-OH of Thr-51 is too far (3.6 Å) to hydrogen bond to the 4' ring oxygen of tyrosyl adenylate in the refined structure of the complex between tyrosyl-tRNA synthetase and its inhibitor, tyrosinyl adenylate (Brown & Blow, 1987; Fig 5.5). The substitution of this residue for cysteine would allow a hydrogen bond to form between the sulphur of Cys-51 and the ring oxygen, since sulphydryl groups are known to form longer hydrogen bonds (3.5 Å compared with about 2.8 Å for those between oxygen and nitrogen atoms). The crystal structure of the reduced enzyme and the coordinates of the inhibitor tyrosinyl adenylate taken from the refined structure mentioned above is shown (Fig 5.6). The sulphur of Cys-51 is nearest (3.08 Å) to the 3'OH of the inhibitor. It could be postulated to form a good hydrogen bond with the 4' oxygen atom, if it is assumed that the substrate and/or enzyme would relax slightly on formation of the tyrosyl adenylate complex. Unfortunately, the tyrosyl adenylate structure contains a disulphide bridge, and it is therefore not possible to prove the existence of this hydrogen bond in the mutant E.Tyr-AMP complex. As was seen in chapter 3, assumptions about the structure of enzyme bound intermediates which are based on the crystal structures of free unligated enzyme are tenuous. There does not, however, seem to be any reason why such a hydrogen bond should not exist in the enzyme bound tyrosyl adenylate complex in solution. It is

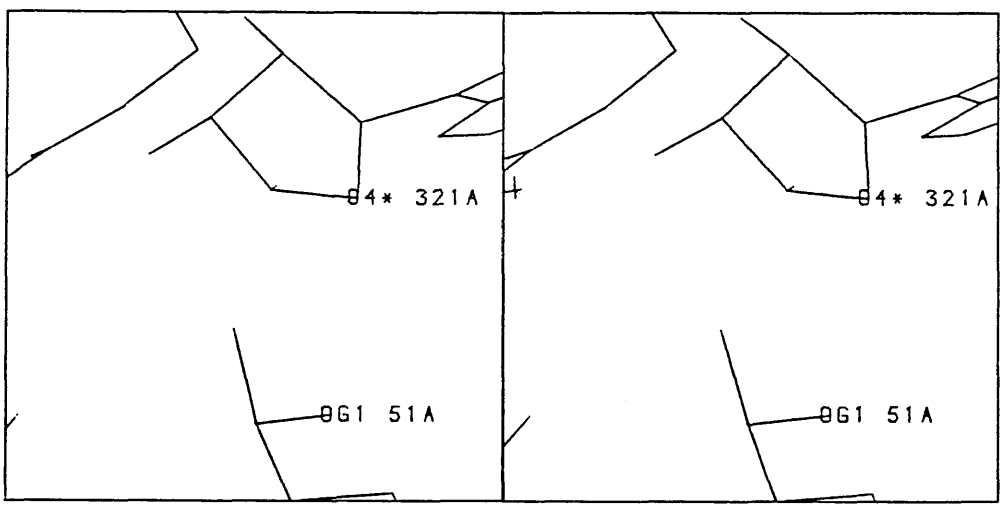


Fig 5.5 The active site region of the refined structure of tyrosyl-tRNA synthetase complexed with the inhibitor, tyrosinyl adenylate. The ribose ring oxygen is 3.6 Å from the γ-oxygen of Thr-51.

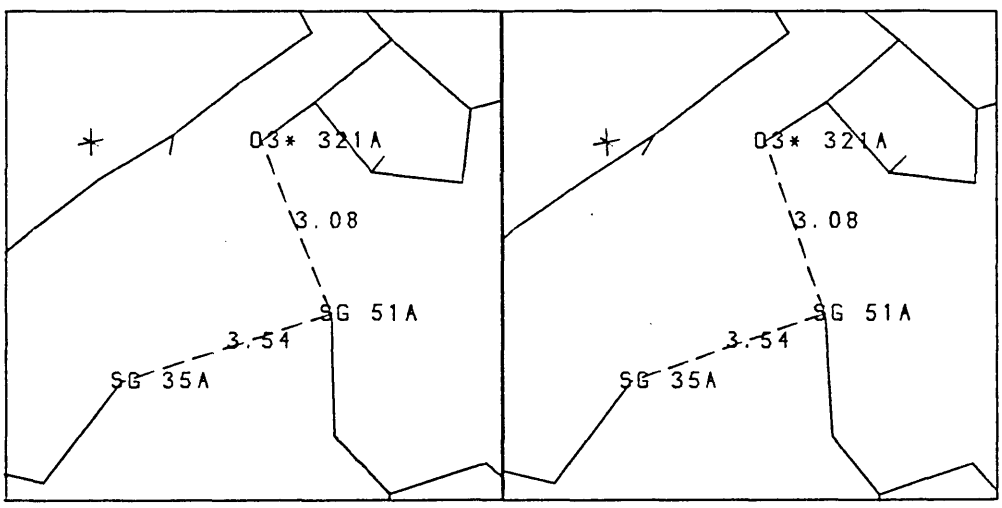


Fig 5.6 Same as Fig 5.5 but the model of the enzyme has been substituted with the refined structure of the reduced form of the mutant Thr→Cys-51. The inhibitor structure is taken from the native structure used in Fig 5.5. Note the proximity between the γ-sulphur of Cys-51 and the 3'OH group of the inhibitor.

very unlikely that the disulphide could exist in the presence of the reducing agent, dithiothreitol, used in the kinetic studies (Fersht *et al.*, 1985; Ho & Fersht, 1986). The overall conclusion must therefore be that the original hypothesis (Fersht *et al.*, 1985) was essentially correct, but as only a crystallographic analysis could reveal, the acceptor group was the 3'OH group of the ribose rather than the ring oxygen as originally proposed.

CHAPTER 6 Analysis of Mutant Asp→Asn-194

6.1.1 Introduction

Crystallographic studies of tyrosyl-tRNA synthetase suggest that Asp-194 is close to but does not make any direct interactions with the α-phosphate moiety of tyrosyl adenylate. This is not surprising, since both groups are negatively charged. Kinetic studies of the mutant Asp→Asn-194, however, show that the rate constant for tyrosyl adenylate formation of about 10^{-3} s^{-1} compared with 20 s^{-1} for the wild type enzyme. The binding of the Michaelis complex, E.Tyr.Mg.ATP, the product complex E.Tyr-AMP.PP_i and E.Tyr-AMP (tyrosyl adenylate) were not affected. Based on the kinetic results alone, it was suggested (Leatherbarrow *et al.*, 1985; Fersht *et al.*, 1986) that the loss in activity in this class of mutation is caused by the removal of an interaction specific to transition-state stabilization and not by a gross structural change in the enzyme. In order to test the above hypothesis, one would need to determine the structures of both the ground and transition-states. Since no transition-state analogue for the reaction is available, only the former structure is accessible by diffraction methods. This study was therefore devoted to the crystallographic analysis of a typical transition-state mutant, Asp→Asn-194, in its ground state.

6.1.2 Purification and Crystallisation.

TyrTS(Asp→Asn-194) was purified as described in chapter 2. Crystals obtained were typically 0.1 x 0.4 x 0.4 mm and grew in the

same form as the wild-type enzyme (Irwin et al., 1976), in 50% ammonium sulphate. A single large crystal (0.4 mm in smallest dimension) was chosen for data collection.

6.1.3 Data Collection and Structure Refinement.

A complete set of data for the complex with tyrosine was collected to 2.5 Å resolution as described in chapter 2. A total of 40935 reflections were reduced to 19181 independents giving an R-merge of 10.2%. These data were good to 2.7 Å resolution.

6.2.1 Difference Map of the Complex With Tyrosine.

Electron density maps were computed and displayed as described in chapter 2. The current residual after several cycles of restrained least squares refinement using PROLSQ (Hendrickson, 1985) is 22.7% at 2.7 Å resolution compared with 21% (2.1 Å resolution) for the native structure (Blow & Brick, 1985). Comparison of the native and mutant structures shows an overall rms difference of 0.19 Å, comprising 0.10 in main and 0.25 Å in side chains respectively. The average B value for the structure was 17.76 $Å^2$ compared with 15.66 $Å^2$ for the native enzyme. The mean temperature factor value for residue 194 rose in line with the general increase in disorder in this structure.

6.3.1 Results of Crystallographic Analysis

The crystal structure of the mutant Asp→Asn-194 shows no structural change after several cycles of refinement. Since the

replacement amino acid is iso-structural and the substitution is merely that of a nitrogen for an oxygen atom. The differences between temperature factors for mutant and wild-type enzyme are shown (Fig 6.1), along with their respective refined structures (Figs 6.2 and 6.3). The fact that very little structural change is observed is not remarkable; kinetic data (Fig 6.4) for the mutation show that the ground state is largely unaffected.

6.4.1 Discussion

Role of Asp-194- Tyrosyl-tRNA synthetase requires Mg^{++} for full catalytic activity. In the absence of Mg^{++}, wild type enzyme catalyses the formation of tyrosyl adenylate with a rate constant of $3x10^{-3}$ s^{-1} compared with 20 s^{-1} in the presence of 10 mM Mg^{++}. Irrespective of the presence or absence of Mg^{++}, both the mutants Asp→Asn-194 and Asp→Ala-194 have rate constants for tyrosyl adenylate formation of about 10^{-3} s^{-1}. The binding of the E.Tyr, E.Mg^{++}.ATP and, in Asp→Asn-194, the E.Tyr-AMP and E.Tyr-AMP.PPi complexes however, is largely unaffected by these mutations (Fig 6.4). This suggests that this residue may bind the magnesium in the transition-state of the enzyme catalysed formation of tyrosyl adenylate.

Crystallography of Asp→Asn-194- The crystal structure of Asp→Asn-194 shows no significant change in the structure of the ground state complexed with tyrosine. So far, ideas about the nature of the transition-state mutants were largely based on the interpretation of kinetic data. In tyrosyl-tRNA synthetase, there is little evidence for any gross structural change on the formation of the transition-state complex. Those residues which may move are discussed in chapter 7. With the notable exception of these residues, the major structural

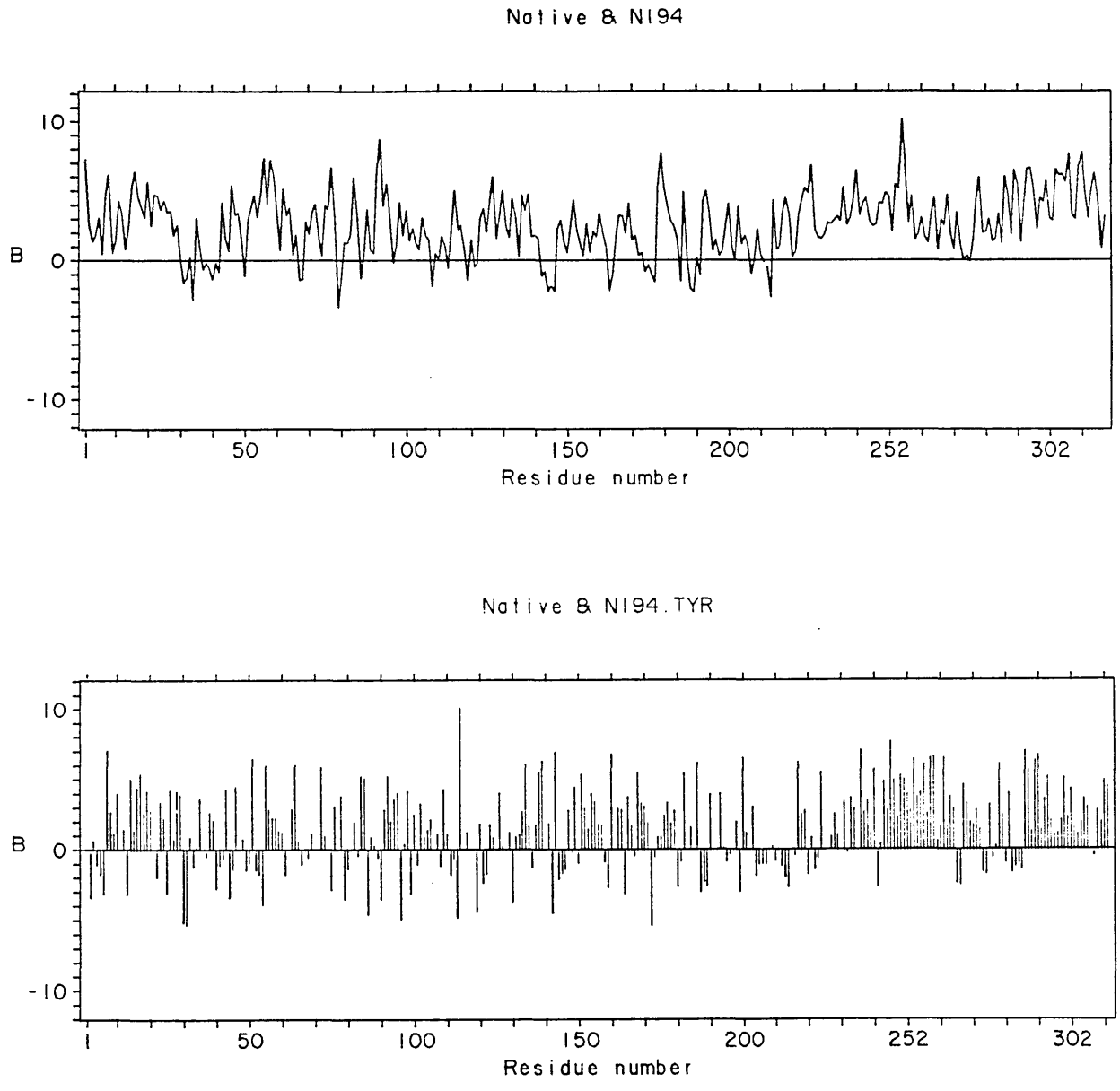


Fig 6.1 A plot of the difference between the crystallographic temperature factors for the main (above) and side chain atoms of the mutant Asp→Asn-194 and that of the native structure. This shows that the mutation is quite benign in its effect. The three main chain peaks correspond to areas of the protein which are already the most mobile in the structure.

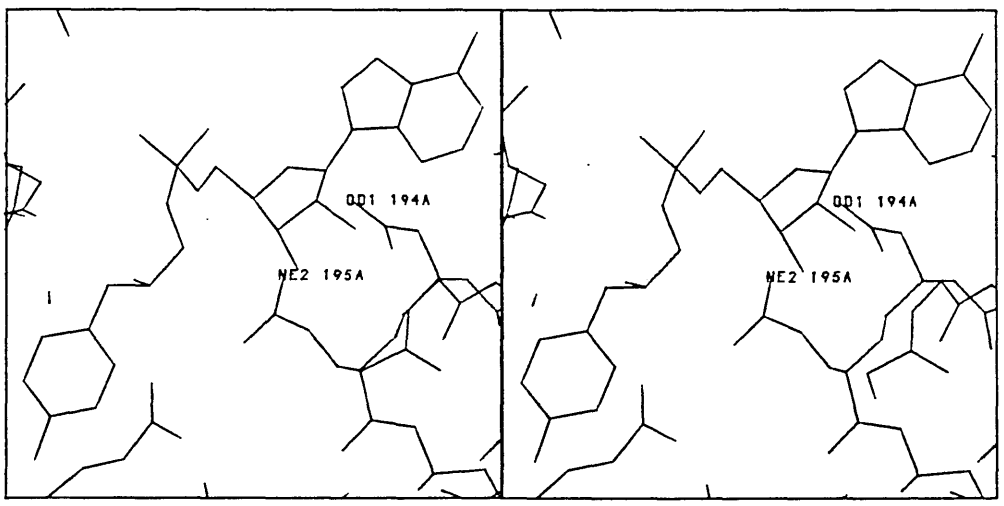


Fig 6.2 The active site region of the refined structure of tyrosyl-tRNA syntheyase complexed with the inhibitor, tyrosinyl adenylate. Residue Asp-194 is shown.

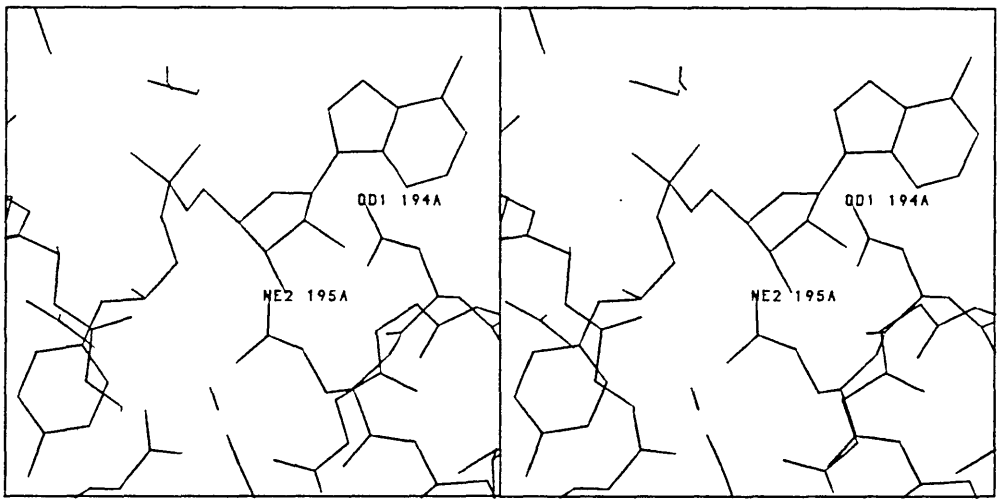


Fig 6.3 The refined structure of the mutant Asp→Asn-194.

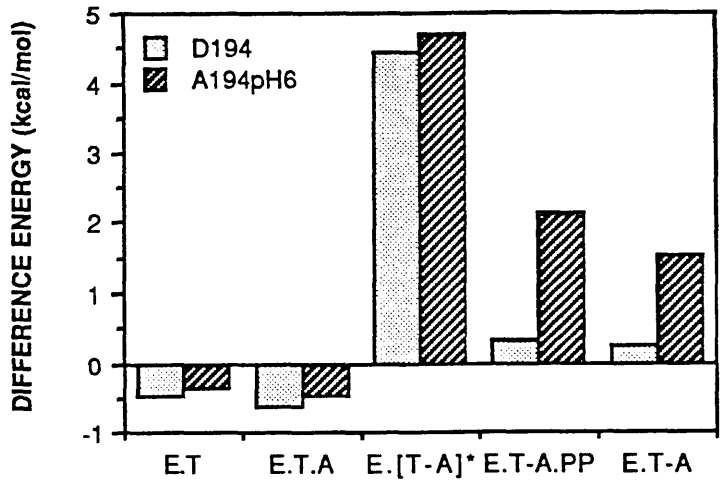


Fig 6.4 Difference free energy diagram of mutants Asp→Asn-194 and Asp→Ala-194. Kinetics were performed at pH 6 for the latter enzyme because of the instability of the E.Tyr-AMP complex.

change occuring on the formation of the transition-state complex is the change in geometry about the α-phosphorus as it is attacked by the carboxyl of the tyrosine. If, for the purposes of this argument, no change in structure of the enzyme is assumed to occur, then a simple model of the behaviour of these residues can be constructed. A transition-state mutant must be an enzyme which lacks an interaction specific to the geometry of the α and, hence (see chapter 1), β and γ phosphates, or, as discussed above, the magnesium, in the transition-state of the reaction. The removal of such interactions should create an enzyme in which transition-state stabilization (i.e. rate) alone was reduced. For removal of any such interaction to affect any of the ground states (E.Tyr.ATP or E.Tyr-AMP.PP_i) a gross structural change of the enzyme would have to occur as an artefactual result of the mutation itself. The structural change would have to be of sufficient magnitude to interfere with the geometrical arrangement of those residues which are believed to interact with any of the E.Tyr.ATP, E.Tyr-AMP.PP_i, or E.Tyr-AMP complexes (see chapter 1). Such a structural change should be detectable in the ground state. No such structural change is observed in the mutant Asp→Asn-194. This suggests that an interaction specific to transition-state stabilization has been removed, causing at most only minimal localized structural change in the transition-state itself in this class of mutation. Another argument based on kinetic data arises from the discovery of linear free energy relationships in tyrosyl-tRNA synthetase (Fersht, 1986; chapter 1). The linear free energy plot shown (Fig 6.5) has a value of $\beta=\infty$, which is what would be expected for a series of mutants which affect the rate of the reaction but not its equilibrium constant. The fact that linear free energy relationships show a general trend is useful in this case

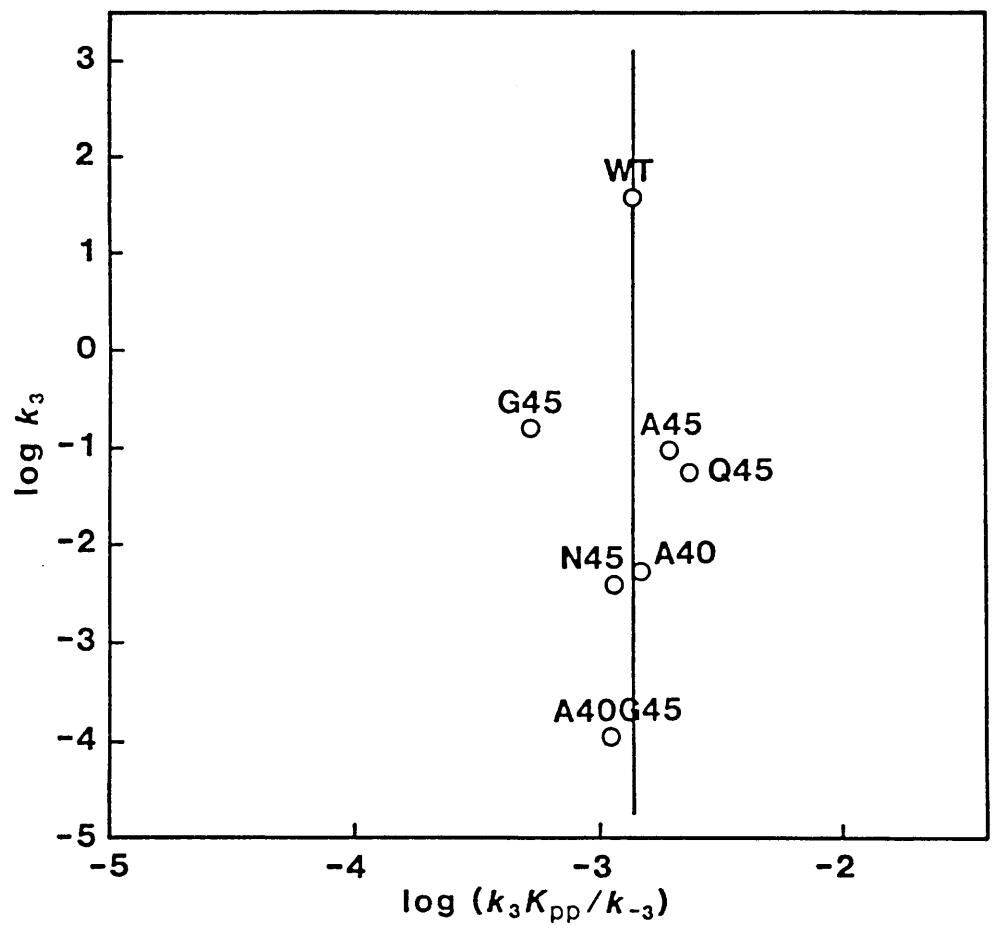


Fig 6.5 A linear free energy relationship between the E.Tyr-ATP$^{\neq}$ complex and the equilibrium constant for the formation of the E.Tyr-AMP complex. Reproduced from Fersht *et al.*, (1986).

because it is further evidence that structural perturbations caused by the mutations are likely to be small given that they are always designed to be as conservative as possible.

In spite of the above kinetic arguments, however, Gerlt (1987) has said

"*since Fersht reported no crystallographic data for any of his mutants, this correlation* (linear free energy relationship) *is exceedingly important evidence that the rather interesting conclusions about the roles of several residues in catalysis are likely to be reliable*".

The determination of this crystal structure has provided further evidence that large changes in structure of the ground state (and by inference, the transition-state) are not, on the whole, caused by conservative mutations of this class. This lends support to the "rather interesting conclusion" that they make interactions specific to the enzyme-transition-state complex.

CHAPTER 7 Transition State Model

7.1.1 Introduction

The transition-state model built from that of tyrosyl adenylate and described previously (Leatherbarrow *et al.*, 1985; chapter 1) has been further confirmed by the discovery of linear free energy relationships (LFERs) in tyrosyl-tRNA synthetase (Fersht *et al.*, 1986). They show that 79% of the binding energy used in the formation of tyrosyl adenylate is taken up in the stabilization of the transition-state for the reaction. This strongly suggests that the structure of tyrosyl adenylate and the transition-state for its formation are similar. Recent work has shown, however, that the model could be augmented. Studies of the mobile loop region of tyrosyl-tRNA synthetase, notably residues Lys-82, Arg-86, Lys-230, Lys-233 and Glu-235, suggest that these residues contribute binding energy to the transition-state for tyrosyl adenylate formation (Fersht *et al.*, 1988). Residues 230, 233 and 235 are 10-15 Å away from the phosphate moiety of tyrosyl adenylate as revealed by X-ray crystallography. Hence a complete model of the transition-state for the reaction will require modelling the loop region in a closed conformation and a Mg^{++} site coordinated to Asp-194 (discussed in detail in preceding chapter). In this chapter we present such a model.

7.1.2 Model Building.

Modelling of the mobile loop region of tyrosyl-tRNA synthetase was carried out using the program FRODO (Jones, 1985) and the

procedure described in Jones & Thirup (1986). A rough model of the α-carbon backbone of the region 220 to 240 of the sequence of tyrosyl tRNA synthetase (Winter *et al.*, 1982) was constructed using FRODO. Then segments of six or seven residues were matched with structurally homologous regions of known crystallographically determined proteins. This procedure was repeated through the target sequence. Segments were chosen which allowed the residues of interest (230 and 233) to make interactions with the phosphate binding site of the enzyme. The geometry of the joined segments was regularized and then the matching procedure was repeated again, staggering the segments matched in the previous cycle of model building. Eventually, a polypeptide segment was arrived at which displayed plausible backbone geometry when plotted on a Ramachandran diagram (Ramakrishnan & Ramachandran, 1965). Side chain conformations were chosen to be both chemically and geometrically reasonable. As far as possible the chi angles of all modelled side chains were engineered to fall within the limits and classes described in Ponders & Richards (1987). The side chains of Lys-82, Arg-86 and Asp-194 were also adjusted, but the main chain was left unchanged.

7.2.1 Results of Model Building

The current model of the complex between tyrosyl-tRNA synthetase and the substrate tyrosyl adenylate is shown (Fig 7.1) (Rubin *et al.*, 1981). The model of the transition-state described by Leatherbarrow *et al.*, 1985 (see chapter 1) implicated residues Thr-40 and His-45 in the binding of the proposed penta-coordinate transition-state (Fig 7.2). Subsequent mutagenesis studies (Leatherbarrow *et al.*, 1985) showed these

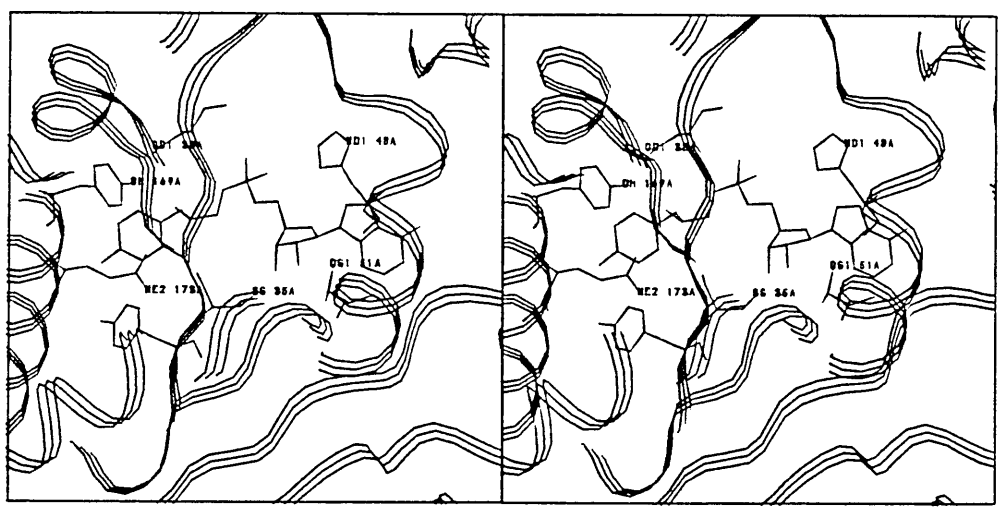


Fig 7.1 The active site region of the refined structure of tyrosyl-tRNA synthetase complexed with the inhibitor, tyrosinyl adenylate.

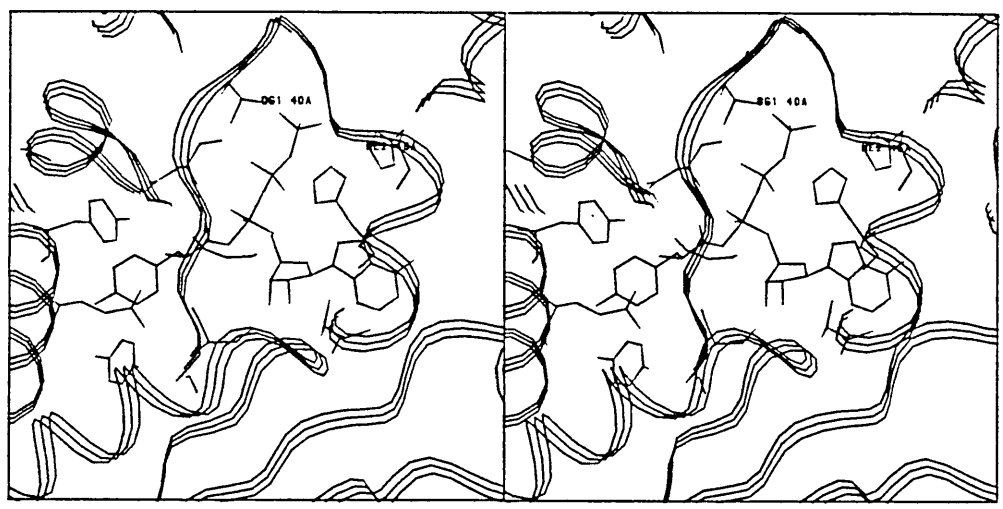


Fig 7.2 The penta-coordinate transition-state as described in Leatherbarrow *et al.*, (1985).

residues to contribute almost all of their binding energy to transition-state stabilization. Further work (Fersht *et al.*, 1988) deleting residues Lys-82, Arg-86, Lys230 and Lys 233 showed that these groups contributed about 3, 5, 3.5 and 5 kcal/mol to the transition-state for the formation of tyrosyl adenylate respectively (Fig 7.3). These residues all correspond to regions of the molecule which have the highest crystallographic temperature factors (Fersht, 1988) and the entire loop region containing residues 230 and 233 is disordered in the wild type crystal structure (Fig 7.4). This loop region (Fig 7.5) was proposed to fold over and bind the phosphate moiety of the transition-state (Fersht *et al.*, 1988) in an induced fit mechanism. A possible model of the folded loop conformation is shown (Fig 7.6). A detailed model of the active site region (Fig 7.7) shows the magnesium coordinated to the β and γ phosphates and solvent. This is in accordance with previous work (Connolly *et al.*, 1980) which showed the magnesium to be coordinated β/γ rather than α/β in yeast phenylalanyl-tRNA synthetase. The β and γ phosphates of the pentacoordinate transition-state as modelled by Leatherbarrow have been moved in order to permit Asp-194 to interact with the magnesium via solvent. This arrangement necessarily involves the introduction of bridging waters between residues Thr-40 and His-45 to bind the phosphates. This may at first seem to be a compromise between the work of Leatherbarrow and data for the mutants at position 194 (described in chapter 6), but it has already been suggested (Fersht, 1988) that water molecules are released during the course of the reaction.

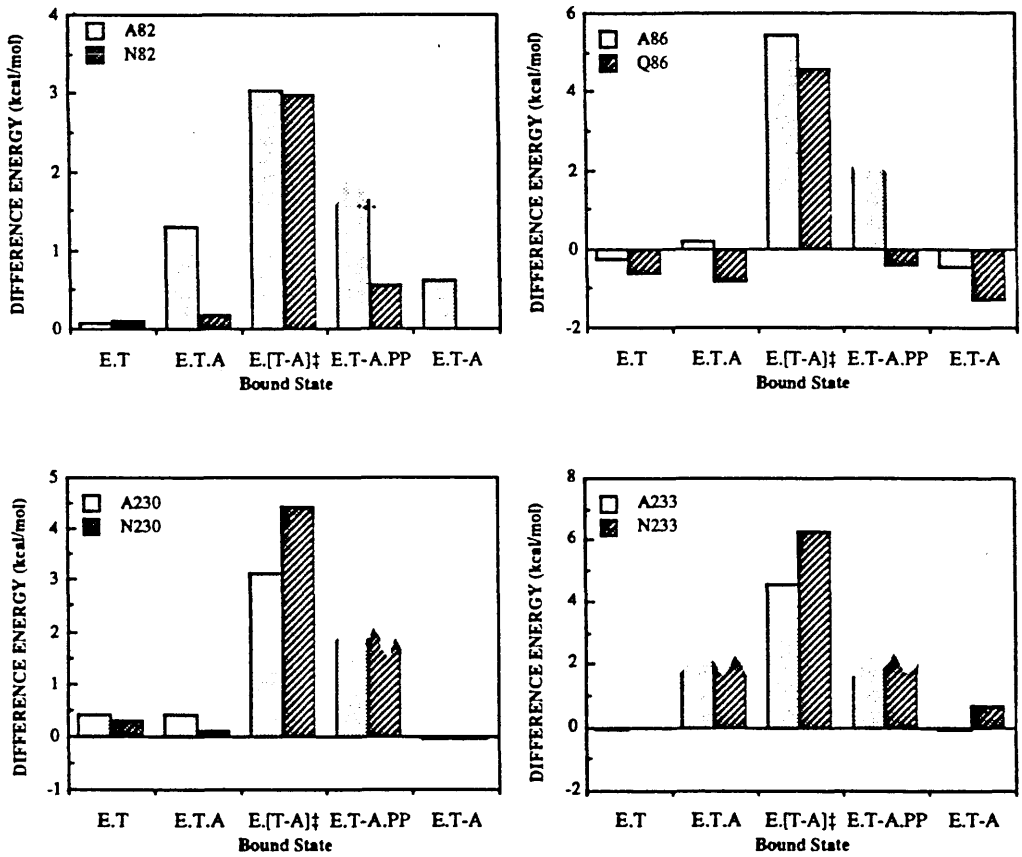


Fig 7.3 Difference free energy diagrams for the active site mutants Lys→Ala or Asn-82; Arg→Ala or Gln-86; also Lys→Ala or Asn-230 and Lys→Ala or Asn-233 which are in the mobile loop. Severed bars indicate that enzyme complex bound too weakly to allow accurate kinetic determinations to be made. Reproduced from Fersht *et al.*, (1988).

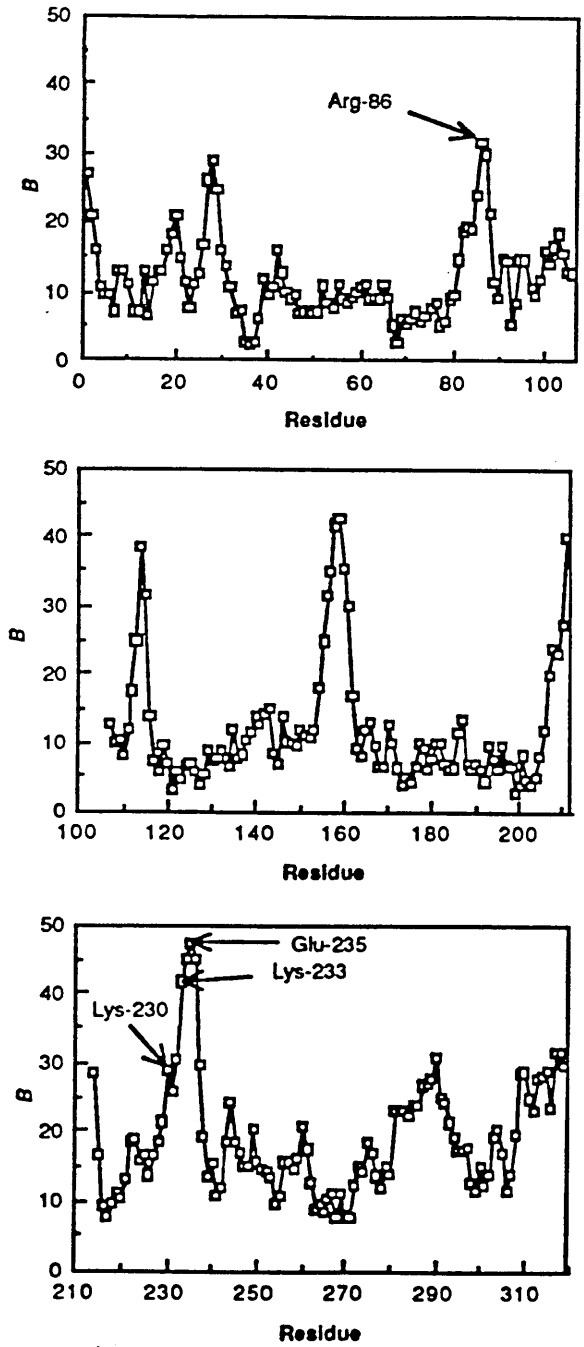


Fig 7.4 Crystallographic temperature factors for main chain. B values averaged for backbone C, N and C_α taken from Brick & Blow (1987) and unpublished data.

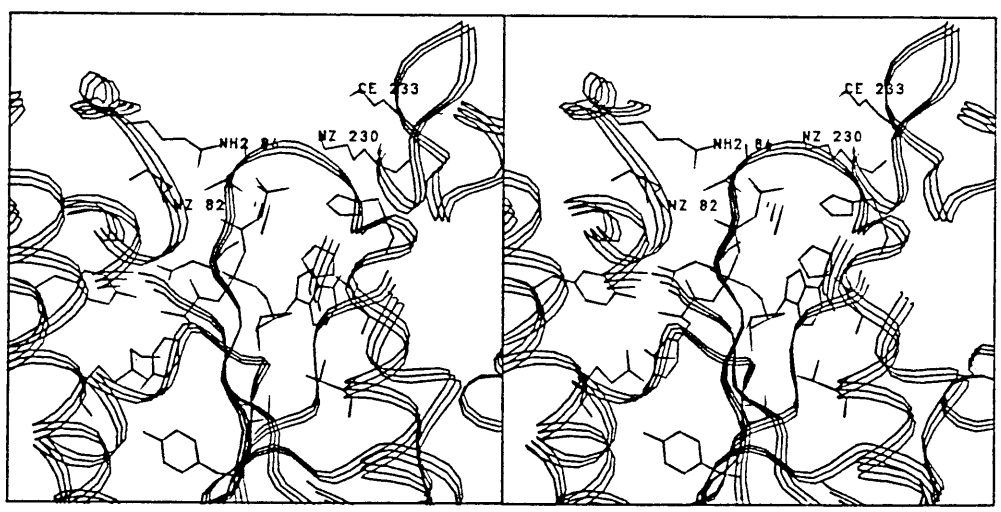


Fig 7.5 Representation of the active site region of tyrosyl-tRNA synthetase showing lysines 82, 230, 233 and arginine 82.

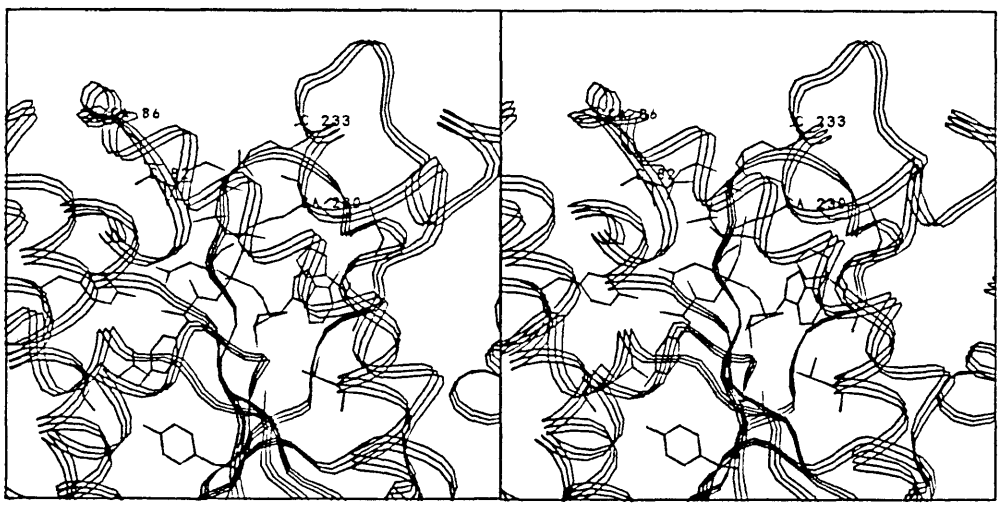


Fig 7.6 Representation of a model of the folded loop conformation of tyrosyl-tRNA synthetase. Note the interactions made between residues 82, 86, 230, 233 and the β and γ phosphates of the penta-coordinate transition-state.

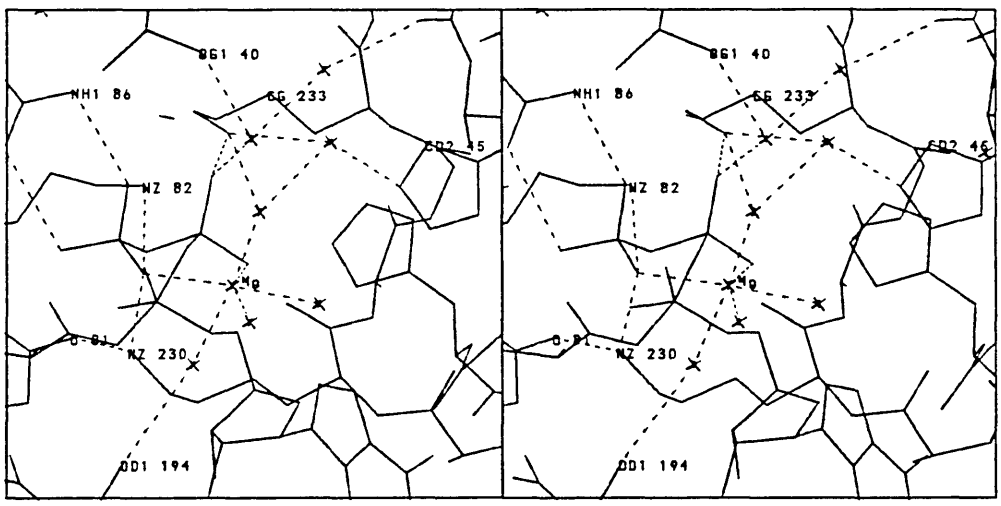


Fig 7.7 A close up view of Fig 7.6, concentrating on the active site region around the α, β and γ phosphates of the penta-coordinate transition-state. Residues 82, 86, 194, 230 and 233 are shown. The magnesium is coordinated to four water molecules and the oxygens of the β and γ phosphates. The penta-coordinate α-phosphate is at the back of the figure.

7.3.1 Discussion

The construction of this model was designed to answer a few elementary questions. Could the mobile loop region be successfully modelled into a conformation which allowed lysines 230 and 233 to interact with the phosphates of the pentacoordinate transition-state? The answer is yes. However, another residue, Glu-235, was mutated in along with Lys-82, Arg-86, Lys-230 and Lys-233 (Fersht, 1988) and was found to contribute several kcal/mol to the E.Tyr.ATP complex and 1.8 kcal/mol to transition-state stabilization. It was proposed (Fersht, 1988) that Glu-235 could interact with the magnesium in the Michaelis complex and the transition-state respectively. The modelling efforts reported here suggest, however, that it would be difficult to build residues 230 233 and 235 in any conformation remotely resembling a published crystallographically determined sequence while simultaneously stabilizing the phosphates and the magnesium. Glu-235 probably interacts with the magnesium in the Michaelis complex and then relinquishes it to Asp-194 in the transition-state. The interaction energy in the transition-state is only 1.8 kcal/mol, and this may represent a subtle interaction within the loop stabilizing it in the closed conformation.

A second question was the role of Asp-194. It has been shown that a chemically reasonable model of the penta-coordinate transition-state could be built where the magnesium interacts with the β and γ phosphates and Asp-194, albeit via a water molecule. Furthermore, interactions based on other mutagenesis work can also be modelled simultaneously and overall the results of work from a diverse range of experiments on the tyrosyl-tRNA synthetase seems to have

enough internal self-consistency to allow the construction of such a model.

Another aim of this study was to identify further residues to mutate and further probe the enzyme. However, it is not possible to test the validity of the model by further mutagenesis as the residues implicated in transition-state stabilization all have long side chains and do not seem to be involved in intra-chain hydrogen-bond networks.

CHAPTER 8 Conclusions

In this study, no gross changes in structure were caused by any of the single amino acid mutations subjected to crystallographic analysis. Such alterations which did occur involved rearrangements of side-chains around the mutated residue. Such small changes in structure are not easy to detect by other techniques such as NMR spectroscopy. The fact that they can be determined, however, allows protein engineering experiments to be interpreted at the molecular level. What are the implications of such structural changes? The catalytic groups of most enzymes are side chains, and a precise knowledge of the geometry of the active site region is vital for mechanistic studies in many cases. A mutation which affects the conformation of an active site residue involved in the formation of an enzyme bound covalent intermediate could cause a large reduction in catalytic activity, yet leave the gross tertiary structure of the enzyme unaffected. The precise determination of such an effect is only possible by X-ray crystallography. Local rearrangements in structure can make protein engineering experiments more difficult or even impossible to interpret. For example, in the mutant Cys→Gly-35, the fact that the two sets of double mutant data were consistently non-additive by 0.4 kcal/mol could have been coincidental. Determination of the crystal structures of the enzyme complexed with tyrosine, however, prompted the construction of the final cycle appearing in Fig 3.7; this suggested that residues 35 and 51 behaved independently of one another if Cys-35 was mutated to glycine and Thr-51 to either cysteine or proline. In the case where there was a glycine at residue 35 and a threonine at residue 51, then there was an interaction between the two worth 0.4 kcal/mol. The structure of the complex with tyrosyl adenylate showed that the mechanistic interpretation was that of a perturbation effect, rather than a

permanent change in structure of the enzyme. Dissection of structure-activity relationships in this detail for mutant enzymes is not possible by kinetic analysis alone. Arguments put forward to explain the behaviour of mutant enzymes rely on assumptions about their effect on the structure of the enzyme as well as its function. Linear free energy relationships are probably the most convincing evidence from kinetic studies that gross structural perturbations have not occured in the construction of the mutants of the tyrosyl-tRNA synthetase described in this thesis. Fine structure analysis, however, requires X-ray crystallography. For example, it was always assumed that transition-state mutants (defined in chapter 6) such as Thr→Ala-40, His→Asn-45, or Asp→Asn-194 caused little or no perturbation in the structure of the ground state. In the case of Asp→Asn-194, although the crystallographic result is very trivial it provides structural information which is of vital importance to the mechanistic enzymologist that cannot be derived or inferred from other sources in such a manifest and detailed way. Similarly, with the mutant Tyr→Phe-34 the aim was to use crystallography to show that two criteria were fulfilled at the molecular level. The first was to discover whether a structural change had occured as a result of the mutation. The second was if the X-ray analysis would unambiguously reveal whether or not a water molecule had been trapped in the active site of the enzyme. If these two conditions could be satisfied, as far as the enzymologist was concerned, a clear picture of this mutant would appear; either the free energy of a paired or unpaired hydrogen bond had been determined.

The effect of mutations at residue Thr-51 of tyrosyl-tRNA synthetase has been analysed in detail by K. Brown (Brown & Blow, 1986; Brown, 1988). The mutants Thr→Ala-51, Thr→Cys-51, Thr→Pro-51 have k_{cat}/K_M values which, in ascending order, are higher than that of

the wild type enzyme. Furthermore, the mutants Thr→Gly-51 and Thr→Ser-51 both have lower values than that of the wild type enzyme. The theory put forward in Brown (1988) is that non-polar interactions rather than hydrogen bonds contributed to the enhanced binding of transition-state and tyrosyl adenylate in these mutants. This may well be the case for Thr→Ala-51 and Thr→Pro-51, but in the case of Thr→Cys-51 the extra binding energy may also arise from the creation of a new hydrogen bond interaction between the sulphur of the cysteine and the 3'OH group of the ribose moiety of tyrosyl adenylate. Of course, without a crystal structure of the reduced sulphydryl form complexed with tyrosyl adenylate it remains speculative, but there is no hint from kinetic or crystallographic data that the conformation of the Cys-51 would change significantly on the formation of tyrosyl adenylate.

The extent to which assumptions made about a protein engineering experiment occur in reality, and whether the measurements made are quantitative is central to the above discussion. A kinetic analysis of a mutant enzyme results in a set of apparent free energy changes, relative to the wild-type molecule, across the experimentally accessible stages of the reaction pathway. Until crystal structures of each stage on the reaction pathway have been determined, efforts to relate apparent binding energies of groups on the enzyme to theoretical models of their function must be undertaken with care. Conclusions about the contribution of particular residues, and to a lesser extent, general trends of a series of mutants must be made with caution. The existence of linear free energy relationships and double mutant data may lend strong support for a particular theory, but in the final analysis direct structural evidence is always necessary.

It is likely that model-building will always be required to help understand the catalytic behaviour of enzymes. Even when detailed

kinetic studies have are possible, and high resolution structures of the free and substrate bound enzyme are available, it can be difficult to unravel the catalytic mechanism. Model building can provide structures of putative intermediates based on known crystallographically determined enzyme substrate or product complexes. Protein engineering experiments can be used to test such models and if the results allow an unambiguous interpretation, then such model building is easily justified. It becomes less easy to defend, however, when the results of model building are inconclusive, or suggest no further experiments that can be done on the enzyme. The model described in chapter 7 showed fairly conclusively that the mobile loop region could bind the β and γ phosphates of the penta-coordinate transition-state described in chapter 1 (Leatherbarrow *et al.*, 1985), but it is difficult to identify further residues for study by protein engineering.

REFERENCES

Alber, T., Dao-pin, S. Wilson, K., Wozniak, J. A., Cook, S. P. & Matthews, B. W. (1987) *Nature 330*, 41-46.

Barker, D. G., & Winter, G. (1982) *FEBS Lett. 145*, 191-193.

Brown, K. A. (1988) Ph. D. thesis, University of London.

Brown, K. A., Brick, P. & Blow, D. M. (1987) *Nature 326*, 416-418.

Bhat, T. N. Blow, D. M., Brick, P., & Nyborg, J. (1982) *J. Mol. Biol. 158*, 699-709.

Blow, D. M., & Brick, P. (1985) in *Biological Macromolecules and Assemblies: Nucleic Acids and Interactive Proteins* (Jurnak, F., & McPherson, A., Eds.) Vol. 2, pp 442-469, Wiley, New York.

Brick, P., & Blow, D. M. (1987) *J. Mol. Biol. 194*, 287-297.

Bryan, P. N., Rollence, M. L., Pantoliano, N. W., Wood, J., Finzel, B. C., Gilliland, G. L., Howard, A. J., & Poulos, T. L. (1986) *Proteins: Structure, function and Genetics 1*, 326-334.

Calendar, R., & Berg, P. (1966) in *Procedures in Nucleic Acids Research* (Cantoni, G. L., & Davies, D. R., Eds.) p 384, Harper & Row, New York.

Carter, P. & Wells, J. A., (1987) *Science 237*, 394-399

Carter, P. & Wells, J. A., (1988) *Nature*, in press.

Carter, P. J., Winter, G., Wilkinson, A. J., & Fersht, A. R. (1984) *Cell (Cambridge, Mass) 38*, 835-840.

Connolly, B. A., Von der Haar, F., Eckstein, F. (1980) *J. Biol. Chem. 255*, 11301-11307.

Fersht, A. R., (1975) *Biochemistry 14*, 5-12.

Fersht, A. R., (1975), Mulvey, R. S., & Koch, G. L. E. *Biochemistry 14*, 13-18.

Fersht, A. R. (1985), *Enzyme Structure and Mechanism*, W. H. Freeman, New York and Oxford, U. K., *chapter 2.*

Fersht, A. R. (1987), *Biochemistry, 26*, 8031-8037.

Fersht, A. R. (1988), *Biochemistry, 27*, 1577-1580.

Fersht, A. R., Ashford, J. S., Bruton, C. J., Jakes, R., Koch, G. L. E., Hartley, B. S. (1975) *Biochemistry 14* 1-13.

Fersht, A. R., Shi, J. P., Knill-Jones, J., Lowe, D. M., Wilkinson, A. J., Blow D. M., Brick P., Carter P., Waye M. M. Y., & Winter G. (1985)a *Nature (London) 316*, 656-657.

Fersht, A. R., Wilkinson, A. J., Carter P. J. & Winter, G. (1985)b *Biochemistry 24*, 5858-5861.

Fersht, A. R., Leatherbarrow, R. J., & Wells, T. N. C. (1986) *Nature (London) 322*, 284-286.

Fersht, A. R., Knill-Jones, J. W., Bedouelle, H. & Winter, G. (1988) *Biochemistry, 27*, 1581-1587.

Fox, G. C., & Holmes, K. C. (1966) *Acta Crystallogr. sect A 20*, 886-891.

Gibson, T. (1984) Ph D. thesis, University of Cambridge.

Gerlt, J. A., (1987), *Chem. Rev., 87*, 1079-1105.

Grutter, M. G., Gray T. M., Weaver, L. H., Alber, T., Wilson, K. & Matthews, B. W. (1987) *J. Mol. Biol. 197*, 315-329.

Hendrickson, W. A. & Konnert, J. H. (1980) In *Computing in Crystallography* (Diamond, R., Ramasethan, S. & Venkatesan, K., eds), pp 13.01-13.23, Indian Academy of Sciences, Bangalore.

Hendrickson, W. A. (1985) *Met. Enzymol. 115* pp 253-270.

Ho, C. K. & Fersht, A. R. (1986) *Biochemistry 25*, 1891-1897.

Irwin M. J., Nyborg, J., Reid, B. R., & Blow D. M. (1976) *J. Mol. Biol. 105*, 577-586.

Jones, T. A. (1985) *Met. Enzymol. 115* pp 157-171.

Jones, T. A. (1986) *EMBO J. 5 (4)*, 819-822.

Laemmli, U. K., (1970) *Nature, 227* 680-685.

Lau, F. T. K., (1988) Ph. D. thesis, University of London.

Leatherbarrow, R. J. & Fersht, A. R. & Winter, G. (1985) *Proc. Natl. Acad. Sci. USA. 82*, 7840-7844.

Leatherbarrow, R. J. & Fersht, A. R. (1986) *Protein Engineering, 1*, 7-16.

Leberman, R., Berthet-Colominas, C., Cusack, S., & Hartlein, M. (1987) *J. Mol. Biol. 193*, 423-425.

Leslie, A. G. W. (1987). In: *Computational Aspects of Protein Crystal Data Analysis*, (Helliwell, J. R., Machin, P. A., & Papiz, M. Z., eds), pp 39-50, SERC, Daresbury.

Lowe, G., & Tansley, G., (1984) *Tetrahedron Lett.*, 113-117.

Lowe, D. M., Fersht, A. R., Wilkinson, A. J., Carter, P., & Winter, G. (1985) *Biochemistry 24*, 5106-5109.

Matsumura, M., Becktel., W. J. & Matthews, B. W., (1988) *Nature 334*, 406-410.

McPherson, A. (1982) *The Preparation and Analysis of Protein Crystals* Wiley, New York.

Messing, J. (1979) *Recombinant DNA tech. bull. 2*, 43-48.

Messing, J. (1983) *Met. Enzymol. 101*, 20-78.

Messing, J., Crea, R. and Seeburg, P. H. (1981) *Nucleic Acids Res., 9* 309-321.

Monteilhet, C., Blow, D. M. & Brick, P. (1984) *J. Mol. Biol. 173*, 477-485.

Nyborg, J., & Wonnacott, A. J. (1977) *The Rotation Method in Crystallography* North-Holland, Amsterdam.

Perona, J. J., Robert, S., Steitz, T. A., & Soll, D. (1988) *J. Mol. Biol. 202*, 121-126.

Ponder, J. W., & Richards, F. M. (1987) *J. Mol. Biol. 193*, 775-791.

Ramakrishnan, C. & Ramachandran, G. N. (1965) *Biophys. J. 5*, 909-933.

Rubin, J., & Blow, D. M., (1981) *J. Mol. Biol. 145*, 489-500.

Russel, M., Kidd, S. & Kelly, M. R. (1986) *Gene 45*, 333-338.

Villafranca, J. E., Howell, E. E., Oatley, S. J., Xuong, N. & Kraut, J. (1987) *Biochemistry 26*, 2182-2189.

Waye, M. M. Y., Winter, G., Wilkinson, A. J. & Fersht, A. R. (1983) *EMBO J. 2*, 1827-1829.

Wells, T. N. C. (1987) Ph. D. thesis *chapter 6*, University of London.

Wells, T. N. C., & Fersht, A. R. (1986) *Biochemistry 25*, 1881-1886.

Wetzel, R. (1987) *TIBS 12*, 478-482.

Winter, G., Fersht, A. R., Wilkinson, A. J., Zoller, M., & Smith, M. (1982) *Nature (London) 299*, 756-758.

Winter, G., Koch, G. L. E., Hartley, B. S., & Barker, D. G., (1983) *Eur. J. Biochem., 132* 383-387.

Zelwer, C., Risler, J. L., & Brunie, S. (1982) *J. Mol. Biol. 155*, 63-81.

Zoller, M. J., & Smith, M. (1983) *Met. Enzymol., 100*, 468-501.

Appendix A: Details of Data Collected on Mutant Enzymes.

Enzyme	Cys→Gly-35	Cys→Gly-35	Asp→Asn-194
Crystallisation[1]	Tyrosine (1 mM)	Tyr (1 mM) ATP (50mM)	Tyr (1 mM)
Mother liquor[2]	"	Tyr (1 mM) ATP (10 mM)	"
Wavelength (Å)	0.88	1.488	1.488
Temperature (° C)	-5	-5	-5
Collected Resolution (Å)	2.5	2.5	2.5
Accepted Resolution (Å)	2.5	2.7	2.7
Number of film packs	14	14	14
Oscillation range (°)	2.5	2.5	2.5
Number of measurements	43782	42188	40935
Number of independents	20549	19912	19181
Merging R-factor[3]	5.3%	10.6%	10.2%
Cell dims[4].	64.58	64.43	64.52
(Å)	238.11	238.57	237.89

[1] In addition to the above, the following reagents were present in all crystallization trials; 50% ammonium sulphate, 100 mM Tris-acetate pH 7.3 and 10 mM $MgCl_2$.

[2] As in 1 above, except mother liquor contained 55% ammonium sulphate.

[3] This defined to be $\Sigma(I(i)- \langle I \rangle)/\Sigma I(i)$, where I(i) are the intensity values of actual measurements, and <I> their respective mean values.

[4] Upper figure is for *a* and *b* axes, lower is that of the *c* axis.

Appendix A (contd.)

Enzyme	Thr→Cys-51	Thr→Cys-51	Tyr→Phe-34
Crystallisation†	Tyramine (17 mM) (ATP 50 mM)	Tyr (1 mM)	Tyr (1 mM)
Mother liquor†	"	Tyramine (17 mM) ATP (50 mM)	"
Wavelength (Å)	1.488	1.488	0.88
Temperature (° C)	-5	-5	4
Collected Resolution (Å)	2.5	2.5	2.5
Accepted Resolution (Å)	2.5	2.7	2.7
Number of film packs	14	14	14
Oscillation range (°)	2.5	2.5	2.3
Number of measurements	42874	43029	52718
Number of independents	19980	20047	19113
Merging R-factor†	6.3%	10.6%	8.4%
Cell dims†.	64.5	64.35	95.30*
(Å, °)	238.1	238.77	67.26*
-			61.30*
-			β=90.82

† Footnotes as in preceding page, except for the mutant Tyr→Phe-34, where the crystallisation was performed in the presence of 12% polyethylene-glycol (PEG), 100 mM Tris-acetate, pH 7.3 and 10 mM $MgCl_2$. Mother liquor was as above, except 14% PEG was used. The cell dimensions similar to the monoclinic form previously reported (Brick & Blow, 1987).

* These are the *a*, *b* and *c* axes, respectively, of the monoclinic form.

Appendix B: Refinement Statistics for Mutant Enzymes.

Enzyme		Cys→Gly-35	Cys→Gly-35	Asp→Asn-194
Ligand		Tyrosine I*	Tyrosine II*	Tyrosine
R-factor		24.3%	23.6%	22.4%
Resolution (Å)		6.0-2.5	6.0-2.5	6.0-2.7
Deviations[1] from ideality	σ	rms	rms	rms
Distances (Å)				
Bonds (1-2) neighbour	0.02	0.013	0.013	0.013
Angles (1-3) neighbour	0.04	0.047	0.046	0.050
Intraplanar (1-4) neighb.	0.05	0.050	0.049	0.053
Planar groups (Å)	0.02	0.012	0.012	0.013
Chiral centres ($Å^3$)	0.15	0.14	0.14	0.14
Torsion angles (deg.)				
Staggered[2]	15	18.2	18.2	19.2
Transverse[3]	45	29.5	29.6	29.8
Contacts (Å)				
Single torsion	0.5	0.20	0.20	0.21
Multiple Torsion	0.5	0.31	0.29	0.29
Thermal factors ($Å^2$)				
Main-chain[4] bond	1.5	2.51	2.47	2.60
Main-chain[5] angle	2.25	3.85	3.85	4.11
Side-chain bond	1.5	3.04	2.99	3.14
Side-chain angle	2.25	4.52	4.46	4.77

* I and II are independently refined structures of the two alternate conformations of Thr-51 in the mutant Cys→Gly-35 (chapter 3); conformation I is similar to that of the native enzyme, and conformation II differs.

[1] The values of σ given are those input to the refinement program and determine the relative weights of the corresponding geometric restraints (Hendrickson & Konnert, 1980). The root-mean-square (rms) deviations from ideality of the refined structure are quoted.

[2] e.g., aliphatic $\chi 1$.

[3] e.g., aromatic $\chi 2$.

[4] (1-2) neighbour.

[5] (1-3) neighbour.

Appendix B: (contd.)

Enzyme		Cys→Gly-35	Cys→Gly-35
Ligand		Tyr-AMP I*	Tyr-AMP II*
R-factor		23.9%	23.6%
Resolution (Å)		6.0-2.7	6.0-2.7
Deviations† from ideality	σ	rms	rms
Distances (Å)			
Bonds (1-2) neighbour	0.025	0.017	0.017
Angles (1-3) neighbour	0.035	0.038	0.038
Intraplanar (1-4) neighb.	0.05	0.042	0.041
Planar groups (Å)	0.02	0.012	0.012
Chiral centres ($Å^3$)	0.15	0.15	0.15
Torsion angles (deg.)			
Staggered†	15	18.5	18.9
Transverse†	45	29.9	30.3
Contacts (Å)			
Single torsion	0.3	0.19	0.19
Multiple Torsion	0.3	0.27	0.27
Thermal factors ($Å^2$)			
Main-chain† bond	1.75	2.44	2.47
Main-chain† angle	2.25	3.73	3.77
Side-chain bond	2.0	3.11	3.16
Side-chain angle	2.5	4.54	4.59

* I and II are identical to those in the preceding table except the mutant, Cys→Gly-35, is complexed with tyrosyl adenylate instead of tyrosine.

† Footnotes as in preceding table.

Enzyme		Thr→Cys-51	Thr→Cys-51
Ligand		Tyramine	Tyr-AMP
R-factor		23.3%	22.4%
Resolution (Å)		6.0-2.5	6.0-2.7
Deviations† from ideality	σ	rms	rms
Distances (Å)			
Bonds (1-2) neighbour	0.025	0.026	0.024
Angles (1-3) neighbour	0.035	0.053	0.035
Intraplanar (1-4) neighb.	0.05	0.064	0.050
Planar groups (Å)	0.02	0.016	0.016
Chiral centres ($Å^3$)	0.15	0.17	0.18
Torsion angles (deg.)			
Staggered†	15	19.1	19.6
Transverse†	45	28.0	31.7
Contacts (Å)			
Single torsion	0.3	0.20	0.20
Multiple Torsion	0.3	0.28	0.27
Thermal factors ($Å^2$)			
Main-chain† bond	1.75	1.38	1.55
Main-chain† angle	2.25	2.23	2.58
Side-chain bond	2.0	2.20	2.28
Side-chain angle	2.5	3.25	3.55

† Footnotes as in preceding table.

Enzyme		Tyr→Phe-34
Ligand		Tyrosine
R-factor		17.9%
Resolution (Å)		8.0-2.7
Deviations† from ideality	σ	rms
Distances (Å)		
Bonds (1-2) neighbour	0.02	0.018
Angles (1-3) neighbour	0.03	0.044
Intraplanar (1-4) neighb.	0.05	0.056
Planar groups (Å)	0.02	0.017
Chiral centres ($Å^3$)	0.15	0.18
Torsion angles (deg.)		
Staggered†	15	18.3
Transverse†	45	30.3
Contacts (Å)		
Single torsion	0.3	0.19
Multiple Torsion	0.3	0.28
Thermal factors ($Å^2$)		
Main-chain† bond	1.5	3.35
Main-chain† angle	2.25	5.10
Side-chain bond	1.50	3.91
Side-chain angle	2.25	6.00

† Footnotes as in preceding table.

Appendix C: Definitions of ΔG_{app} and ΔG_{bind} (from Fersht, 1988a).

ΔG_{bind}

In the following system,

$$E\text{-}X.w + w.Y\text{-}S \lesseqgtr E\text{-}X.Y\text{-}S + w.w$$

$$\Delta G_{bind} = G_{X.Y} + G_w - G_{X.w} - G_{Y.w}$$

This can be thought of as the free energy change in X and Y going from the solvated to the bound state.

ΔG_{app}

By experiment,

$$\Delta G_{app} = RT\ln(K_S/K'_S)$$

where K_S and K'_S are the measured dissociation constants of the ES (wild-type) and ES' (mutant) complexes (likewise notation for intermediate species) respectively (Wells and Fersht, 1986).

In contrast with the scheme for ΔG_{bind}, which looks specifically at the binding species, the general case for ΔG_{app} above leads to the following;

$$\Delta G_{app} = (G_{E'}-G_E) - (G_{E'S}-G_{ES})$$

where the free energy of whole E and ES complexes are considered. ΔG_{app} is then a measure of the net dissociation energy of the binding reaction combined with any energy associated with changes in protein or solvent structure, as a result of the mutagenesis.

If E and E' are identical in structure, and the substrate (Y) remains hydrated when it binds to E', then $\Delta G_{app} = \Delta G_{bind}$ for this process, when the donor and acceptor species are uncharged.

Appendix D: Bacterial Strains and Media.

Bacterial strains

Strain	Genotype
E. coli TG2 (Gibson, 1984)	K12, Δ(lac-proAB), *thi*, *sup*E, *hsd*Δ5, *Rec*A, *sr*1::Tn 10, [F', *tra*D36, *pro*AB, *lac*Iq, *lac*Z ΔM15]
E. coli JM101 (Messing, 1979)	K12, Δ(lac-proAB), *thi*, *sup*E, [F', *tra*D36, *pro*AB, *lac*Iq, *lac*Z ΔM15]
E. coli HB101F (Russell *et al.*, 1986) (Lau, 1988)	K12, *pro*, *leu*, *thi*, *lac*Y *hsd*20, *end*A, *rec*A, *rps*L20(*str*^{r}) *ara*-14, *gal*K2, *xyl*-5, *mtl*-1, *sup*E44, [F', *kan*R]

Media

Broth: 2 x TY broth was made up of the following ingredients; 16 g bacto-tryptone (Difco), 10 g yeast extract (Difco) and 5 g NaCl per litre of tap water. For culture of *E. coli* HB101F, kanamycin was added at a concentration of 50 mg/L, after freshly sterilized media had cooled to room temperature.

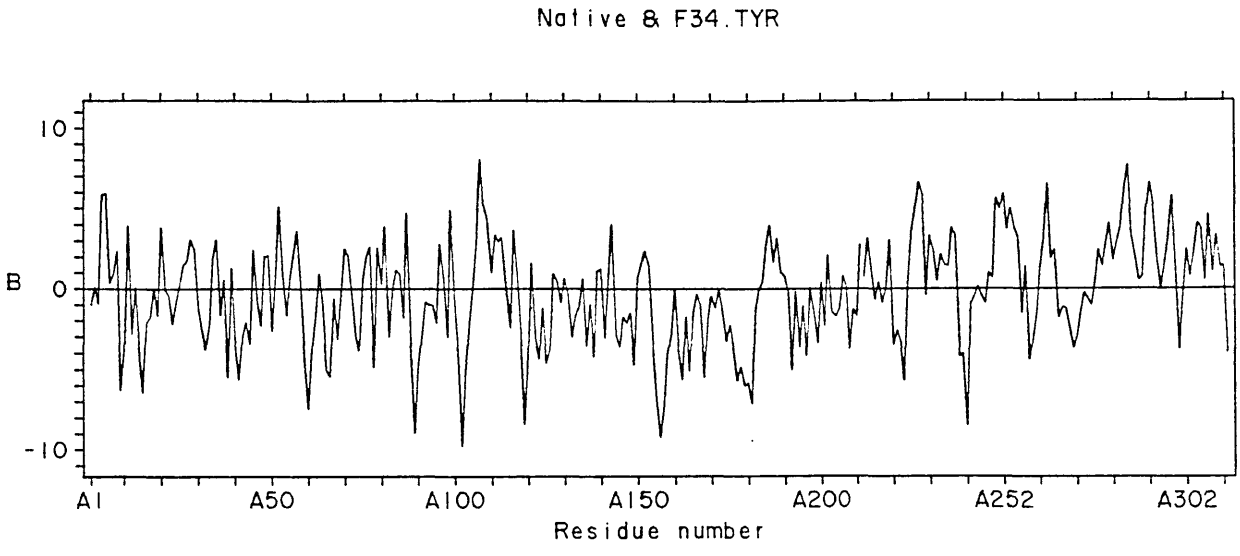
Minimal agar was prepared by adding 100 ml of 5 x minimal media salts (52.5 g K_2HPO_4, 22.5 g KH_2PO_4, 5 g $(NH_4)_2SO_4$ and 2.5 g

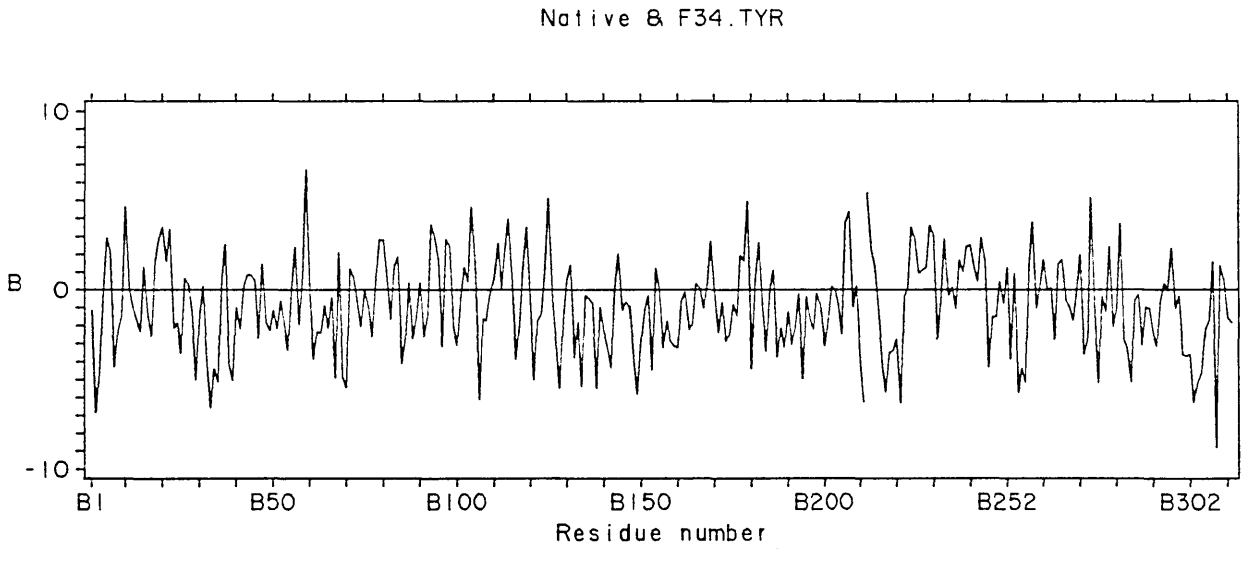
sodium citrate per litre) to 400 ml of water containing 7.5 g of molten agar (Difco). After sterilisation, the mixture was left to cool to 55° C, whereupon 0.25 ml of vitamin B1 (1% w/v), 0.5 ml $MgSO_4$ (20% w/v) and 5 ml glucose (20% w/v) were added.

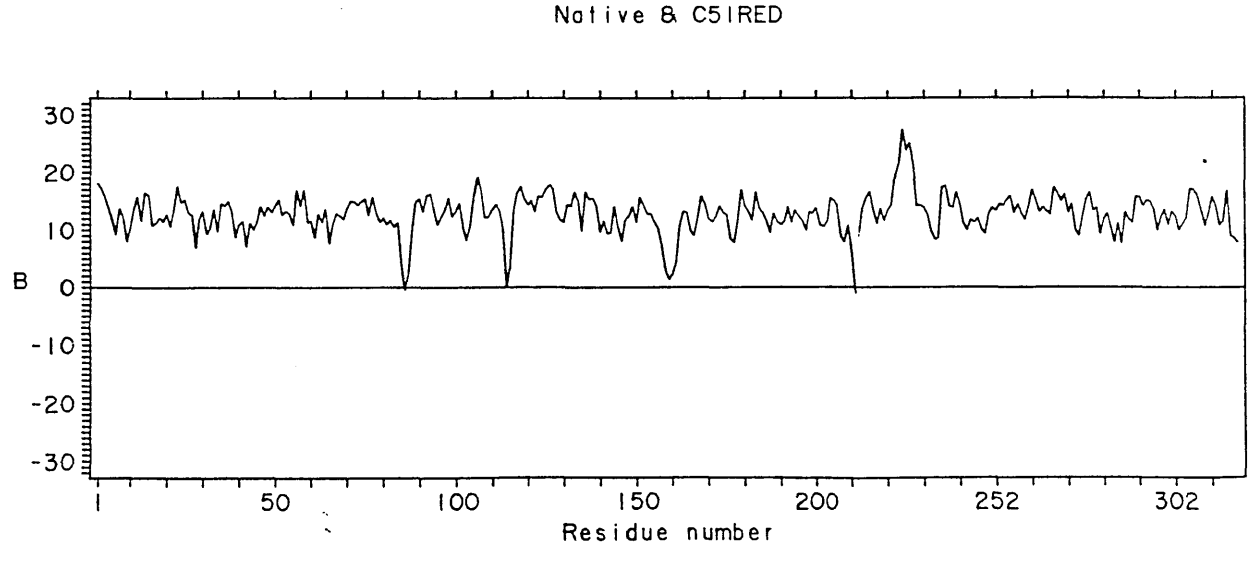
H-top agar consists of 10 g bacto-tryptone (Difco), 6 g bacto-agar (Difco) and 8 g NaCl, per litre. For selection of *E. coli* HB101F, kanamycin (Sigma) was added to freshly autoclaved media at a concentration of 50 mg/L after allowing the media to cool to 55° C.

All media were sterilised by autoclaving at 121° C for 20 mins.

Appendix E: Comparison of Main Chain B Values for Mutant and Native Structures.







Appendix E (contd.)

